THESIS
2
2004

This is to certify that the
dissertation entitled

NEURAL SUBSTRATES OF DIURNALITY IN THE NILE GRASS RAT, *ARVICANTHIS NILOTICUS*

presented by

Michael David Schwartz

has been accepted towards fulfillment
of the requirements for the

Doctoral degree in Neuroscience

Major Professor's Signature

12/6/04

Date

MSU is an Affirmative Action/Equal Opportunity Institution

LIBRARY
Michigan State
University

PLACE IN RETURN BOX to remove this checkout from your record.
TO AVOID FINES return on or before date due.
MAY BE RECALLED with earlier due date if requested.

DATE DUE	DATE DUE	DATE DUE

2/05 p:/CIRC/DateDue.indd-p.1

NEURAL SUBSTRATES OF DIURNALITY IN THE NILE GRASS RAT, *ARVICANTHIS NILOTICUS*

By

Michael David Schwartz

A DISSERTATION

Submitted to
Michigan State University
In partial fulfillment of the requirements
For the degree of

DOCTOR OF PHILOSOPHY

Neuroscience Program

2006

ABSTRACT

NEURAL SUBSTRATES OF DIURNALITY IN THE NILE GRASS RAT, *ARVICANTHIS NILOTICUS*

By

Michael David Schwartz

Circadian rhythms in behavior and physiology differ dramatically in diurnal and nocturnal rodents. However, the neural basis for these differences is unknown. A pacemaker located in the suprachiasmatic nucleus of the hypothalamus (SCN) is responsible for generating and maintaining circadian rhythms in mammals, but current research suggests that cellular and molecular rhythms in the SCN of diurnal rodents are similar to those of nocturnal species. The neural substrates of diurnal or nocturnal phase preference are thus likely to reside downstream of the SCN. The experiments in this dissertation address this issue by examining outputs of the circadian system in a diurnal rodent, the Nile grass rat *Arvicanthis niloticus*. Specifically, experiments assessed the anatomy and function of a major SCN target, the lower subparaventricular zone (LSPV).

In the first set of experiments, expression of the immediate early gene cFos was found to be rhythmic in the LSPV of grass rats and nocturnal lab rats housed in a light-dark cycle. However, the rising phase of this rhythm was advanced by nearly 8 hours in grass rats compared to lab rats, and was endogenous in grass rats, but not lab rats, when kept in constant darkness. Differences in the timing and the persistence of rhythmic activity in the grass rat LSPV suggest that this region could modulate circadian signals differently in diurnal and nocturnal rodents.

In the second set of experiments, the efferent neuroanatomy of the grass rat SCN and LSPV were characterized using microinjections of anterograde tracers. The distribution of efferent fibers from the LSPV was nearly identical to that of the SCN, as has been previously reported in nocturnal rodents. Furthermore, both the SCN and LSPV projected directly onto gonadotropin-releasing hormone neurons, whose rhythmic activity is reversed in grass rats and lab rats. Thus, the efferent projections of the LSPV are consistent with a role in modulating circadian signals. The similarity of SCN and LSPV projections also suggests that both areas work together to communicate circadian information.

Finally, LSPV function was assessed by monitoring general activity rhythms following neurotoxic lesions of the LSPV. Destruction of the LSPV caused profound disturbances in free-running activity rhythms and in entrainment of those rhythms, suggesting that signals from the grass rat LSPV contribute to rhythmic precision and stability in grass rats. However, neither activity rhythms nor the ability to entrain were abolished, indicating that the LSPV is not necessary for expression of either a diurnal phase preference or activity rhythms.

In summary, the LSPV exhibits the basic functional and anatomical characteristics necessary to communicate circadian signals originating in the SCN. Functional circadian rhythms are thus likely to depend on contributions from multiple oscillators that are ultimately coordinated by the master pacemaker, and the LSPV is very likely to be one of those oscillators.

Copyright by

MICHAEL DAVID SCHWARTZ

2006

For my mother and father.

Acknowledgements

First and foremost, I want to thank my advisor and mentor, Dr. Laura Smale, for her curiosity, enthusiasm, support, and her critical comments at every step of the way. Thanks also to the other members of my guidance committee, Dr. Antonio Nunez, Dr. Cheryl Sisk and Dr. John Johnson, whose perspectives have shaped both my personal and professional growth.

Much of this work would not have been possible without my labmates in the Smale and Nunez labs. Anna Baumgras, Joel Breen, Alexandra Castillo-Ruiz, Andrea Kaiser, Dr. Gladys Martinez, Terri McElhinny, Dr. Chidambaram Ramanathan, Jessica Schrader, Nicole Timm and Dr. Russell van Horn all have a hand in this research, and I am lucky to have worked with them all. Special thanks to Drs. Megan Mahoney and Josh Nixon, whose advice, encouragement and friendship over the last 6 years has been, and continues to be, invaluable.

Of course, not all training occurs in the lab. From day one, the Neuroscience Program welcomed me into a truly collaborative training community, and its students, postdocs and faculty continue to be a major part of my development. Thanks to David McFarlane for technical assistance, Dr. Sharleen Sakai for tract-tracing advice, and Dr. Henryk Urbanski for providing the gonadotropin-releasing hormone antibody.

Financial support for my research and training came from the National Institutes of Health (R01-MH53433, awarded to LS, and F31-MH070087, awarded to MDS) and the National Science Foundation (IBN-0130977, awarded

to LS). Additional support was provided by the Neuroscience Program and the Graduate School at Michigan State University.

Thanks to my family and friends who have supported me over the years, and thanks especially to Julia, for her love and her strength.

TABLE OF CONTENTS

LIST OF TABLES

LIST OF FIGURES

Images in this dissertation are presented in color.

INDEX OF ABBREVIATIONS

Abbreviation	Definition
τ	tau
2DG	2-deoxyglucose
3v	Third ventricle
ABC	Avidin-biotin-peroxidase complex
ac	Anterior commissure
ACB	Nucleus accumbens
AHA	Anterior hypothalamic area
AHC	Anterior hypothalamic area, central part
AHP	Anterior hypothalamic area, posterior part
ANOVA	Analysis of variance
Arc	Arcuate nucleus
AVPV	Anteroventral periventricular nucleus
BDA	Biotinylated dextran amine
BNST	Bed nucleus of the stria terminalis
CalB	Calbindin
CM	Centromedial thalamic nucleus
Cry, *Cry*	Cryptochrome
CT	Circadian time
D3v	Dorsal third ventricle
DAB	diaminobenzidine
DBB	Diagonal band of Broca
DD	Constant darkness
DMH	Dorsomedial hypothalamic nucleus
ER	Estrogen receptor
f	Fornix
fr	Fasciculus retroflexus
GnRH	Gonadotropin-releasing hormone
hbc	Habenular commissure
HDB	Horizontal limb of the diagonal band of Broca
ic	Internal capsule
IGL	Intergeniculate leaflet
-ir	immunoreactive
LA	Lateroanterior hypothalamic nucleus
LD	Light: dark cycle
LGN	Lateral geniculate nucleus
LH	Leuteinizing hormone
LHA	Lateral hypothalamic area

LHb	Lateral habenula
LPO	Lateral preoptic area
LSi	Lateral septum, intermediate part
LSPV	Lower subparaventricular zone
LSv	Lateral septum, ventral part
MeA	Medial amygdala
MHb	Medial habenula
MMn	Medial mammillary nucleus, median part
MnPO	Median preoptic nucleus
MPO	Medial preoptic nucleus
mPOA	Medial preoptic area
MS	Medial septum
mt	Mammillary tract
MUA	Multiple-unit activity
NMA	N-methyl-DL-aspartic acid
NDS	Normal donkey serum
NGS	Normal goat serum
ocx	Optic chiasm
opt	Optic tract
OVLT	Vascular organ of the lamina terminalis
PBS	Phosphate-buffered saline
pc	Posterior commissure
Pe	Periventricular hypothalamus
PeF	Perifornical region
Per, *Per*	Period
PF	Parafascicular thalamic nucleus
PH	Posterior hypothalamus
PK2	Prokineticin 2
PLP	4 % paraformaldehyde with lysine and sodium periodate
PMD	Premammillary nucleus, dorsal part
PMV	Premammillary nucleus, ventral part
POA	Preoptic area
PrC	Pre-commissural nucleus
PVG	Periventricular gray
PVN	Hypothalamic paraventricular nucleus
PVT	Paraventricular thalamic nucleus
PT	Parataenial thalamic nucleus
RCh	Retrochiasmatic area
Re	Reuniens thalamic nucleus
Rh	Rhomboid thalamic nucleus
Rt	Reticular thalamic nucleus
SCN	Suprachiasmatic nucleus
SCO	Sub-commissural organ
SHy	Septohypothalamic nucleus
SM	Nucleus of the stria medullaris

sm	Stria medullaris
SON	Supraoptic nucleus
SPF	Subparafascicular nucleus
sPVZ	Subparaventricular zone
st	Stria terminalis
Sub	Submedius thalamic nucleus
SuM	Supramammillary nucleus
TMN	Tuberomammillary nuclei
VDB	Vertical limb of the diagonal band of Broca
VIP	Vasoactive intestinal polypeptide
VLPO	Ventrolateral preoptic area
VMH	Ventromedial hypothalamic nucleus
VMPO	Ventromedial preoptic area
VP	Vasopressin
VTU	Ventral tuberal region
ZI	Zona incerta
ZT	Zeitgeber time

CHAPTER 1

Introduction

General introduction

Nearly all life forms studied to date exhibit circadian rhythms in behavior and physiology (Dunlap et al., 2004). While neurobiological study into the workings of the mammalian circadian clock proceeds at a lightning pace, most of this research focuses on nocturnal rodent models such as the lab rat, mouse and hamster. Diurnal animals (including humans) display dramatically different circadian rhythms, and without a clear understanding of these differences, the extent to which research on nocturnal rodents can be applied to diurnal species is unclear. Yet, the mechanisms that underlie differences between diurnal and nocturnal patterns of behavior and physiology are unknown (reviewed in Smale et al., 2003). This introductory chapter will first review the neural mechanisms underlying the fundamental circadian clock in mammals and present evidence suggesting that it is the same in diurnal and nocturnal species. This will be followed by a discussion of some of the ways in which responses to signals from that clock could differ in diurnal and nocturnal rodents. Finally, summaries of the research questions to be addressed in each chapter will be presented.

Cellular and molecular basis of mammalian circadian rhythms

Circadian rhythms, endogenous 24-hour cycles of behavioral, physiological and molecular processes, are ubiquitous in nature. The first indication that specific genes play central roles in the production of circadian

rhythms was the discovery of the *period* gene in the fruit fly *Drosophila melanogaster* (Konopka and Benzer, 1971). In mammals, discovery of the *tau* mutant hamster, which exhibited an abnormally short circadian period (Ralph and Menaker, 1988), and the *Clock* mouse, which exhibited a long τ followed by disintegration of rhythmicity (Vitaterna et al., 1994), was soon followed by characterization of many more 'clock genes' and a model of how they generated self-sustaining 24-hour oscillations in gene transcription and translation. Although the details of these models are still changing, it is clear that in both prokaryotic and eukaryotic organisms, circadian rhythmicity arises from the interaction of positive and negative feedback loops in gene transcription and translation (Dunlap, 1999; Bell-Pedersen et al., 2005). In mammals, the transcription factors *Clock* and *Bmal* form the positive portion of the loop. Their protein products dimerize, enter the nucleus and activate transcription of three sets of genes. One of these, the mammalian ortholog of *Period*, contains three variants, *Per1, Per2,* and *Per3*; the function of *Per3* is unclear, but the first two are intrinsic to the basic molecular clock. The other genes whose transcription is activated by Clock and Bmal are the *Cryptochrome* genes (*Cry1, Cry2*), and *Rev-Erbα*. Protein products of *Rev-Erbα* inhibit expression of *Bmal* (Reppert and Weaver, 2002). The protein products of the *Per* and *Cry* genes turn dimerize, re-enter the nucleus and repress transcription of their own genes, forming the negative loop, while the simultaneous repression of *Rev-Erbα* leads to increases in *Bmal* transcription (Reppert and Weaver, 2002). The resulting 24-hour oscillations in *Per1* and *Per2* mRNA, and Per1 and Per2 protein are frequently

used as markers for the oscillation of the molecular clock and allow direct observation of its phase.

In mammals, the hypothalamic suprachiasmatic nucleus (SCN) contains the primary circadian pacemaker (reviewed in Weaver, 1998). Complete electrolytic lesions of the SCN abolish circadian rhythmicity in a number of species (Moore and Eichler, 1972; Stephan and Zucker, 1972), and the SCN continues to oscillate after being isolated from other inputs *in vivo* (Inouye and Kawamura, 1979) and *in vitro* (Green and Gillette, 1982; Yamazaki et al., 2000). Furthermore, transplanting SCN tissue into the brain of an arrhythmic host restores locomotor rhythmicity, and does so with the characteristics of the donor, not the host (Ralph et al., 1990). These data and other findings have clearly demonstrated that the SCN contains a self-sustaining circadian oscillator that is necessary for the generation of circadian activity rhythms.

The SCN is similar in diurnal and nocturnal rodents

Theoretically, the SCN could represent a potential source of species differences in the timing of circadian rhythms in behavior. However, this does not appear to be the case, as in many respects the SCN is similar in diurnal and nocturnal species. For example, SCN metabolic activity measured by 2-deoxyglucose uptake (2DG) peaks during the subjective day in an array of diurnal and nocturnal species (Schwartz, 1991), and rhythms in multiple-unit electrical activity peak during the day in the SCN of the nocturnal lab rat and the diurnal Siberian chipmunk (Kubota et al., 1981; Sato and Kawamura, 1984b; Kurumiya and Kawamura, 1988). Furthermore, daily rhythms in expression of

the immediate early gene cFos are similar in the SCN of diurnal grass rats and nocturnal lab rats (Katona et al., 1998; Nunez et al., 1999). These data suggest that rhythmic activity in the SCN is similar at a general level in several diurnal and nocturnal species. Nevertheless, species differences have been reported in some features of SCN structure and function. For example, the SCN's response to stimulation by light is different in lab rats and diurnal *Octodon degus* (Krajnak et al., 1997; Jiao et al., 1999), and responses to infusions of muscimol, a GABA-A agonist, into the SCN are different in grass rats and hamsters (Novak and Albers, 2004). It thus remains possible that mechanisms associated with diurnality involve changes in specialized subpopulations of cells within the SCN. However, in diurnal grass rats, rhythms in the SCN's responsiveness to light are similar to those of nocturnal species (Mahoney et al., 2001), and both light pulses and muscimol injection have similar effects on *Per* expression in the SCN of grass rats and hamsters (Novak et al., 2006). Taken together, the data suggest that although some features of SCN function vary across species, most features of SCN function and anatomy are similar in nocturnal and diurnal species.

Accumulating evidence suggests that one fundamental component of the SCN that is the same across species is the core molecular clock that it contains. The SCN of diurnal rodents such as grass rats, 13-lined ground squirrels and *Arvicanthis ansorgei* express high levels of *Per1* and *Per2* mRNA in the subjective day (Mrosovsky et al., 2001; Caldelas et al., 2003; Lambert et al., 2005; Novak et al., 2006), as has been demonstrated in lab rats (Yan and Okamura, 2002) mice (Hastings et al., 1999; Bae et al., 2001) and hamsters

(Hamada et al., 2004). These similarities are also seen in rhythms of Per1 and Per2 proteins in the SCN of diurnal grass rats (Ramanathan et al., 2006) and nocturnal lab rats (Amir et al., 2004), mice (Hastings et al., 1999; Field et al., 2000) and hamsters (Nuesslein-Hildesheim et al., 2000). Although the molecular clock includes many components whose function could conceivably differ, the similarity in phase of *Per* mRNA and protein oscillations suggests that the molecular clock is very likely to be similar in nocturnal and diurnal species.

The mechanisms coupling the molecular clock within the SCN to output rhythms are poorly understood at the molecular level. However, several proteins and peptides are emerging as candidate output molecules that communicate clock information to systems regulating physiological and behavioral events. Proteins such as prokineticin 2 (PK2; Cheng et al., 2002), transforming growth factor-alpha (Kramer et al., 2001) and cardiotrophin-like cytokine (Kraves and Weitz, 2006) may play roles in communicating circadian information to SCN targets that regulate behavior. In addition, vasopressin (VP) and vasoactive intestinal polypeptide (VIP) may function as SCN signals regulating neuroendocrine rhythms. In all cases in which molecular outputs have been examined in diurnal species they have been the same as those documented in nocturnal ones (Reppert et al., 1983; Krajnak et al., 1998; Lambert et al., 2005; Mahoney et al., 2006). Taken together, the data on the SCN of nocturnal and diurnal species suggest that the primary mechanisms underlying diurnality are likely to lie downstream of the SCN, in cells that receive direct or indirect input from it.

Outputs of the SCN

The SCN appears to use a combination of signaling methods, paracrine and synaptic, to communicate with its targets. Diffusible signals can induce 2DG and Per rhythms *in vitro* (Allen et al., 2001), and can restore locomotor rhythms in arrhythmic hamsters *in vivo* (Silver et al., 1996a). However, SCN transplants that reinstate locomotor rhythms in hamsters reinstate *Per* rhythms in some but not other peripheral targets (Guo et al., 2006), and also fail to reinstate neuroendocrine rhythms (Meyer-Bernstein et al., 1999). Thus, diffusible signals are unable to sustain the full panoply of circadian rhythms seen in intact hamsters, implying that neural efferents from the SCN are an essential aspect of circadian output (de la Iglesia et al., 2003; de la Iglesia and Schwartz, 2006). Virtually nothing is known about the roles of axonal projections of the SCN, or diffusible signals that might be released by it, in the regulation of rhythms in animals other than nocturnal rodents.

SCN efferents have been characterized using anterograde and retrograde neural tracers in lab rats and hamsters (Watts and Swanson, 1987; Watts et al., 1987; Morin et al., 1994; Leak and Moore, 2001; Kriegsfeld et al., 2004). In mice, SCN projections have been examined indirectly via immunohistochemical analysis of VP and VIP fibers originating in the SCN (Abrahamson and Moore, 2001). Although some species differences in efferent fiber distributions have been reported (Morin et al., 1994), these studies have all found that the SCN of lab rats, mice and hamsters projects widely within the hypothalamus. These projections are especially concentrated in the medial hypothalamus, are present but more moderate in the limbic forebrain and midline thalamus, and almost, if

not completely, absent in the midbrain, hindbrain and cerebral cortex. There are no published data on the efferent projections of the SCN in diurnal rodents, although at least some of them are likely to be similar (Mahoney and Smale, 2005b). A major goal of this thesis, therefore, is to evaluate whether these projections differ in grass rats compared to lab rats or hamsters, as well as to identify pathways by which circadian signals could reach target populations of cells whose activity is inverted in diurnal and nocturnal species.

The lower subparaventricular zone

Mechanisms underlying diurnality could be located outside of the SCN such that its output signals are the same in nocturnal and diurnal species but are interpreted differently at, or downstream of, one or more SCN targets. The subparaventricular zone (sPVZ) is one promising candidate for such a downstream site. This is a relatively cell-sparse region adjacent to the hypothalamic periventricular nucleus extending dorsally and caudally from the dorsal border of the SCN to the ventral border of the hypothalamic paraventricular nucleus (PVN; Watts et al., 1987; PVN; Morin et al., 1994; Smale and Boverhof, 1999). The SCN of both nocturnal and diurnal species sends massive AVP- and VIP-immunoreactive (-ir) projections into the sPVZ. In nocturnal species, the sPVZ is known to project in turn to nearly all of the same targets as the SCN (Watts et al., 1987; Morin et al., 1994; Kriegsfeld et al., 2004). Based on these data, it has been suggested that circadian signals from the SCN are amplified by the sPVZ en route to their targets (Watts and Swanson, 1987).

The lower part of the subparaventricular zone (LSPV) is located immediately dorsal to the SCN and includes parts of the terminal field of VP- and VIP-ir axons emanating from the SCN (Watts and Swanson, 1987; Watts et al., 1987; Lu et al., 2001). However, while the latter includes the entire terminal field extending dorsally and caudally to the PVN, the LSPV includes only the part of the terminal field that is immediately dorsal to the SCN. Under a 12:12 light-dark cycle (LD), cFos-ir in the SCN of diurnal grass rats, like that of the nocturnal lab rats, peaks early in the light phase and declines steadily thereafter (Nunez et al., 1999). However, cFos rhythms in the LSPV are very different in the two species. In the grass rat LSPV, cFos rises sharply at Zeitgeber time (ZT) 17 [1] and remains high until several hours after lights-on. cFos-ir in the LSPV of lab rats, by contrast, does not rise until 8 hours, later, at ZT 1. While the rising phase of the LSPV and SCN rhythms are in phase in lab rats, this is not the case in grass rats. In summary, the LSPV, a direct target of the SCN in both diurnal and nocturnal species, exhibits a rhythm in cFos expression with a rising phase that is advanced by approximately 9 hours in a diurnal species relative to a nocturnal one and almost reversed from the rhythm seen in the SCN in a diurnal species, but not a nocturnal one. It is not yet known whether these patterns reflect

[1] In circadian biology, time is denoted in either zeitgeber time (ZT) or circadian time (CT), depending on the lighting conditions. Zeitgeber hours are equivalent to clock hours, and referenced to the timing of the light-dark transition; in a 12:12 LD cycle, ZT 0 corresponds to lights-on and activity onset for a diurnal animal, and ZT 12 corresponds to lights-off and activity onset for a nocturnal animal. Under constant lighting conditions, circadian hours are referenced to subjective daylength, where one circadian hour is equal to $1/24^{th}$ of the organism's free-running circadian period (τ). CT 0 corresponds to the start of the subjective day and activity onset in a diurnal animal, and CT 12 corresponds to the start of subjective night and activity onset for a nocturnal animal. For a more detailed review see
Moore-Ede MC, Sulzman FM, Fuller CA (1982) The clocks that time us: physiology of the circadian timing system. Cambridge, Mass.: Harvard University Press..

endogenous mechanisms as the data described above were all collected from animals maintained in LD conditions. However, these data raise the possibility that the LSPV might modulate circadian signals originating in the SCN, and do so differently in diurnal and nocturnal species.

Overview of chapters

The experiments in this thesis, broadly speaking, will explore output mechanisms used by the circadian system, whether these mechanisms might differ in some way in diurnal and nocturnal rodents, and, if so, how those differences might contribute to determining whether an animal exhibits a diurnal or nocturnal pattern of rhythmicity. The latter could theoretically occur in several ways. Circadian output signals sent by the SCN to other brain regions could differ in diurnal and nocturnal rodents. Although differences could still exist that have not yet been identified, the phases of rhythms that are intrinsic to the molecular clock, and of the rhythms in SCN output signals that have been identified, are similar in diurnal and nocturnal species (see above). Existing data thus suggest that the key to diurnality lies beyond the SCN. A very plausible alternative is that SCN targets of diurnal and nocturnal species respond differently to circadian signals sent to them by the SCN. This thesis will evaluate a specific variant of this hypothesis that has emerged from consideration of the results reviewed above. In this model, circadian signals originating within the SCN are modulated by the LSPV in different ways in nocturnal and diurnal species. This leads, in turn, to different patterns of coupling between the SCN and its other downstream targets. This then leads to reversed circadian patterns

of intracellular rhythms in those target cells, and to reversed patterns of behavioral rhythms in diurnal and nocturnal species. Several predictions emerge from this hypothesis:

Prediction$_1$: If the LSPV is necessary for maintaining diurnal patterns of rhythmicity, then its rhythmic activity should be endogenous. In chapter two, this prediction is tested by comparing rhythms in cFos expression in grass rats and lab rats kept in constant darkness. Additional experiments evaluate the time course of cFos expression in the LSPV when animals are kept in an LD cycle, and further characterize the neurochamical anatomy of the LSPV.

Prediction$_2$: If the LSPV provides a signal to areas of the brain important for maintaining circadian rhythms, then it should have some mechanism of communicating with those areas. This prediction is tested in studies described in chapters three and four. In chapter three, injections of the anterograde tracer biotinylated dextran amine (BDA) are used to map the efferent projections of both the SCN and the LSPV of grass rats. Chapter four examines whether the SCN and/or the LSPV project directly onto a population of cells whose rhythmic activity is reversed in diurnal and nocturnal species by comparing appositions between gonadotropin-releasing hormone neurons and fibers from the SCN and LSPV.

Prediction$_3$: If the LSPV is a necessary component for the maintenance of diurnal patterns of physiological and behavioral rhythms, its destruction should significantly alter or abolish these rhythms. Chapter five evaluates this prediction by examining general activity rhythms in grass rats with neurotoxic lesions of the LSPV that spare both the SCN and its efferent fibers.

In lab rats, the region dorsal to the SCN appears to be an important target of the SCN that plays a key role in regulation of a variety of rhythms (Watts and Swanson, 1987; Watts et al., 1987; Saper et al., 2005). These include rhythms in neuroendocrine processes associated with estrous cyclicity (Arendash and Gallo, 1979; Docke et al., 1982; Watts et al., 1989; Fernandez-Galaz et al., 1999), sleep-wake cycles (Lu et al., 2001) and locomotor rhythms (Lu et al., 2001; Moore and Danchenko, 2002; Abrahamson and Moore, 2006). The experiments described in this thesis will help to identify features of this output system that may generalize from lab rats to other species, including ones showing very different patterns of rhythmicity. These studies will also evaluate ways in which the LSPV differs across species and test the hypothesis that it contributes to emergence of a diurnal phase preference. If the LSPV does not specifically mediate diurnality in the grass rat, it may still be integrally involved in output of SCN timing signals, in the production of rhythms, or in the interaction between the clock and rhythmic behavior. These experiments will therefore make important contributions to our understanding of diurnality specifically as well as of circadian output systems more generally.

CHAPTER 2

Schwartz MD, Nunez AA, Smale L (2004) Differences in the suprachiasmatic nucleus and lower subparaventricular zone of diurnal and nocturnal rodents. Neuroscience 127:13-23.

CHAPTER 2

Differences in the suprachiasmatic nucleus and lower subparaventricular zone of diurnal and nocturnal rodents

Introduction

The suprachiasmatic nucleus (SCN) of the hypothalamus is the site of the principal circadian pacemaker in mammals (Moore and Leak, 2001), and in many respects the SCN is similar in diurnal and nocturnal mammals. For example, rhythms in multiple-unit activity (MUA) peak during the day in the SCN of both lab rats and the diurnal Siberian chipmunk (Kubota et al., 1981; Sato and Kawamura, 1984b; Kurumiya and Kawamura, 1988), and glucose utilization measured by uptake of 2-deoxyglucose (2DG) peaks during the subjective day in both nocturnal and diurnal mammals (reviewed in Schwartz, 1991). Diurnal rodents such as the 13-lined ground squirrel and *Arvicanthis ansorgei* express high levels of mRNA for the clock genes *per1* and *per2* in the SCN in the subjective day (Mrosovsky et al., 2001; Caldelas et al., 2003), as has been demonstrated in the lab rat (Yan and Okamura, 2002) and mouse (Hastings et al., 1999; Bae et al., 2001). Overall these data imply that, with respect to some very basic functions, the SCN is more similar than different in diurnal and nocturnal species. However, diurnal *Octodon degus* differ from lab rats with respect to the pattern of responsiveness of SCN cells to light (Krajnak et al., 1997; Jiao et al., 1999). Furthermore, light-unresponsive SCN cells exhibit circadian rhythms in spontaneous firing rate *in vivo* in lab rats, but not in degus (Jiao et al., 1999). The SCN is a functionally and anatomically heterogeneous nucleus, and

differences within some SCN neurons could lead to divergent patterns of rhythmicity.

It is also possible that differences between diurnal and nocturnal patterns of circadian rhythmicity emerge from processes downstream of the SCN. For example, SCN targets may interpret output signals differently in one species relative to another. This could occur in a decentralized fashion whereby re-interpretation occurs at many sites receiving input from the SCN. Alternatively, a single target could modulate signals coming from the SCN differently in diurnal and nocturnal species. Different patterns of signals could then be broadcast from this central location to multiple distal targets.

The hypothalamic subparaventricular zone (sPVZ) is one possible location for a modulator of SCN efferent signals. Extending dorsally and caudally from the dorsal border of the SCN to the paraventricular hypothalamic nucleus, the sPVZ is one of the major targets of the SCN in lab rats (Watts and Swanson, 1987; Watts et al., 1987; Watts, 1991; Moore and Leak, 2001), mice (Abrahamson and Moore, 2001) and hamsters (Morin et al., 1994). Cells in the sPVZ project to many of the same regions as do cells in the SCN in lab rats (Watts and Swanson, 1987; Watts et al., 1987; Watts, 1991) and in hamsters (Morin et al., 1994; Orpen and Steiner, 1994; Kriegsfeld et al., 2004). Here we focus on the ventral portion of the sPVZ, which extends outward from the dorsal border of the SCN and overlaps partially with the perisuprachiasmatic region. We refer to this region as the lower subparaventricular zone or LSPV. The daily rhythm in expression of the immediate early gene product cFos in the LSPV is

dramatically different in nocturnal lab rats as compared to a diurnal rodent, the unstriped Nile grass rat, *Arvicanthis niloticus* (referred to hereafter as the grass rat; (Nunez et al., 1999). Specifically, in lab rats, the number of cFos-immunoreactive (-ir) cells in the LSPV displayed a sharp peak at Zeitgeber time (ZT) 1 and declined rapidly thereafter, whereas in grass rats, the rising phase of the rhythm began at ZT 17, and cFos was still high at ZT 1, after which it began to decline. These species differences raise the possibility that the LSPV is a central point at which a common efferent signal emanating from the SCN could be modulated differently in one species relative to the other, leading ultimately to differential patterns of coupling between SCN output and behavioral rhythms (Nunez et al., 1999).

The present work sought to characterize further the grass rat LSPV and to compare its rhythmic activity to that of lab rats. The first study had two primary goals: to assess whether cFos in the grass rat LSPV remains high through the night, and to determine when cFos begins to rise in the lab rat LSPV. In the second study, we determined whether daily rhythms in this region are endogenous by releasing grass rats and lab rats into constant darkness (DD) for two to three weeks, and sacrificing them at different phases of their rhythms in general activity. Because cells containing calbindin (CalB) had been previously seen within and around the grass rat SCN (Mahoney et al., 2000), we processed tissue from these animals for visualization of both cFos and CalB-ir to assess the degree to which cFos expression overlaps with that of CalB in the LSPV. Finally, we mapped the distribution of cFos-positive cells in the grass rat LSPV in relation

to cells immunopositive for vasopressin (VP), vasoactive intestinal peptide (VIP) and CalB to characterize the LSPV anatomically in relation to the SCN, and to assess the utility of CalB-ir as a peptidergic marker for the LSPV.

Experimental Procedures:

Animals:

Animals were adult male Sprague-Dawley lab rats obtained from Charles River Laboratories (Wilmington, MA), and adult male grass rats obtained from a breeding colony at Michigan State University (Katona and Smale, 1997). Animals were singly housed in Plexiglas cages (lab rats: 26 x 48 x 20 cm; grass rats 34 x 28 x 17 cm) with access to food (lab rats: Harlan Teklad 8640, Madison, WI; grass rats, PMI Nutrition Prolab RMH 2000, Brentwood, MO) and water *ad libitum* in a 12:12 light: dark (LD) cycle (lights on at 06:00). A red light (<5 lux) remained on constantly for animal care purposes. All experiments were performed in compliance with guidelines established by the Michigan State University All-University Committee on Animals Use and Care, and the NIH Guide for the Care and Use of Laboratory Animals. All efforts were made to minimize the number of animals used and their discomfort.

General immunocytochemical procedure:

At the time of sacrifice, animals were given an overdose of sodium pentobarbital and perfused transcardially with 0.01M phosphate-buffered saline (PBS), pH 7.2, followed by 4% paraformaldehyde (Sigma, St. Louis, MO) in 0.1M phosphate buffer, unless otherwise noted. Animals sacrificed during the dark phase or in DD were fitted with a light-tight hood prior to perfusion to prevent

acute exposure to light. Brains were post-fixed for 1-2 hours, transferred to 20% sucrose solution overnight, and then stored in cryoprotectant at -20°C until sectioning. Brains were sectioned coronally at 30 μm on a freezing microtome, and sections were either placed into PBS for immediate processing or into cryoprotectant for further storage.

Unless noted otherwise, incubations were conducted at room temperature for 1 hour on a shaker, and tissue was rinsed 3 x 10 minutes in PBS between incubations. Free-floating sections were rinsed in PBS, and then incubated in (i) 5% normal serum in PBS with 0.3% Triton-X, followed by (ii) primary antibody on a rotator for 48 hours at 4°C. Following primary incubation, tissue was incubated in (iii) biotinylated secondary antibody, followed by avidin-biotin peroxidase complex (ABC Vectastain Kit, Vector Laboratories, Burlingame, CA). Protein was visualized by reacting with diaminobenzidine (DAB; 0.5mg/mL; Sigma) in Trizma buffer (Sigma), catalyzed with hydrogen peroxide. For cFos/CalB double-labeling, cobalt chloride was added to the cFos reaction, yielding a blue-black rather than brown reaction product. The reaction was quenched in PBS, then rinsed and incubated with the second primary antibody. Reagents for each reaction were as follows. cFos: (i) normal goat serum (NGS; Vector), (ii) rabbit anti-cFos (Santa Cruz Biochemistry, Santa Cruz, CA, 1:25,000), (iii) biotinylated goat anti-rabbit; (Vector, 1:200). VP: (i) NGS, (ii) guinea pig anti-VP (Peninsula Laboratories, CA, 1:10,000), (iii) biotinylated goat anti-guinea pig (Vector, 1:200). VIP: (i) 5% normal donkey serum (NDS; Jackson Laboratories, CA), (ii) guinea pig anti-VIP (Peninsula, 1:2000), (iii) biotinylated donkey anti-guinea pig

(Jackson, 1:200). CalB: (i) NDS, (ii) mouse anti-CalB (Sigma, 1:20,000), (iii) biotinylated donkey anti-mouse (Jackson, 1:200). Specificity of CalB and Fos labeling was verified by blocking experiments in which the primary antibody was pre-incubated with its antigen (CalB: Swant, Bellinzona, Switzerland, 3 μg/mL; cFos: Immunostar, CA, 5 μg/mL); in both cases pretreatment with blocking peptide dramatically reduced or eliminated staining (data not shown). Specificity of VP and VIP labeling in the grass rat SCN was previously documented in (Smale and Boverhof, 1999). Primary deletion controls for each peptide also resulted in absence of stain (data not shown). Tissue was mounted, dehydrated, and coverslipped with Permount.

cFos rhythms in LD:

To evaluate cFos rhythms in the SCN and LSPV of entrained animals, 35 grass rats and 30 lab rats were kept in 12:12 LD and perfused at ZT 1, 5, 13, 17, 20, or 23 as described above except that 1.3% lysine and 4% sodium periodate were added to the 4% paraformaldehyde. Every third section through the rostrocaudal extent of the SCN was used for single-label cFos immunocytochemistry.

Two sections through the mid- to caudal SCN were selected from each animal for analysis. All cFos-positive neurons were counted within the SCN, and within a region of the LSPV defined by a 215 µm x 160 µm rectangle placed immediately dorsal to the SCN and lateral to the third ventricle (Fig. 2.1). Bilateral counts for each area were averaged across the 2 sections.

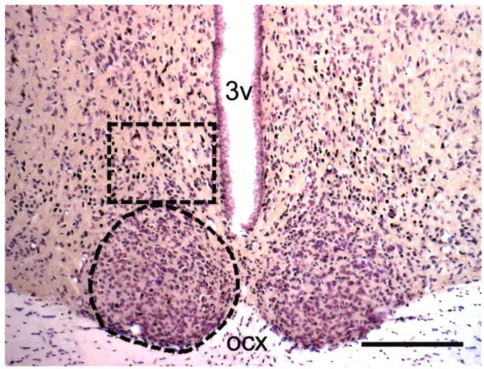

Figure 2.1: Photomicrograph of the SCN and LSPV of a grass rat perfused at ZT 22 and stained for cFos-ir and Nissl. The SCN is outlined on the left, and the sampling region used for LSPV counts is drawn to scale and placed above the SCN. The section depicted here corresponds to the map of cFos-ir in the mid-SCN of the series depicted in Fig. 2.6. 3v: third ventricle; ocx: optic chiasm. Scale bar = 200 μm.

cFos Rhythms in DD:

To assess the rhythmicity of cFos-ir in the SCN and LSPV under constant conditions, 20 grass rats and 23 lab rats were first housed in 12:12 LD with infrared motion detectors placed directly over the cage to monitor general activity rhythms. Activity data was collected and viewed on a PC running the Dataquest 3 program (Data Sciences International, St. Paul, MN). After an acclimation period of 1-2 weeks, lights were turned off at the normal time (18:00) and remained off from this point onwards.

Animals were allowed to free-run in DD for 21-22 days (grass rats) or 16-17 days (lab rats). At the end of this time, actograms for each animal were examined and activity onsets were eye-fitted independently by two investigators. All animals were randomly assigned to specific circadian times (CT) for sacrifice, where CT 0 = activity onset (grass rats), or CT 12 = activity onset (lab rats). Grass rats were sacrificed at CT 5 (n=6), CT 13 (n=8), or CT 22 (n=6); lab rats were sacrificed at CT 1 (n=5), CT 5 (n=6), CT 13 (n=5), or CT 22 (n=7). Every third section through the SCN and LSPV was processed for double-label cFos/CalB immunocytochemistry. Bilateral maps were made of 2 sections through the mid- to caudal SCN and LSPV as described above using a camera lucida, and counts were made of the numbers of cells positive for cFos only, CalB only, and cells positive for both cFos and CalB.

Statistical analyses:

Cell counts from each species were analyzed by single-factor analyses of variance (ANOVA) using Statview (SAS Institute) followed by posthoc pairwise Tukey comparisons (LD experiment) or a Bonferroni correction (DD). Differences for all tests were considered significant at the $P<0.05$ level. All counts were made by an investigator unaware of the time of sacrifice of each animal.

Anatomical characterization of the LSPV region:

Two male grass rats kept in 12:12 LD were perfused at ZT 22 (when we found cFos-ir in the LSPV to be maximal; see below). To identify the boundaries between the SCN and the surrounding region in a more traditional manner, three series through the SCN of one animal were processed for cFos-ir, VP-ir, and VIP-ir, respectively. Maps were made of the VP, VIP and cFos cell distributions in the SCN and LSPV through 5 sections extending from just rostral to the SCN to just caudal to it. Following mapping, the coverslips were removed from the cFos-ir series, tissue was Nissl-stained, and re-coverslipped in order to determine the Nissl-defined boundary of the SCN. To evaluate the spatial relationship between cFos and one potential marker for this region, we processed one series from the second animal for cFos/CalB double-labeling. Maps were made of the cFos and CalB cell distributions in the SCN and LSPV through 5 sections extending from just rostral to the SCN to just caudal to it. Following mapping, the coverslips were removed from the series, tissue was Nissl-stained, and re-coverslipped in order to determine the Nissl-defined boundary of the SCN.

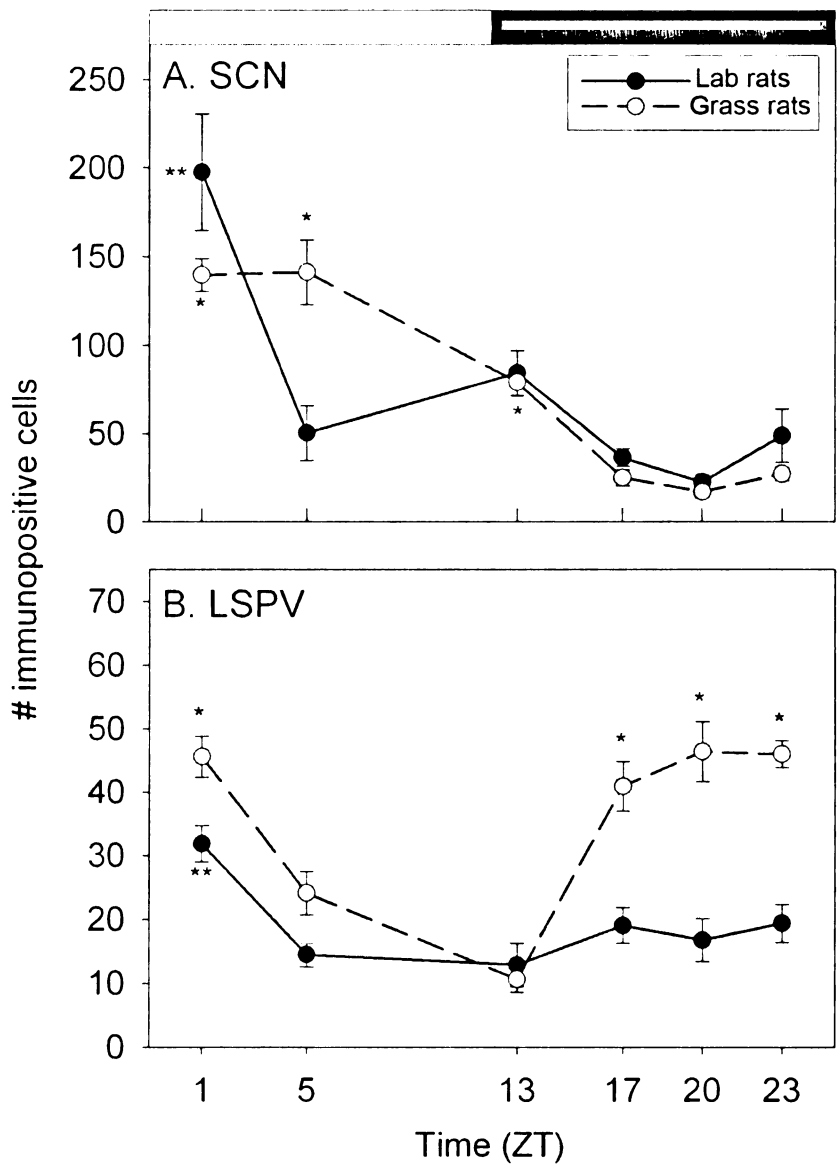

Figure 2.2: Numbers of cFos-positive cells in (A) the SCN, and (B) the LSPV of grass rats (open circles) and lab rats (filled circles) kept in a 12:12 LD cycle. Asterisks indicate time points where numbers of cFos-positive cells are significantly elevated relative to other time points in (*) grass rats, (**) lab rats.

Results:

cFos rhythms in LD:

SCN: In both grass rats ($F_{5,29} = 44.696$, $p < .0001$) and lab rats ($F_{5,24} = 14.079$, $p < .0001$), the numbers of cFos-positive cells in the SCN peaked early in the day and decreased steadily thereafter. In grass rats, cFos was highest from ZT 1-5 and lowest from ZT 17-23 (Fig. 2.2a, 2.3). In lab rats, cFos was also highest at ZT 1 but declined to a trough by ZT 5, and remained low for the rest of the day (Fig. 2.2a, 2.3). cFos-positive nuclei appeared throughout the SCN in both species, with no clear regional differences emerging at any time point. Thus, under a 12:12 LD cycle, both species displayed basically similar daily cFos rhythms in the SCN, though in lab rats cFos-ir declined more rapidly from peak values than in grass rats.

LSPV: In the grass rat LSPV, there was a significant effect of time ($F_{5,29} = 19.548$, $p < 0.001$) on the numbers of cFos-positive cells in the SCN. Posthoc comparisons revealed that the number of cFos-positive cells at ZT 5 and ZT 13 were significantly lower than at all other time points (Fig. 2.2b, 2.3). The number of cFos-positive nuclei rose sharply from ZT 13 to ZT 17 and remained high through ZT 1. In lab rats, cFos was also rhythmic ($F_{5,24} = 5.416$, $p = .0018$), but in contrast to the pattern seen in grass rats, the number of cFos-positive cells did not rise until the interval between ZT 23 and ZT 1, and had declined back to baseline levels by ZT 5 (Fig. 2.2b, 2.3). Low levels were maintained for the remainder of the day and night. Thus, both species displayed

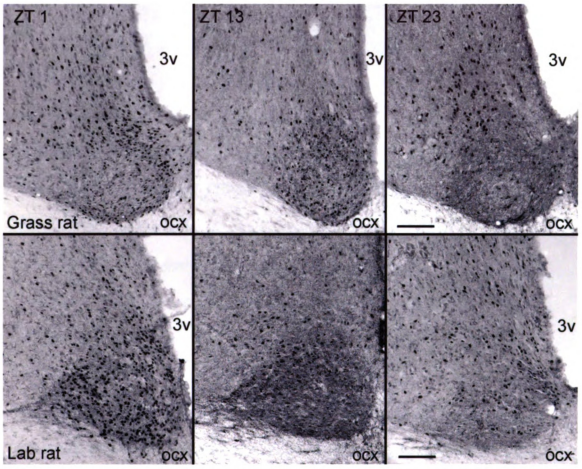

Figure 2.3: Photomicrograph of the SCN and LSPV of representative grass rats (top row) and lab rats (bottom row) perfused at ZT 1 (left), ZT 13 (middle) or ZT 23 (right) and processed for cFos-ir. 3v: third ventricle; ocx: optic chiasm. Scale bar = 100 μm.

daily rhythms in cFos-ir in the LSPV under LD, but in grass rats cFos rose ~8 hours earlier and remained elevated ~8 hours longer.

cFos and CalB rhythms in DD:

SCN: In the grass rat SCN, cFos remained rhythmic after animals had been in DD for 3 weeks ($F_{2,17}$= 9.701, p = .0015; Fig. 2.4a). Posthoc comparisons indicated that the number of single-labeled cFos-positive nuclei was higher at CT 5 than at either CT 13 or CT 22, a pattern similar to that seen in LD. The cFos rhythm in the SCN was only found in cells that did not contain CalB; no effect of time was seen on double-labeled cells ($F_{2,17}$ = 0.689, p = .5164). The number of single-labeled CalB-positive cells also did not vary as a function of time ($F_{2,17}$ = 0.070, p =.9327). In grass rats cFos-ir appeared throughout the SCN, with no clear regional differences. At all time points, a small number of CalB-positive cells were scattered throughout the SCN in rostral and middle sections but in the caudal SCN these cells were concentrated in a roughly circular region slightly lateral to the center of the nucleus. Double-labeled cells were rare, and were not restricted to any subregion of the SCN.

In lab rats there were no effects of time on the number of single-labeled cFos-positive nuclei ($F_{3,19}$ = 2.070, p = .1382), single-labeled CalB-positive cells ($F_{3,19}$ = 0.029, p = .9931), or in the number of double-labeled cells ($F_{3,19}$ = 2.425, p =.0973) in the SCN after 2 weeks in DD (Fig. 2.4b). cFos-positive nuclei tended to be concentrated in the dorsomedial SCN, whereas CalB-positive cells were fewer in number and scattered throughout the SCN.

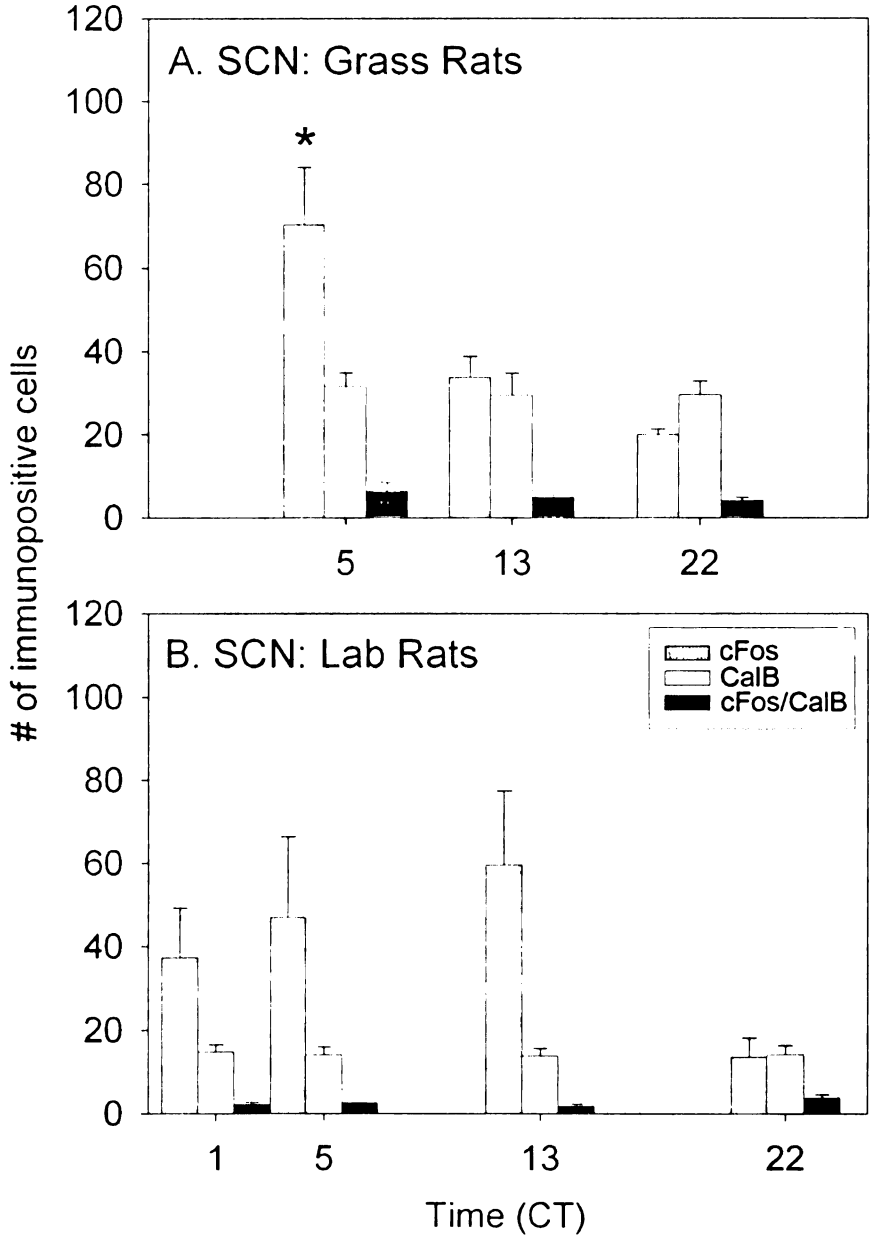

Figure 2.4: Counts of cells positive for cFos only (grey bars), CalB only (white bars), and cells positive for both cFos and CalB (black bars) in the SCN of A) grass rats, B) lab rats, after 2-3 weeks in DD. Asterisks indicate time points where numbers of cFos-positive cells (*) are significantly elevated relative to other time points, p=.0015.

LSPV: In the grass rat LSPV, there were significant effects of time on the number of cells singly labeled for cFos ($F_{2,17} = 27.801$, $p < .0001$; Fig. 2.5a), such that cFos-ir was higher at CT 22 than at either CT 5 or CT 13. This pattern was also observed in cells that contained both cFos and CalB ($F_{2,17} = 19.068$, $p < .0001$; Fig. 2.5a) Thus, cFos increased at night both inside and outside of CalB-positive cells. The total number of CalB-positive cells was also affected by time ($F_{2,17} = 5.795$, $p = .0201$; data not shown), and was higher at CT 22 than at CT 5. However, there was no effect of time on numbers of CalB-positive cells that did not contain cFos ($F_{2,17} = 1.460$, $p = .2600$; Fig. 2.5a). Thus, CalB increased at night, but only in cells also positive for cFos.

In the lab rat LSPV, there were no effects of time on the number of single-labeled cFos-positive nuclei ($F_{3,19} = 0.058$, $p = .9811$), single-labeled CalB-positive cells ($F_{3,19} = 0.516$, $p = .6759$), or the number of double-labeled cells ($F_{3,19} = 0.087$, $p = .9663$; Fig. 2.5b).

Distributions of cFos, VP, VIP and CalB in the SCN/LSPV*:*

SCN: In order to characterize in more detail the distribution of cFos-ir in the LSPV in relation to the SCN, we compared labeling for VP and VIP, two peptides commonly used to demarcate the SCN, with labeling for cFos at ZT 22, when cFos-ir is highest in the LSPV. The distributions of VP and VIP within the SCN of a grass rat perfused at ZT 22 were similar to those described previously (Smale and Boverhof, 1999) (Fig. 2.6). VP-positive neurons were distributed in a roughly crescent-like pattern within the lateral, dorsal and medial SCN. The dorsal

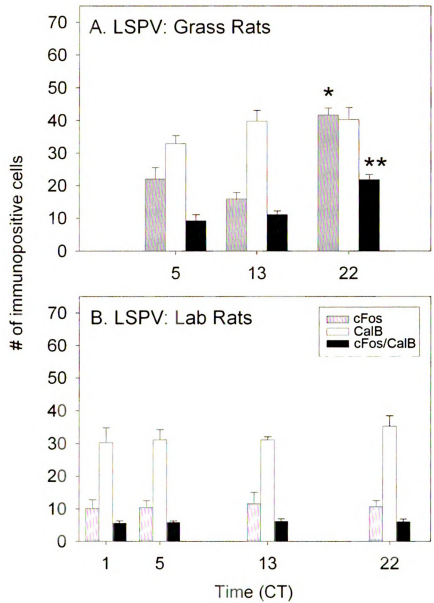

Figure 2.5: Counts of cells positive for cFos only (grey bars), CalB only (white bars), and cells positive for both cFos and CalB (black bars) in the LSPV of A) grass rats, B) lab rats, after 2-3 weeks in DD. Asterisks indicate time points where numbers of cFos-positive cells (*) or double-labeled cells (**) are significantly elevated relative to other time points, $p<.0001$.

boundary of the region containing VP-positive cells coincided almost perfectly with the dorsal boundary of the SCN as defined by Nissl in an alternate series (one section is shown in Fig. 2.1). VIP-positive neurons were concentrated in the ventral SCN, extending to the optic chiasm. The lateral edge of the VIP-positive cell-containing region corresponded to the lateral border of the SCN as defined by Nissl. Distributions of VP-ir and VIP-ir overlapped slightly along the medial and lateral edges of the SCN, but not along its dorsal or ventral regions. Neither VP- nor VIP-positive cells were found outside the boundaries of the SCN as defined by Nissl. VP-positive fibers extended dorsally from the SCN, and coursed dorsally and caudally to the PVN; VIP-positive fibers were present in approximately the same regions, but to a somewhat lesser extent. At ZT 22 few cFos-positive cells were observed within the SCN, whereas large numbers were seen dorsal and dorsolateral to the nucleus (Fig. 2.1, 2.6). Similarly, few cFos-positive cells were found either rostral to the SCN or caudal to it.

In tissue processed for cFos/CalB-ir from a grass rat perfused at ZT 22, a few cFos-positive nuclei were observed in the SCN as indicated by a blue-black reaction product (Fig. 2.7). CalB-positive cells were light brown, and both perikarya and fibers were visible within the SCN. CalB-positive cells were scattered evenly through the SCN from its rostral to its middle regions (Fig. 2.8). However, in the caudal SCN they were concentrated in a round subnucleus near the center of the SCN (Fig. 2.7b), as seen in the previous experiment. The distribution of CalB within the caudal SCN appears to be similar to that of gastrin-releasing peptide (GRP)-containing cells seen previously in the grass rat SCN

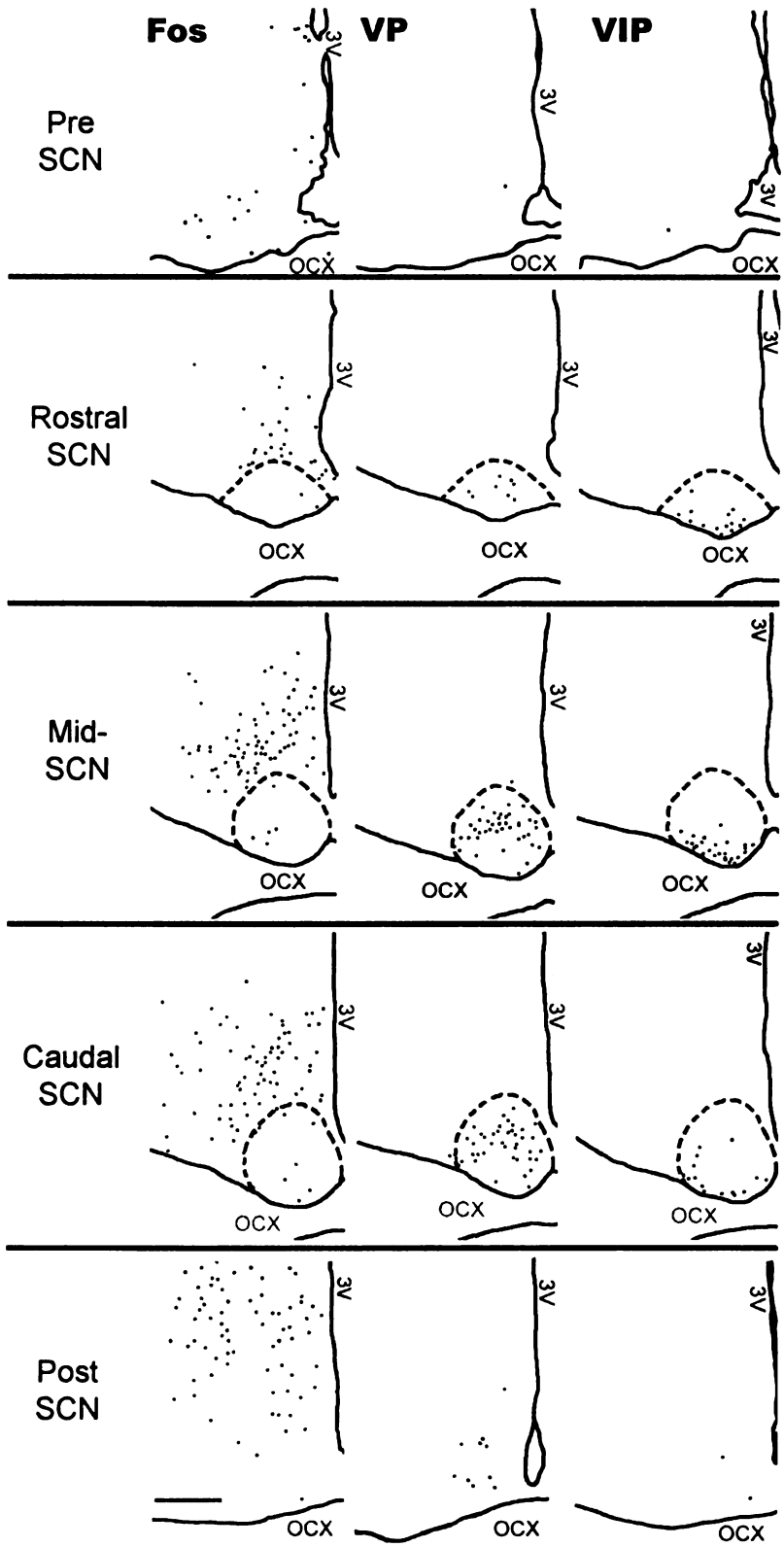

Figure 2.6: Distributions of AVP, VIP and cFos-ir through sections rostral to the SCN, in the SCN, and caudal to the SCN of a grass rat perfused at ZT 22. 3v: third ventricle; ocx: optic chiasm. Scale bar = 100 μm.

(Katona et al., 1998; Smale and Boverhof, 1999). The CalB-positive region of the caudal SCN was clearly separated from the LSPV by a more CalB-sparse zone around it (Fig. 2.7b).

LSPV: In a grass rat perfused at ZT 22, many cFos-positive nuclei were observed just dorsal and dorsolateral to the SCN (Fig. 2.6, 2.7a, 2.8). In the rostral-most sections, cFos-positive cells were located in the area immediately dorsal to the SCN. In more caudal sections, cFos-positive cells increased in density and spread out both dorsally and to a lesser extent laterally, such that in mid- and caudal sections cFos-positive cells were present from the periventricular hypothalamic nucleus (Pe) to the anterior hypothalamic area (AHA). cFos labeling was restricted to the area dorsal and dorsolateral to the SCN; few cFos-positive cells were visible directly lateral to the SCN at any rostrocaudal level (Fig. 2.6, 2.7a). The region containing the highest concentration of cFos-positive cells at ZT 22 was clearly outside the SCN as defined by Nissl stain, and did not overlap with either VP- or VIP-positive cell bodies (Fig. 2.1, 2.6).

In tissue processed for cFos/CalB-ir, the distribution of cFos-positive cells was very similar to that described above (Fig. 2.7a, 2.8). A large number of CalB-positive cells were interspersed with cFos-positive cells at all rostrocaudal levels of the LSPV. These CalB-positive cells extended dorsally and laterally from the outer boundaries of the SCN in a pattern similar to that of cFos-positive cells (Fig. 2.8). However, there were more CalB-positive than cFos-positive cells lateral to the SCN in caudal sections. CalB-positive cells in the LSPV were not

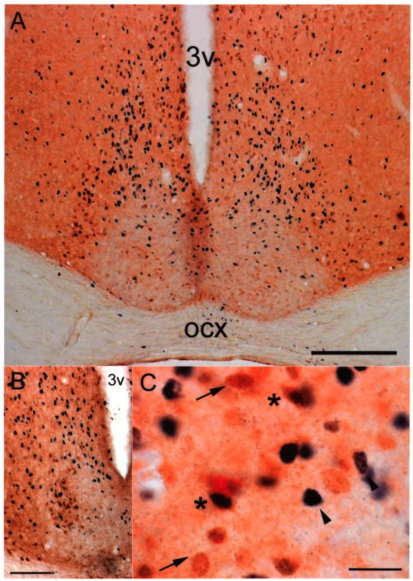

Fig. 2.7. (A) Photomicrograph of the SCN and LSPV of a grass rat perfused at ZT 22 showing the distributions of cFos and CalB-ir; scale bar? = 200 ? μm. (B) Detail of the caudal SCN in the same animal. The section pictured here is the one from which the map of cFos and CalB-ir in the caudal SCN are drawn in Fig. 2.8. Scale bar?= 200 ?μm. (C) Double-labeled cells in the LSPV of the same animal shown in (A) and (B) taken at 100x, showing cFos-ir (arrowheads), CalB-ir (arrows), and double-labeled cells (asterisks); scale bar?= 20 μm. ocx, optic chiasm; 3v, third ventricle.

densely packed in a nucleus, but were clearly more numerous in the LSPV than in the dorsal SCN, which contained little to no CalB-ir. While significant numbers of CalB-positive cells were observed in a subnucleus near the center of the caudal SCN (see above), this cell group was separated from the LSPV by a CalB-sparse zone around it. Double-labeled cells were easily identifiable at high power (Fig. 2.7c).

Discussion:

These experiments serve to expand on and clarify the species differences in cFos-ir rhythms in the LSPV reported earlier (Nunez et al., 1999). Our results establish that the daily rhythm in LSPV cFos-ir differs in grass rats and lab rats with respect to both its phase and its waveform, that both the SCN and LSPV cFos rhythms are endogenous in the diurnal grass rat, but not in the nocturnal lab rat, and that in grass rats the LSPV cFos rhythm is paralleled by a rhythm in CalB-ir within cFos-positive cells.

Neuroanatomy of the grass rat LSPV:

At a time of peak cFos-ir in the LSPV (as demonstrated in experiments 1 and 2), the distribution of cFos-ir did not overlap with the distributions of two peptides (VP and VIP) that clearly mark the boundaries of the SCN. Moreover, the distribution of cFos-ir was unambiguously outside the Nissl-defined border of the SCN. Thus, the cFos-positive LSPV region of grass rats that we sampled represents an area outside the conventional boundaries of the SCN. CalB-positive cells were numerous outside of the SCN, where their distribution overlapped with that of cFos-positive cells surrounding the SCN. While it is

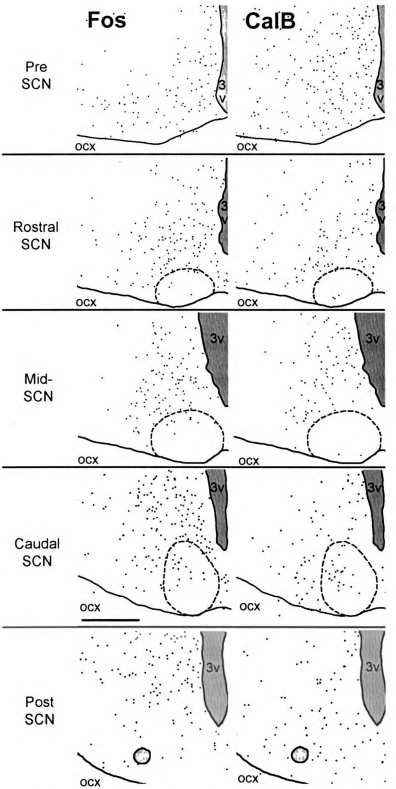

Figure 2.8: Distributions of cFos- and CalB-ir in the SCN and LSPV of a grass rat perfused at ZT 22. 3v: third ventricle; ocx: optic chiasm. Scale bar = 100 ?μm.

difficult to assign a discrete outer boundary of the LSPV based on these data, it may be thought of as the edge of a region dorsal and dorsolateral to the SCN that contains both CalB-positive cells and cells that express cFos in the late night. This region overlaps well with the distribution of VP and VIP-ir efferent fibers from the SCN that characterize the sPVZ in lab rats (Watts and Swanson, 1987; Watts et al., 1987; Watts, 1991) and grass rats (Smale and Boverhof, 1999). However, it is distinct from the perisuprachiasmatic region in that the overlap of cFos- and CalB-ir is markedly higher in the area dorsal to the SCN, than in the areas lateral, rostral or caudal to the SCN. The inner boundary of the LSPV is easier to identify than its outer boundary because it is delineated by the borders of the SCN, as defined by the VP cells of the nucleus or by Nissl stain. To summarize, the mapping data presented here clearly show that at ZT 22, cFos-ir in the region that we call the LSPV is outside the SCN. This cFos-ir occupies a region roughly dorsal to the SCN that corresponds to the ventral-most aspect of the sPVZ as defined in the lab rat by Watts and Swanson (1987) and Watts et al. (1987).

cFos rhythms in the SCN:

The daily cFos rhythm in the SCN was fundamentally similar in grass rats and lab rats kept in a 12:12 LD cycle, with a peak early in the light phase, at ZT 1, followed by a decline to levels that remained low through the dark phase. However, in grass rats cFos did not decline until after ZT 5, whereas in lab rats it had already dropped to basal levels by that time. Although previous studies of cFos in the SCN of grass rats (Katona et al., 1998; Nunez et al., 1999) and lab

rats (Nunez et al., 1999) have found varying results at ZT 5, all reveal elevated cFos expression in the SCN of both species in the hour after light onset, followed by decreases from the light to the dark phase of the cycle. A rapid decline in cFos expression circa ZT 5 could be responsible for the differences between experiments.

After 2-3 weeks in DD, grass rats, but not lab rats, displayed a robust endogenous cFos rhythm in the SCN very similar to that seen in LD. In grass rats, this cFos-ir was not restricted to regions of the SCN defined by a particular neuronal phenotype (i.e. CalB, VP, VIP). The lack of cFos/CalB double-labeling in the grass rat SCN indicates that the cFos rhythm was specifically outside of the CalB-positive subpopulation of cells. The high levels of cFos expression during the subjective day (CT 5) seen here in the SCN of grass rats was not detected in a previous study in which grass rats were sampled at CT 6 after only 24 hours in DD (Mahoney et al., 2001). The difference between the two studies could reflect the emergence of a rhythm following extended periods in DD. Alternatively, cFos may have been low at CT 6 in the study of Mahoney et al (2001), and high at CT 5 in the current study, because cFos declines rapidly around this time (see above).

In lab rats, we observed no effect of time on cFos-ir in the SCN after 2 weeks in DD. In contrast, several reports have described an endogenous rhythm in *cfos* mRNA (Guido et al., 1999a; Schwartz et al., 2000) and protein (Sumova et al., 1998; Guido et al., 1999a; Schwartz et al., 2000; Beaule et al., 2001) in the dorsomedial SCN of lab rats as well as hamsters (Guido et al., 1999b).

Differences in the time points chosen for sampling (between 4-24 time points in a 24-hour period), and/or the duration of exposure to DD (2 days or less in earlier studies, versus 2 weeks in the present study) may account for the divergent findings. To our knowledge, this is the first report examining spontaneous cFos expression in the SCN of either lab rats or a diurnal species after more than 5 days in DD. More work is needed to determine the functional implications of this species difference in SCN cFos expression.

cFos rhythms in the LSPV:

In 12:12 LD, there were clear species differences in the daily cFos rhythm in the LSPV. In grass rats the rising phase of the rhythm in the LSPV was out of phase with that of the SCN rhythm (in grass rats), and with rhythms in both regions in lab rats. In an earlier study, grass rats kept in LD exhibited increased cFos-ir in the LSPV at ZT 16 relative to ZT 4 (Smale et al., 2001), but in another this trend did not reach statistical significance (Mahoney et al., 2000). Thus, the rising phase of Fos in the LSPV may occur rapidly between ZT 16-17 in the grass rat. The cFos rhythm in the LSPV differed not only with respect to the phase of the rise but also its waveform, in that cFos remained elevated considerably longer in grass rats than in lab rats. The divergent patterns of cFos-ir in the LSPV of these species may therefore reflect two distinct processes, one promoting an increase in cFos expression and another promoting its maintenance. The cFos rhythm in the grass rat LSPV also differs from that of lab rats in that it is clearly endogenous, as it persisted for 3 weeks in DD without a reduction in amplitude. These species differences in both the phase and the

dependence on light of the cFos rhythm suggest a functional role for the grass rat LSPV that is distinct from that of the lab rat.

In addition to the rhythm in single-labeled cFos-positive cells, a parallel rhythm in numbers of CalB-positive cells containing cFos was evident in the LSPV of grass rats kept in DD. Interestingly, a sizable proportion of the total CalB cells in the LSPV did not contain Fos, and the numbers of CalB cells without cFos did not change over time. Thus, there seem to be two distinct populations of CalB-positive cells in the LSPV: one that does not change with respect to either CalB or cFos expression, and another in which both CalB and cFos expression increase from CT 5 to CT 22.

The functional significance of CalB in either the SCN or the LSPV of the grass rat is unclear at present. In hamsters, a CalB-positive SCN subnucleus is essential for maintenance of circadian locomotor rhythms (LeSauter and Silver, 1999). In that species, cells in this region are both responsive to light (Silver et al., 1996b) and extensively interconnected with cells in other subregions in the SCN (LeSauter et al., 2002; Jobst et al., 2004). Although the CalB cells themselves do not exhibit a spontaneous daily rhythm in firing rate (Jobst and Allen, 2002) or cFos expression (Silver et al., 1996b), the distribution of CalB in the cell nucleus relative to the cytoplasm is rhythmic (Hamada et al., 2003). Furthermore, treatment with antisense to CalB causes time-dependent changes in light-dependent *per1* induction in the SCN and light-induced behavioral phase shifts (Hamada et al., 2003). Thus, in at least one nocturnal species, CalB-positive cells in the SCN contribute in a crucial way to the regulation of circadian

rhythms in the SCN and in behavior. Whether CalB-positive cells inside or above the SCN of the grass rat are necessary for circadian rhythms, or similarly organized in terms of function, remains to be determined.

In lab rats, cFos-ir in the LSPV was not rhythmic after 2 weeks in DD, revealing a second species difference in the pattern of cFos expression in this region. Spontaneous rhythms in multiple-unit activity in the region surrounding the SCN (including but not limited to the LSPV) persist in blinded rats kept in DD (Inouye and Kawamura, 1979). A lack of rhythmicity in cFos-ir, then, may not reflect a total loss of rhythmic neural activity in the region. For example, in lab rats, MUA rhythms in the area around the SCN could be driven by the SCN and thus persist in the absence of photic input, whereas cFos rhythms may be dependent on light. In grass rats, however, cFos rhythms in the LSPV are endogenous. The species differences in both the phase of the LSPV cFos rhythm and its dependence on light suggest that the function of the cFos rhythm, and possibly the LSPV itself, is very different in these two species.

The only other data available comparing daily rhythms within and adjacent to the SCN of diurnal animals comes from MUA records. In the diurnal Siberian chipmunk, MUA outside the SCN peaked during the day and was low at night (Sato and Kawamura, 1984b), whereas in lab rats, MUA outside the SCN peaked at night and was low during the day (Inouye and Kawamura, 1979). Thus, daily rhythms in MUA outside the SCN were reversed in a diurnal species relative to a nocturnal one, and in the nocturnal species the rhythms outside the SCN were reversed relative to those in the SCN. In the present study of cFos, rhythms in

the LSPV also differed in a diurnal species relative to a nocturnal one, but in this case it was the diurnal species in which these rhythms were out of phase with those in the SCN. Thus, MUA rhythms in diurnal Siberian chipmunks and cFos rhythms in diurnal grass rats were not in phase with each other. This may reflect a basic species difference in the region, or perhaps cFos-ir does not reflect the same type of activity as MUA. In either case, these species differences in the area around the SCN, contrasted with the similarities seen within the SCN, are consistent with the hypothesis that differences between nocturnal and diurnal species may arise from direct targets of the SCN, or from SCN cells that project to these targets.

Conclusions:

The precise function of either the LSPV, or the sPVZ, in either a diurnal or nocturnal species has not been firmly established, but seems likely to be closely tied in with the circadian system. In lab rats, anterograde and retrograde tract tracing revealed that the sPVZ projects to almost all of the same targets as the SCN, but to a greater degree (Watts and Swanson, 1987; Watts et al., 1987), leading the authors to suggest that the sPVZ might modulate SCN output signals (Watts and Swanson, 1987; Watts, 1991). Several lines of evidence suggest that the sPVZ may be involved in the timing of estrus-related events in lab rats (Nunez and Stephan, 1977; Arendash and Gallo, 1979; Docke et al., 1982; Watts et al., 1989; van der Beek et al., 1997b; Fernandez-Galaz et al., 1999). The sPVZ may also be involved in the regulation of circadian locomotor rhythms in lab rats (Lu et al., 2001; Moore and Danchenko, 2002), although if this is the

case, fibers projecting from the SCN to the sPVZ are probably not necessary for this (Brown and Nunez, 1986; Watts et al., 1989). It should be noted furthermore that these studies considered the sPVZ as a whole, and that similar manipulations targeting the LSPV more specifically could yield different results. Although many questions remain, it appears that the sPVZ in lab rats is involved with a subset of the SCN's output, and may in addition help integrate this information with other factors such as hormonal state to organize timing of estrus-related neuroendocrine events and behaviors. If so, then a near-reversal in the rhythmic activity in the region, as indicated by cFos-ir, could be part of a mechanism mediating differences in the timing of expressed circadian rhythms in nocturnal and diurnal species. In lab rats, in which a nocturnal pattern of behavior is expressed, rhythmic cFos expression in the LSPV is either in phase with the SCN (LD) or nonexistent (DD). In grass rats, however, the 8-hour difference in the rising phase of the daily cFos rhythms in the LSPV as compared to the SCN could reflect a mechanism promoting a diurnal pattern of behavioral and physiological rhythms. For example, neurons in the grass rat LSPV could receive rhythmic signals from the SCN, transform those signals, and then transmit them to downstream targets. More work is needed to determine if and how the LSPV may modulate the outputs of the SCN in diurnal and nocturnal species.

In conclusion, the LSPV of the grass rat, a region that receives substantial input from the SCN, displays a daily rhythm in cFos expression that differs from that of lab rats with respect to 1) its rising phase, 2) the duration of the peak, 3)

its phase relationship relative to cFos rhythms in the SCN, and 4) its dependence on a LD cycle. Furthermore, an endogenous rhythm in CalB expression within cFos-positive cells parallels that of cFos in the LSPV of grass rats, but not lab rats. Cellular processes mediated by cFos and CalB, such as gene expression and calcium regulation, are likely to be timed very differently in the LSPV of these two species. These data may reflect a species difference in the mechanisms whereby efferent signals from the SCN are coupled to their downstream targets. It is tempting to speculate that differences in this coupling could lead to the dramatic differences in daily rhythms in physiology and behavior seen between diurnal and nocturnal rodents.

CHAPTER 3

Efferent projections of the suprachiasmatic nucleus and lower subparaventricular zone in the Nile grass rat *(Arvicanthis niloticus)*

Introduction

Diurnal and nocturnal species display marked differences in a host of behavioral and physiological rhythms. The hypothalamic suprachiasmatic nucleus (SCN) houses the central circadian pacemaker in mammals (Weaver, 1998), but the phase of rhythms that have been examined in the SCN appears similar in diurnal and nocturnal species. This is the case for daily rhythms of multiple-unit activity (Kubota et al., 1981; Sato and Kawamura, 1984b; Kurumiya and Kawamura, 1988), 2-deoxyglucose uptake (Schwartz, 1991) and clock gene expression (Hastings et al., 1999; Mrosovsky et al., 2001; Yan and Okamura, 2002; Caldelas et al., 2003; Ramanathan et al., 2006), as well as for rhythms in mRNA for the clock-controlled genes prokineticin 2 (Cheng et al., 2002; Lambert et al., 2005) and vasopressin (Dardente et al., 2004). While differences between day- and night-active species could result from unidentified processes or cells within the SCN, they are more likely to arise from processes occurring downstream of the SCN.

One region that could play an important role in such a process is the hypothalamic subparaventricular zone (sPVZ). The sPVZ extends dorsally and caudally from the SCN to the ventral edge of the hypothalamic paraventricular

nucleus (Watts, 1991; Saper et al., 2005), and is a major target of the SCN in the nocturnal laboratory rat (Watts and Swanson, 1987; Watts et al., 1987; Moore and Leak, 2001), mouse (Abrahamson and Moore, 2001) and hamster (Morin et al., 1994; Orpen and Steiner, 1994; Kriegsfeld et al.). The sPVZ in turn projects to many of the same efferent targets as the SCN in lab rats (Watts and Swanson, 1987; Watts et al., 1987) and hamsters (Morin et al., 1994; Orpen and Steiner, 1994). Daily rhythms in cFos expression in the lower part of the subparaventricular zone (LSPV) are dramatically different in diurnal Nile grass rats and nocturnal lab rats (Nunez et al., 1999; Schwartz et al., 2004), and daily rhythms in multiple-unit activity adjacent to the SCN are reversed in diurnal Siberian chipmunks compared to nocturnal lab rats (Inouye and Kawamura, 1979; Sato and Kawamura, 1984b). The grass rat LSPV also displays daily rhythms in immunoreactivity for calbindin and for the clock gene products Per1 and Per2 (Schwartz et al., 2004; Ramanathan et al., 2006). Thus, this region may have functional characteristics that would enable it to modulate circadian timing signals originating in the SCN, and to do that differently in diurnal and nocturnal animals (Watts, 1991; Schwartz et al., 2004; Saper et al., 2005). If this is the case, then signals from the LSPV should interact with those from the SCN either at, or downstream of, SCN targets. The projections of the SCN and LSPV, however, have not yet been described in a diurnal species.

In the present study, we have mapped the efferent projections of the grass rat SCN and LSPV using the anterograde tract tracer biotinylated dextran amine (BDA), and compared the distributions of fibers from these two areas. We report

that the efferent projections of the SCN and LSPV are quite similar to those reported for nocturnal species, with projections extending through the diencephalon, and the densest innervation in a relatively small subset of midline hypothalamic and thalamic nuclei. Taken together with reports from nocturnal species, these data suggest that the efferent neuroanatomy of the SCN and LSPV is highly conserved in rodents, and that the LSPV has projections that may enable it to modulate the responsiveness of target cells to signals coming from the SCN.

Experimental Procedures

Animals:

Adult female grass rats obtained from a breeding colony at Michigan State University (Katona and Smale, 1997) were singly housed in Plexiglas cages (34 x 28 x 17 cm) with access to food (PMI Nutrition Prolab RMH 2000, Brentwood, MO) and water *ad libitum*. Animals were kept in a 12:12 light: dark cycle; a red light (<5 lux) remained on constantly for animal care purposes. All experiments were performed in compliance with guidelines established by the Michigan State University All-University Committee on Animals Use and Care, and the NIH Guide for the Care and Use of Laboratory Animals.

Surgical procedures and tissue processing:

All animals received a unilateral iontophoretic injection of 10,000 MW BDA (Molecular Probes; Eugene, OR) directed at the SCN or LSPV. Animals were deeply anesthetized with sodium pentobarbital (50mg/kg i.p.) prior to surgery, and then the head was shaved, wiped with betadine, and injected with lidocaine

(0.03cc s.c.). The animal was then placed into a stereotaxic apparatus (Stoelting Co.; Wood Dale, IL) with the incisor bar set to -6.0 mm and the micropipette set at an angle of 10 degrees, and a 1-2 cm incision was made in the scalp to expose the skull. Final injection coordinates were: 1.4 mm anterior to bregma, 1.2 mm lateral to bregma, and 6.3 mm ventral to dura. A small hole was drilled in the skull, and dura was gently broken to allow uninterrupted passage of the micropipette. A glass micropipette (WPI; Sarasota, FL) with inner tip diameter of 10-15 μm was then filled with 10% BDA in 0.01 M phosphate-buffered saline (PBS; pH 7.4) and lowered slowly to injection depth. Injections were made under 5 mA positive alternating current at a rate of 7 seconds on/ 7 seconds off, for 7 minutes, followed by a 7-minute rest period. Micropipettes were then withdrawn slowly under negative current. The incision was closed with autoclips, and animals were given 0.06 cc buprenorphine i.m. and 1.0 cc sterile saline s.c. Seven days later, animals were given an overdose of sodium pentobarbital and perfused transcardially with 0.01M phosphate-buffered saline (PBS), pH 7.2, followed by 4% paraformaldehyde (Sigma, St. Louis, MO) in 0.1M phosphate buffer. Brains were post-fixed for 4 hours, then transferred to 20% sucrose solution overnight. Brains were sectioned coronally at 30 µm on a freezing microtome into 3 series of sections, which were then stored in cryoprotectant at -20°C until processing began.

One series of free-floating sections were rinsed 3 x 10 minutes in PBS at room temperature, and then incubated in avidin-biotin peroxidase complex (ABC Vectastain Kit, Vector Laboratories, Burlingame, CA). Protein was visualized by

reacting with diaminobenzidine (0.5mg/mL; Sigma) in Trizma buffer (Sigma) enhanced with nickel sulfate. Tissue was mounted, dehydrated, and coverslipped with Permount. An alternate series from each animal with a successful injection was reacted as above, mounted and counterstained with neutral red to assist in mapping brain regions. Injections were considered successful if they were isolated to either the SCN or the LSPV, with no spread to the other area. Data presented come from 2 injections localized to the SCN and 4 injections localized to the LSPV (Fig. 3.1).

Microscopy:

Sections were analyzed on a Zeiss Axioskop microscope (Zeiss, Germany) under brightfield illumination, and all photomicrographs were taken using a Zeiss Axiocam MR (Zeiss) and processed in Adobe Photoshop 7.0 (Adobe Systems; Mountain View, CA). Labeled fibers were mapped from two representative cases (SCN: # 74, LSPV: # 34), using selected sections through the hypothalamus. For each single-labeled (i.e. non-counterstained) section, a series of photomicrographs was taken at 10x and combined in Photoshop to form a composite photomicrograph of the section. Images were adjusted for sharpness, brightness and contrast. BDA-ir fibers were traced in Photoshop using a drawing pad (Wacom; Vancouver, WA). Although BDA can be carried in a retrograde direction (Reiner et al., 2000), we saw very few BDA-ir cell bodies that were not associated with the injection sites in each of the cases analyzed. All anatomical landmarks and nuclear boundaries were drawn based on comparison between neutral-red counterstained and single-labeled sections in

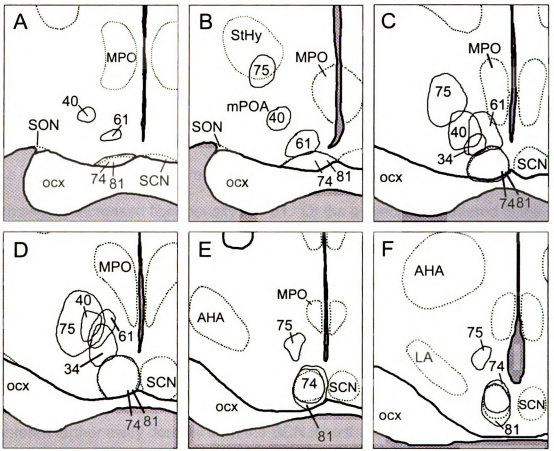

Figure 3.1: Line drawings depicting the location of biotinylated dextran amine (BDA) injections in all cases described in the present study. See page *xv-xvi* for abbreviations.

the representative cases. The map of the injection sites was prepared in Photoshop using # 74 as a template, with outlines of injection sites for other cases traced in.

Results

Injection sites:

Both of the injections centered in the SCN filled the entire SCN (Fig. 3.1). However, injection spread in # 74 was limited to the boundaries of the SCN, whereas # 81 included a small amount of spread into the retrochiasmatic area. The distribution of BDA-labeled fibers in these two cases was overall very similar, with slightly increased fiber density in # 81. Of the 4 injections centered in the LSPV (Fig. 3.1), cases 34 and 61 were the most similar with respect to placement, extending up to 400 μm from the dorsal and dorsolateral edges of the mid- to caudal SCN. They were also similar with respect to the distribution of labeled fibers. Case 40 was centered slightly more rostrally than # 34 and # 61, but overlapped with both of these injections at their centers. Case 75 was centered farther away dorsally from the SCN than the other 3 cases, and was similar to # 40 in its rostrocaudal placement. Fiber distributions of these two cases were very similar to each other, and while generally similar to those of # 34 and # 61, exhibited some important differences. Of these 4, # 34 was the smallest injection and # 75 the largest. None of the 4 injections centered in the LSPV labeled cells in the SCN as revealed by neutral red counterstaining in alternate sections. Cases 74 and 34 will be described in detail as representative

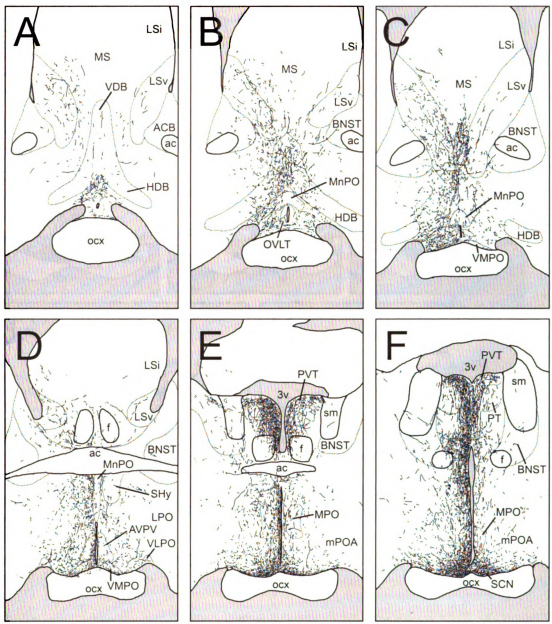

Figure 3.2: Line drawings depicting the distribution of BDA- labeled fibers following an injection centered in the suprachiasmatic nucleus (SCN; case 74). Panels are arranged rostral-to-caudal, and were traced from sections as described in text. See page *xv-xvi* for abbreviations.

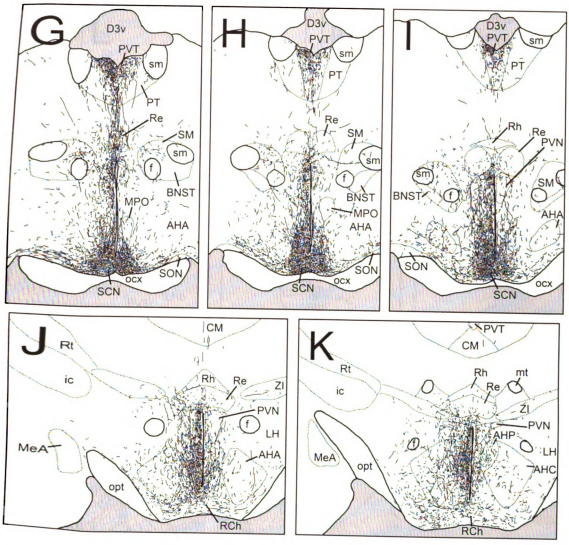

Figure 3.2 (continued).

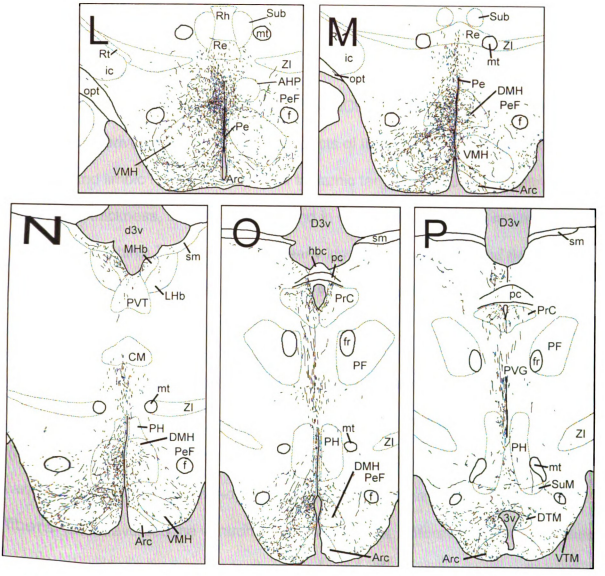

Figure 3.2 (continued).

hits in the SCN and LSPV respectively, with descriptions of the other cases included when they differ.

Injections centered in the SCN:

Following injections centered in the SCN, BDA-labeled fibers were most dense in periventricular and medial aspects of the hypothalamus, parts of the basal and limbic forebrain, and a few thalamic targets (Fig. 3.2). Fibers were of variable thickness, usually varicose, and in most cases exhibited moderate to heavy branching. This pattern was nearly identical in cases 74 and 81, with slightly increased fiber density overall in # 81 compared to # 74.

Rostral Paths:

Rostrally-directed fibers from the SCN were organized in two pathways. The first coursed ventrally along the ocx through the medial preoptic area (mPOA), terminating in the diagonal band of Broca and the vascular organ of the lamina terminalis (Fig. 3.2a-d). This pathway included a dense group of thick fibers that traversed the ventromedial preoptic area, anteroventral periventricular nucleus and medial preoptic nucleus, and more diffuse, mixed-caliber fibers that innervated more dorsal parts of the mPOA (Fig. 3.2c-d). The ventrolateral and lateral preoptic areas were lightly innervated. Rostral to the mPOA, thin fibers branched laterally and dorsally to innervate the vertical and horizontal diagonal band, with many fibers terminating in and around the vascular organ of the lamina terminalis (Fig. 3.3a). Few fibers were observed rostral to the vascular organ.

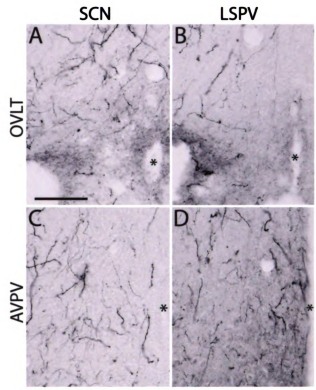

Figure 3.3: Photomicrographs of BDA- labeled fibers in the vascular organ of the lamina terminalis (OVLT; A, B) and anteroventral periventricular nucleus (AVPV; C, D) of cases 74 (A, C) and 61 (B, D). * = 3rd ventricle. Scale bar = 100 µm.

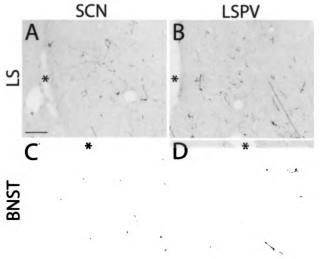

Figure 3.4: Photomicrographs of BDA- labeled fibers in the lateral septum (LS; A,B) and bed nuclei of the stria terminalis (BNST; C,D) of cases 74 (A,C) and 61 (B, D). * = lateral ventricle. Scale bar = 100 µm.

The second rostrally-directed pathway ran more dorsally through the hypothalamic periventricular nucleus and medial preoptic nucleus, then continued rostrally and laterally into the septal region (Fig. 3.2a-e). These rostrally-directed fibers coursed under and around the edge of the anterior commissure to innervate more dorsal and lateral aspects of the mPOA and the medial septum before terminating in the ventral and, to a lesser extent, the intermediate lateral septum (Fig. 3.4a). These fibers were thin, and once past the anterior commissure became very straight with few branches or varicosities. Once in the lateral septum, however, abundant branching, varicosities and terminals were observed.

Midline thalamic paths:

Dorsally-projecting fibers also continued caudal to the anterior commissure to densely innervate the anterior paraventricular thalamus (PVT), the parataenial nucleus, and, to a lesser extent, medial aspects of the bed nuclei of the stria terminalis (Fig. 3.2e-g). More fibers were present in medial divisions of the bed nuclei in # 81 than in # 74, and neither case exhibited fibers in the oval nucleus of the bed nuclei (Fig. 3.4c). A moderate number of fibers branched dorsal to the third ventricle to innervate the contralateral PVT. Some of these fibers also continued caudally to innervate the mid- and posterior PVT; however, fibers were far more dense in the anterior PVT than more caudal aspects of the nucleus. At all levels of the PVT, fibers were visible along the ependymal wall lining the dorsal third ventricle (Fig. 3.5a).

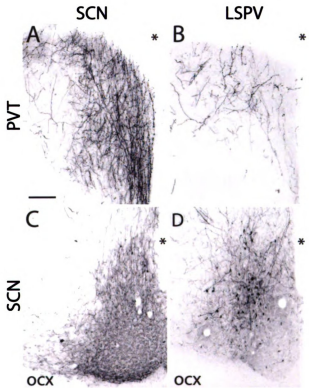

Figure 3.5: Photomicrographs of BDA- labeled fibers in the paraventricular thalamic nucleus (PVT; A, B) and the centers of the injection sites (C, D) of cases 74 (A, C) and 61 (B, D). * = 3rd ventricle. Scale bar = 100 µm.

Lateral Path:

A moderate to dense plexus of fibers exited the SCN and coursed laterally along the optic chiasm to the supraoptic nucleus. The majority of these fibers either terminated just outside the supraoptic nucleus or continued rostrally, although some fibers did enter the supraoptic nucleus. A few fibers followed the optic tract from the SCN to the ventral lateral geniculate nucleus and intergeniculate leaflet (IGL). These fibers were thin, largely without varicosities or branches, and appeared sparse as they coursed along the optic tract and through the ventral lateral geniculate. However, the terminal field in the IGL was quite robust (Fig. 3.6a). Fibers within the IGL were thin and spindly in appearance, with clear terminal morphology on the ipsilateral and contralateral IGL. This path was the most bilateral of all the paths; fiber density in the IGL was nearly equal on the two sides of the brain. A few sparse fibers were seen in the amygdala close to the optic tract in # 81 but not in # 74; these were localized to the medial amygdalar nucleus and its immediate vicinity.

Caudal paths:

Caudally-directed fibers from the SCN were organized into two pathways. The first and most dense of these was in the sPVZ, particularly the area immediately dorsal to the SCN which we have previously described as the LSPV (Fig. 3.2g-k; Schwartz et al., 2004). Branching and terminals were evident immediately as these fibers exited the SCN such that the entire region surrounding the SCN was moderately innervated with thin and thick fibers. The

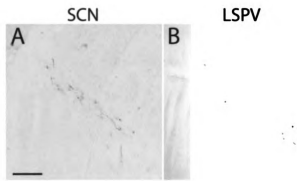

Figure 3.6: Photomicrographs of BDA- labeled fibers in the intergeniculate leaflet of cases 74 (A) and 34 (B). Scale bar = 100 µm.

distribution of these fibers overlapped almost completely with that of cFos and calbindin-positive cells previously reported in the grass rat LSPV (Schwartz et al., 2004), and fiber density in the LSPV (dorsal to the SCN) was noticeably greater than in the area lateral to the SCN (Fig. 3.5c). This plexus of fibers continued dorsocaudally to innervate the dorsal sPVZ, the PVN (Fig. 3.2i-k), and the dorsomedial hypothalamic nucleus (DMH; Fig. 3.2m-p). While many fibers terminated in the sPVZ just ventral to the PVN, many were also evident within periventricular and dorsal parvocellular compartments of the PVN, with fewer in the medial parvocellular compartments and only sparse fibers in the magnocellular subnuclei (Fig. 3.8a, 3.8c). A few fibers continued past the PVN dorsally as far as the Reuniens nucleus and medial zona incerta (Fig. 3.2j-k). Caudal to the sPVZ and PVN, labeled fibers surrounded the area dorsal and medial to the ventromedial hypothalamic nucleus, with some fibers penetrating the nucleus itself (Fig. 3.2l-n). These fibers were thin and twisted, with many terminals and moderate branching (Fig. 3.9a, 3.9c). All parts of the DMH were innervated, though fibers were particularly concentrated in the pars compacta of the DMH, with fewer fibers in other subregions (Fig. 3.2n-o; Fig 3.8e, 3.8g). Dorsal to the DMH, thin spindle-like fibers ran dorsocaudally through the periventricular gray to the habenula and precommissural nucleus (Fig. 3.2n-p). Caudal to the DMH, a plexus of fibers that was sparse to moderately dense was observed in the dorsal tuberomammillary nucleus, with some of these fibers continuing caudally to innervate the supramammillary nucleus.

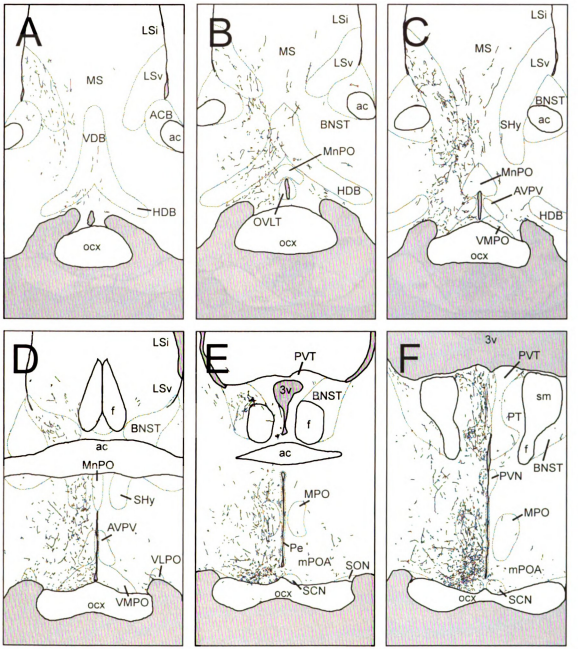

Figure 3.7: Line drawings depicting the distribution of BDA- labeled fibers following an injection centered in the lower subparaventricular zone (LSPV; case 34). Panels are arranged rostral-to-caudal, and were traced from sections as described in text. See page *x-xii* for abbreviations.

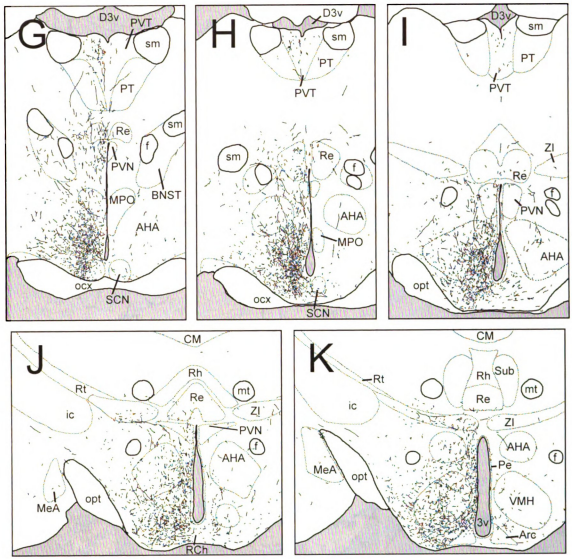

Figure 3.7 (continued).

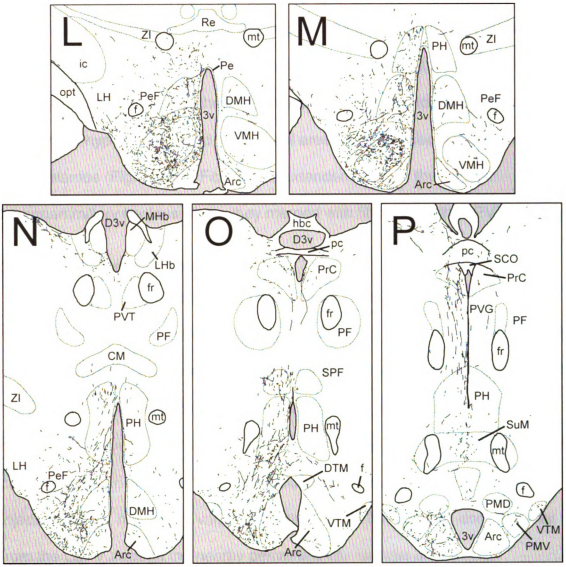

Figure 3.7 (continued).

The final fiber pathway projected caudally through the retrochiasmatic area to innervate more ventral and ventrolateral aspects of the hypothalamus. These fibers spread throughout the ventral tuberal region of the hypothalamus, providing moderate input to the ventromedial nucleus, low-to-moderate input to the anterior hypothalamic and perifornical areas, and few fibers in the lateral hypothalamus (Fig. 3.2l-o). Fibers also extended towards the dorsal tubermammillary nucleus where they merged with fibers from the sPVZ pathway.

Injections centered in the LSPV:

The distribution of BDA-ir fibers following injections into the LSPV was quite similar to that described following injections into the SCN. However, LSPV efferents tended to be more evenly distributed along the medial-lateral axis of the hypothalamus than were SCN efferents, which were more concentrated in the medial and periventricular zones. LSPV fibers, like SCN fibers, were of variable caliber, often varicose, and displayed frequent branching. Proximal to the injection center, many thin, varicose fibers radiated dorsally and dorsolaterally from the LSPV through the nearby periventricular nucleus and anterior hypothalamic area. Very few fibers penetrated the SCN, and these were restricted to the area closest to the injection site (Fig. 3.5d). Sparse fibers were also visible in the ependymal layer near the SCN, as well as in the contralateral LSPV.

Rostral paths:

Anterior to the SCN, fibers extended rostrally from the LSPV along the ocx to innervate the ventromedial preoptic area and the anteroventral periventricular

nucleus (Fig. 3.7a-d), and to a lesser extent the ventrolateral preoptic area and the vascular organ of the lamina terminalis. Fibers also lined and entered the ependymal wall of the third ventricle around the anteroventral periventricular nucleus (Fig. 3.3b, 3.4d). While this was still a substantial projection, the fibers were thinner and fewer in overall number than those seen after SCN injections.

A larger fiber plexus radiated dorsolaterally from the LSPV through the mPOA. These fibers spread out from the midline at more rostral levels to provide a diffuse input to an area extending from the basal forebrain and diagonal band of Broca to the lateral septum (Fig. 3.7b-c). The medial septum was most heavily innervated close to the anterior commissure, and in # 34 more fibers were seen at the ventricular edges of the lateral septum than in all other cases. Fibers were denser in the horizontal than the vertical limb of the diagonal band in # 34 and # 40, whereas in # 61 and # 75 the inputs to the two limbs were similar. While the septum was also heavily innervated by the SCN, in general the LSPV projection along this path was more dense than that of the SCN (Fig. 3.4a-b).

Midline thalamic paths:

A third major fiber plexus ran dorsally from the LSPV to the PVT and, to a lesser extent, the anterior aspects of the parataenial and Reuniens nuclei (Fig. 3.7f-g). These fibers were longer and thinner than those emanating from the SCN, branched significantly and had many boutons and terminals. As they did following injections into the SCN, labeled fibers in the PVT entered the ependymal layer, sometimes contacting the dorsal third ventricle (Fig. 3.5b). Fibers also extended into the bed nuclei of the stria terminalis just anterior to the

PVT, innervating medial aspects and avoiding the oval nucleus (Fig.7e). Whereas fibers in the PVT were somewhat less dense than those seen following injections of the tracer into the SCN, labeled fibers in the bed nuclei were slightly more dense following injections into the LSPV (Fig. 3.4c-d).

Lateral paths:

A small group of fibers coursed along the optic chiasm laterally from the SCN to lightly innervate the supraoptic nucleus (Fig. 3.7g). Some of these fibers continued to follow the optic tract, and entered the amygdala. In cases 34 and 61, where injections were centered squarely in the LSPV, fiber density in the amygdala was sparse, whereas more rostral injections (# 40 and # 75) resulted in greater numbers of labeled fibers. The medial amygdalar nucleus was the only part of the amygdala with BDA-ir fibers in all 4 cases of injections into the LSPV. Because the increased innervation of the amygdala was associated with more rostrally-centered injections, it seems likely that some of these fibers originated in the caudal preoptic area or anterior hypothalamus rather than the LSPV.

In cases 34 and 75, a few sparsely-distributed fibers were visible in the IGL (Fig. 3.6b), but none were observed in # 40 and # 61. Given the similarity in location of injections 34 and 61, and the fact that the larger injection of the two (# 61) did not label fibers in the IGL, it is not possible to confirm a projection from the LSPV to the IGL. However, the injection site for # 34 and # 75 extended slightly further laterally than those of # 61 and # 40, so the fibers seen in # 34

and # 75 could have arisen from this region. Further studies will be necessary to verify the location of neurons in and around the SCN that project to the IGL.

Caudal paths:

Caudal to the SCN, fibers from the LSPV coursed along two pathways. The majority of these efferents extended dorsocaudally through the sPVZ, with some fibers terminating ventral to the PVN and others continuing into the nucleus (Fig. 3.7h-j). Although some fibers were present in the periventricular subregion, the most substantial input from the LSPV was in the caudal parvocellular subregion (Fig. 3.8b), where fibers spread out laterally, generally avoiding magnocellular cell bodies. Innervation of the medial zona incerta was more dense, and the Reuniens nucleus less dense, than that seen following SCN injections (Fig. 3.7j-l). These fibers were far more extensive in cases 61 and 75 than in # 34, whereas in # 40 no fibers were seen in the zona incerta or dorsal to the PVN, and magnocellular paraventricular neurons were heavily interweaved by BDA-ir fibers, suggesting that projections from the area just rostral to the LSPV are very different from those of the LSPV itself. The perifornical region was sparsely- to moderately innervated by fibers that extended caudally and laterally from the sPVZ, PVN and zona incerta in # 34 and # 61 (Fig. 3.7l-n), while in # 40 and # 75, fibers were dense in the perifornical region. In the DMH, the overall density of labeled fibers was lower after injections into the LSPV than the SCN, but fiber density increased in the pars compacta region as was noted for SCN efferents (Fig. 3.7l-n, Fig. 3.8e-h). From this point, fibers continued

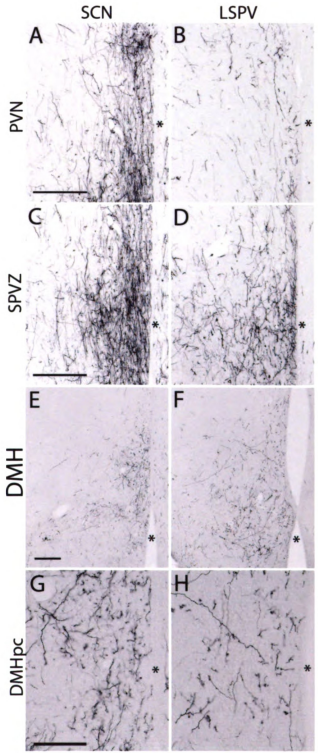

Figure 3.8: Photomicrographs of BDA- labeled fibers in the paraventricular hypothalamic nucleus (PVN; A, B), dorsal subparaventricular zone (SPVZ; C, D), and dorsomedial hypothalamic nucleus (DMH; E-H) of cases 74 (A, C, E, G) and 61 (B, D, F, H). A detail of the DMH pars compacta (DMHpc) is pictured in panels G and H. * = 3rd ventricle. Scale bar = 200 µm (A-F), 100 µm (G, H).

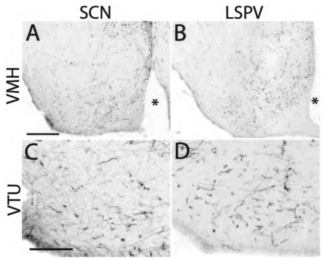

Figure 3.9: Photomicrographs of BDA- labeled fibers in the ventromedial hypothalamic nucleus(VMH; A,B) and adjacent ventral tuberal region (VTU; C,D) of cases 74 (A,C) and 34 (B,D). * = 3rd ventricle. Scale bar = 300 µm (A, B), 100 µm (C, D).

dorsally and caudally past the DMH to innervate the posterior hypothalamic area, subparafascicular nucleus and periventricular gray (Fig. 3.7n-o), eventually reaching the habenula and precommissural nucleus. Fibers were thin and straight until the precommissural nucleus where they branched and terminated.

A ventral group of fibers proceeded caudally from the LSPV along the basal edge of the hypothalamus to innervate the retrochiasmatic area, as well as ventral and lateral aspects of the anterior hypothalamic area (Fig. 3.7i-j); labeled fibers were relatively diffuse in these regions. These fibers eventually surrounded and entered the ventromedial hypothalamic nucleus and the ventral tuberal region lateral to it (Fig. 3.7l-n). Fibers were thin, often short, with numerous branches and boutons. These fibers also provided input to the perifornical region and the DMH. In contrast to the SCN efferents, LSPV fibers were more dense within the ventromedial nucleus than in the DMH, particularly in the central and ventrolateral subregion as well as the perinuclear region (Fig. 3.9b, 3.9d). As they extended caudally past the ventromedial nucleus, these fibers projected to the dorsal and to a lesser extent, the ventral tuberomammillary nuclei, and gradually decreased in density until they were no longer seen.

Discussion

The observed distributions of SCN and LSPV efferents in grass rats are very similar to those previously reported for nocturnal species, consisting of overlapping projections to the hypothalamus, thalamus and limbic forebrain. This suggests, first, that the basic efferent circuitry of the circadian system is highly conserved in diurnal and nocturnal species. Second, while some differences in

the relative density of projections from the SCN and LSPV were apparent, nearly all areas receiving fibers from the SCN also received at least some input from the LSPV, and vice versa. These findings are consistent with the hypothesis that convergence of LSPV terminals on SCN targets could play a role in the promotion of differences in circadian rhythms seen in diurnal and nocturnal species.

Common output pathways of the SCN and LSPV:

The major projections from the SCN are very similar to those of the LSPV and can be organized into 6 pathways according to their respective termination points as follows: 1) an anterior ventral pathway to the mPOA and diagonal band, 2) an anterior dorsal path extending into the septal region, 3) a dorsal pathway to the PVT, 4) a lateral pathway to the supraoptic nucleus and IGL, 5) a dorsocaudal pathway through the sPVZ to the DMH, and 6) a caudal pathway innervating the ventral aspect of the caudal hypothalamus. A very similar distribution for SCN and LSPV efferents exists in lab rats (Watts and Swanson, 1987; Watts et al., 1987), and in hamsters (Morin et al., 1994; Orpen and Steiner, 1994; Kriegsfeld et al.). Thus, the gross organization of SCN/LSPV outputs is essentially the same in diurnal grass rats and at least two nocturnal species.

The majority of projections from the SCN and LSPV were restricted to the hypothalamus, particularly in the medial and periventricular zones. However, direct projections to hypothalamic areas involved with sleep/wake behavior such as the ventrolateral preoptic area and median preoptic nucleus were comparatively sparse. Circadian signals may influence sleep/wake regulation

indirectly through projections to the mPOA, sPVZ and DMH (Deurveilher and Semba, 2004; Saper et al., 2005). These sites, in turn, project to the ventrolateral preoptic area (Deurveilher et al., 2002), the median preoptic nucleus (Deurveilher and Semba, 2003) and arousal-promoting groups such as the tuberomammillary nuclei and the orexin neurons in the perifornical area (Deurveilher and Semba, 2004). The preoptic area, sPVZ, and DMH are also extensively interconnected in lab rats (Simerly and Swanson, 1986; ter Horst and Luiten, 1986; Watts and Swanson, 1987; Watts et al., 1987; Simerly and Swanson, 1988; Thompson et al., 1996; Gu and Simerly, 1997; Thompson and Swanson, 1998; Deurveilher et al., 2002; Deurveilher and Semba, 2003, 2004), and may comprise part of an integrative network regulating multiple behaviors (Swanson, 2000), including locomotor activity and the sleep/wake cycle. Thus, complex rhythms such as those in sleep-wake behavior could be coordinated both through converging SCN/LSPV projections onto this medial hypothalamic circuit, and by interactions between the components of that circuit.

In contrast, direct projections from the SCN/LSPV to more specialized populations of cells may play a greater role in circadian regulation of neuroendocrine functions, particularly those associated with reproduction (de la Iglesia and Schwartz, 2006). Circadian rhythms in mating behavior (Mahoney and Smale, 2005a), the ovulatory surge in luteinizing hormone (McElhinny et al., 1999), and cFos expression in gonadotropin-releasing hormone (GnRH) neurons (Mahoney et al., 2004) are reversed in nocturnal and diurnal rodents. Direct projections from the SCN onto GnRH neurons in the preoptic area, and estrogen

receptor- containing neurons in the anteroventral periventricular nucleus have been described in lab rats (van der Beek et al., 1993; de la Iglesia et al., 1995; Van der Beek et al., 1997a), and both VP- and VIP-ir fibers, some of which are presumed to originate in the SCN, form appositions with GnRH- and estrogen receptor-positive neurons in grass rats (Mahoney and Smale, 2005b). In the present study, both SCN and LSPV projections were seen in parts of the septum, diagonal band, vascular organ of the lamina terminalis and mPOA that contain GnRH and estrogen receptor-positive cells (Mahoney and Smale, 2005b). While it is not known if the LSPV is necessary for normal reproductive rhythms in grass rats, neural connections from both the SCN (Meyer-Bernstein et al., 1999; de la Iglesia et al., 2003) and the sPVZ (Watts et al., 1989) appear to play important roles in the circadian control of neuroendocrine rhythms in nocturnal rodents, and at least some of these rhythms are reversed in diurnal rodents (Mahoney et al., 2004). The current data are thus consistent with the hypothesis that convergence of SCN and LSPV projections on neuroendocrine cells might promote the differences in their regulation by the circadian system.

The most robust extrahypothalamic projection from the SCN and LSPV was to the PVT, which projects in turn to several other SCN/LSPV targets within the hypothalamus (Moga et al., 1995). Unlike the SCN and LSPV, however, the PVT also sends major ascending fibers to regions in the telencephalon, including the amygdala and cerebral cortex (Moga et al., 1995); in some cases this may be the most direct route through which SCN signals could reach these areas (Sylvester et al., 2002). The PVT is a primary target of the SCN signaling

molecule prokineticin 2 in both lab rats and grass rats (Cheng et al., 2002; Lambert et al., 2005). In the present study, the PVT was densely innervated by both the SCN and the LSPV throughout its entire rostrocaudal extent, a pattern consistent with a role for the LSPV in modulating circadian signals originating in the SCN. However, daily cFos rhythms in the PVT are somewhat similar in grass rats and lab rats kept in a light-dark cycle (Novak and Nunez, 1998; Novak et al., 2000). This suggests that rhythmic cells within the PVT may respond differently to SCN and/or LSPV input compared to cells in other hypothalamic regions. The PVT also sends a robust projection to the SCN (Moga et al., 1995), and PVT stimulation can phase-shift rhythms in drinking (Salazar-Juarez et al., 2002). It is thus possible that the LSPV could indirectly influence the activity of SCN neurons through the PVT.

Differences in efferents of the SCN and LSPV:

Almost all areas innervated by the SCN were also innervated by the LSPV, and vice versa. The only possible exception to this was the IGL, in which labeled fibers were abundant following all SCN injections, but sparse following some LSPV injections, and absent in other cases. In hamsters (Morin et al., 1992; Vrang et al., 2003; Vidal et al., 2005) and lab rats (Card and Moore, 1989; Moore and Card, 1994), retrograde tracer injections into the IGL labeled small numbers of cell bodies in and around the SCN and large numbers of cells in the retrochiasmatic area, and anterograde tracer injections into the SCN and LSPV each labeled fibers in the IGL (Watts et al., 1987; Morin et al., 1994; Kriegsfeld et al., 2004). In the present study, IGL labeling was consistently associated with

injections centered in the SCN, but not the LSPV. However, the two LSPV injections that did label fibers in the IGL were also centered further laterally than the two that did not. While this difference in location is slight, the SCN is both functionally and anatomically complex (Morin et al., 2006), and such heterogeneity may also exist in the tissue surrounding the SCN (Ramanathan et al., 2006). Retrograde tracing will be necessary to determine exactly which cells within and around the SCN project to the IGL

Functional Implications:

While the SCN and the LSPV of both diurnal and nocturnal species appear to project to essentially the same target areas, several lines of evidence suggest that LSPV outputs may differ functionally from those of the SCN in at least two respects. First and foremost, the SCN is likely to use different neurotransmitters than the LSPV. While is it estimated that the majority of SCN neurons are GABAergic (Moore and Leak, 2001), the SCN of both diurnal and nocturnal species is both functionally and anatomically heterogeneous (Antle and Silver, 2005). At least some SCN peptides are involved in signaling to SCN target cells, as both VP- and VIP-ir SCN neurons send major projections out of the SCN (Van der Beek et al., 1997a; Abrahamson and Moore, 2001; Mahoney and Smale, 2005b), and experimental manipulations of these peptides have revealed a role for them in regulation of neuroendocrine rhythms (Kriegsfeld and Silver, 2006). While the identity of the transmitter(s) used by projection neurons of the LSPV is still unknown, these are likely to differ from those used by SCN neurons, as cells in the LSPV do not express many of the peptides and proteins

seen in the SCN (e.g. vasopressin, vasoactive intestinal polypeptide, gastrin-releasing peptide, corticotropin-releasing factor; Watts and Swanson, 1987; Moore and Silver, 1998; Smale and Boverhof, 1999; Abrahamson and Moore, 2001). This also raises the possibility that some targets may respond more, or differently, to signals from the SCN and LSPV, depending on the type and timing of the signal. A second difference between the grass rat SCN and LSPV is that they exhibit different patterns of rhythmicity at the cellular level. For example, when grass rats are kept on a light-dark cycle cFos in the LSPV rises within 5 hours of lights-off, but does not go up in the SCN until lights-on (Nunez et al., 1999; Schwartz et al., 2004). These differences in the pattern of rhythmic activity, and in the chemical signals used, suggest that in grass rats, the LSPV is more than a relay for SCN signals. Rather, the SCN and LSPV may send distinctly different signals to their various targets.

Although the grass rat LSPV and SCN are different with respect to cell phenotypes and their patterns of rhythmicity, they are similar in other respects. In both regions, cFos rhythms are endogenous (Schwartz et al., 2004) and are buffered against dramatic changes in activity state (Schwartz and Smale, 2005). These data indicate that rhythmic activity in the grass rat LSPV, like that within the SCN, is not dependent on a light-dark cycle, nor is it heavily influenced by sleep/wake state or behavioral arousal. Signals coming from the LSPV are thus more tightly coupled to the pacemaker than to the external environment or internal state. Both the SCN and LSPV also express daily rhythms in expression of the clock gene products Per1 and Per2 (Ramanathan et al, 2006). The

observation that these signals appear to reach nearly all of the same target regions as those from the SCN makes it even more likely that the output of the LSPV is related to timekeeping in grass rats.

Conclusions:

The function of the LSPV in either diurnal or nocturnal species is not fully understood. In lab rats, the lower part of the sPVZ may be involved in regulating the timing of reproduction-related events (Arendash and Gallo, 1979; Docke et al., 1982; Watts et al., 1989; Fernandez-Galaz et al., 1999) and locomotor activity (Lu et al., 2001; Moore and Danchenko, 2002). However, circadian body temperature rhythms persist with reduced amplitudes in animals with ventral sPVZ lesions (Lu et al.), suggesting that, although the ventral sPVZ may be necessary for expression of some rhythmic processes, it is not essential for all. In grass rats, the LSPV displays an endogenous rhythm in cFos expression that is 8 hours advanced relative to that in the SCN, whereas in lab rats, this rhythm is in phase with the SCN rhythm under a light-dark cycle and is not rhythmic under constant dark conditions (Schwartz et al.). Thus, rhythmic activity in the grass rat LSPV is different from both the activity of its own SCN, and from the activity of the LSPV in nocturnal lab rats. The clear parallelism in the efferents of the SCN and LSPV in grass rats demonstrated here is consistent with the hypothesis that projections from the grass rat LSPV may converge with those from the SCN on their target cells. If this is the case, then signals from the LSPV could alter the responses of these cells to signals originating in the SCN, and

perhaps do this differently in diurnal grass rats compared to nocturnal species such as lab rats.

CHAPTER 4

The suprachiasmatic nucleus and the lower subparaventricular zone project onto gonadotropin-releasing hormone neurons in the Nile grass rat (*Arvicanthis niloticus*)

Introduction:

In female rodents, reproductive behavior involves the precise temporal coordination of multiple physiological and behavioral events. The activation of gonadotropin-releasing hormone (GnRH) neurons underlying the ovulatory surge in leuteinizing hormone (LH) requires both a hormonal signal, mediated by circulating levels of estrogen that peak on the day of proestrus, and a daily temporal signal. For example, nocturnal female laboratory rats (*Rattus norvegicus*, hereafter referred to as 'lab rats') given barbiturates on the afternoon of proestrus delay ovulation by 24 hours (Everett and Sawyer, 1950), and ovariectomized female rats with constantly elevated levels of circulating estradiol exhibit daily LH surges (Legan and Karsch, 1975). Rhythms in the timing of the LH surge also free-run in female lab rats housed in constant lighting conditions (Cheung and McCormack, 1983; Takeo, 1984), indicating that the daily signals governing GnRH activation and the LH surge are endogenous. In diurnal rodents such as Nile grass rats (*Arvicanthis niloticus*), mating behavior occurs in the early morning, 180 degrees out of phase with the time of day at which it occurs in lab rats (Mahoney and Smale, 2005a). This difference is accompanied by reversals in rhythms in the LH surge (McElhinny et al., 1999) and cFos expression within

GnRH neurons, and these phase differences persist in constant darkness (Mahoney et al., 2004). However, the neural basis of these species differences is not known.

Circadian influences on reproductive events in rodents are governed by the suprachiasmatic nucleus (SCN), which contains the primary mammalian circadian pacemaker (Moore and Eichler, 1972; Stephan and Zucker, 1972). However, the SCN appears to be similar in day- and night-active species. For example, daily rhythms in expression of the clock genes *per1* and *per2* peak at the same times of day in the SCN of diurnal and nocturnal species (Hastings et al., 1999; Mrosovsky et al., 2001; Yan and Okamura, 2002; Caldelas et al., 2003; Ramanathan et al., 2006). Indices of cellular activity in SCN neurons such as 2-deoxyglucose uptake (Schwartz, 1991) and multiple-unit activity (Sato and Kawamura, 1984b; Kurumiya and Kawamura, 1988) are also similar in diurnal and nocturnal species (but see Jiao et al., 1999). These similarities suggest that the mechanisms underlying differences between diurnal and nocturnal patterns of rhythmicity are located downstream of the pacemaker in the SCN.

The subparaventricular zone (sPVZ) dorsal to the SCN may be part of such a mechanism. The sPVZ extends from the dorsal border of the SCN along the midline to the hypothalamic paraventricular nucleus, and is a major target of the SCN in nocturnal and diurnal species (Watts and Swanson, 1987; Watts et al., 1987; Morin et al., 1994; Abrahamson and Moore, 2001; Moore and Leak, 2001). The sPVZ in turn projects to many of the same target regions as the SCN in both lab rats (Watts and Swanson, 1987; Watts et al., 1987) and in diurnal Nile

grass rats (chapter 3). Daily rhythms in multiple-unit electrical activity immediately outside the SCN are reversed in diurnal Siberian chipmunks compared to lab rats (Kubota et al., 1981; Sato and Kawamura, 1984b), and circadian rhythms in cFos expression in the lower part of the subparaventricular zone (LSPV) are dramatically different in diurnal Nile grass rats and nocturnal lab rats (Nunez et al., 1999; Schwartz et al., 2004). This region thus displays the characteristics necessary to communicate circadian signals indirectly to targets that are also innervated by the SCN, and to do that differently in diurnal and nocturnal animals (Schwartz et al., 2004).

Direct projections from the SCN are likely to play a major role in circadian regulation of neuroendocrine functions, including those associated with reproduction (de la Iglesia and Schwartz, 2006). Direct projections from the SCN onto GnRH neurons in the preoptic area (POA), and estrogen receptor- (ER-) containing neurons in the anteroventral periventricular nucleus (AVPV) have been described in lab rats and hamsters (de la Iglesia et al., 1995; Watson et al., 1995; Van der Beek et al., 1997a). In lab rats, these projections may use vasoactive intestinal polypeptide (VIP; van der Beek et al., 1993) and/or vasopressin (VP; Kalamatianos et al., 2004) as transmitters. In grass rats, both VP and VIP-positive fibers, some of which are thought to originate in the SCN, form appositions with GnRH- and ER-positive neurons (Mahoney and Smale, 2005b). However, rhythms in VP and VIP mRNA in grass rats and lab rats are similar (Krajnak et al., 1998; Mahoney et al., 2006), suggesting that differences in the timing of rhythmic activity in GnRH neurons may be regulated by differences

in responsiveness to SCN signals and/or other sources of inputs to these cells (Mahoney and Smale, 2005a).

In grass rats, both the SCN and the LSPV project to areas containing GnRH- and ER- positive cells, including the medial septum (MS), the diagonal band of Broca (DBB), the vascular organ of the lamina terminalis (OVLT), and the POA (chapter 3). The general distributions of these efferents are consistent with the idea that signals from cells in both the LSPV and the SCN influence rhythms in target cell populations regulating reproduction. However, it is not known whether LSPV neurons project directly onto GnRH neurons in any species. If the LSPV is involved in maintaining a diurnal pattern of circadian rhythmicity, then cells receiving input from it should show different patterns of rhythmicity in diurnal and nocturnal species. Here, we used injections of the anterograde tracer biotinylated dextran amine (BDA), in conjunction with light-level and confocal approaches, to determine if SCN and/or LSPV cells project directly to GnRH neurons, a population of cells that is rhythmically inverted in diurnal and nocturnal species.

Materials and Methods:

Animals

Animals were adult female grass rats (*Arvicanthis niloticus)* obtained from a breeding colony at Michigan State University (Katona and Smale, 1997). Animals were singly housed in Plexiglas cages (34 x 28 x 17 cm) with access to food (PMI Nutrition Prolab RMH 2000, Brentwood, MO) and water *ad libitum.* Animals were kept in a 12:12 light: dark (LD) cycle; a red light (<5 lux) remained

on constantly for animal care purposes. All experiments were performed in compliance with guidelines established by the Michigan State University All-University Committee on Animals Use and Care, and the NIH Guide for the Care and Use of Laboratory Animals.

Surgical Procedures:

All animals received a unilateral iontophoretic injection of 10,000 MW BDA (Molecular Probes; Eugene, OR) directed at the SCN and LSPV. Animals were deeply anesthetized with sodium pentobarbital (50mg/kg i.p.) prior to surgery. The animal's head was shaved, sterilized with betadine, and injected with 0.03 cc lidocaine s.c. The animal was then placed into a stereotaxic apparatus (Stoelting Co.; Wood Dale, IL) with the incisor bar set to -6.0 mm and the micropipette angled 10 degrees, and a 1-2 cm incision was made in the scalp to expose the skull. Injection coordinates were: 1.4 mm anterior to bregma, 1.2 mm lateral to bregma, and 6.3 mm ventral to the dura. A small hole was drilled in the skull, and the dura was gently broken to allow uninterrupted passage of the micropipette. A glass micropipette (WPI; Sarasota, FL) with inner tip diameter of 10-15 μm was then filled with 10% BDA in 0.01 M phosphate-buffered saline (PBS; pH 7.4) and lowered slowly to the final position. Injections were made under 5 mA positive alternating current at a rate of 7 seconds on/ 7 seconds off, for 7 minutes, and were followed by a 7-minute rest period. Micropipettes were then withdrawn slowly under negative current. The incision was closed with autoclips, and animals were given 0.06 cc buprenorphine i.m. and 1.0 cc sterile saline s.c. Seven days later, animals were given an overdose of sodium

pentobarbital and perfused transcardially with 0.01M phosphate-buffered saline (PBS), pH 7.2, followed by 4% paraformaldehyde (Sigma-Aldrich Co., St. Louis, MO) in 0.1M phosphate buffer. Brains were post-fixed for 4 hours and then transferred to 20% sucrose solution overnight. Brains were sectioned into 3 series coronally at 30 μm on a freezing microtome, and sections were stored in cryoprotectant at -20°C until processing. One series of sections was used here; the other two series were used in a separate study (chapter 3).

Light-level analyses:

For analysis of tissue at the light level, we used DAB with and without nickel as the chromagen. Unless noted otherwise, incubations were conducted at room temperature for 1 h on a shaker, and tissue was rinsed 3 × 10 min in PBS between incubations. Free-floating sections were rinsed in PBS, and then incubated in avidin-biotin peroxidase complex (ABC; ABC Vectastain Kit, Vector Laboratories, Burlingame, CA). Tissue was rinsed in sodium acetate buffer and BDA was visualized by reacting with diaminobenzidine (DAB; 0.5mg/mL; Sigma) enhanced with nickel sulfate in acetate buffer. Sections were rinsed in PBS, then incubated in i) 5% normal horse serum (Vector) in PBS with 0.3% Triton X-100, ii) mouse anti-GnRH antibody (1:5000; HU4H antibody characterized in Urbanski, 1991) on a rotator for 48 h at 4 °C, iii) biotinylated horse anti-mouse antibody (1:200; Vector), iv) ABC. Protein was visualized by reacting with diaminobenzidine (0.5mg/mL; Sigma) in Trizma buffer (Sigma). Sections were then mounted, dehydrated, and coverslipped with Permount.

GnRH-ir neurons with and without BDA-ir appositions (also referred to as contacts) were counted in 3 rostrocaudal zones encompassing the MS and DBB (6 sections), the OVLT (2 sections), and the POA and SCN (6 sections). Sections were examined for appositions on a Zeiss Axioskop microscope (Zeiss, Göttingen, Germany) under brightfield illumination using a 100x oil immersion lens. A GnRH-ir neuron was considered to be contacted by a BDA-ir fiber if, in the same plane of focus, a swelling on a BDA-ir axon (blue-black fiber) was observed abutting a GnRH-ir cell body (brown cell), or a labeled process emanating from a GnRH-ir cell body. All photomicrographs were taken using a Zeiss Axiocam MR (Zeiss) and processed in Adobe Photoshop 7.0 (Adobe Systems; Mountain View, CA). The 'sharpen' filter was applied once to each image, and then images were adjusted for brightness and contrast.

Confocal analysis:

Free-floating sections were rinsed in PBS, and then incubated in i) ABC, ii) biotinylated tyramide from a Renaissance TSA-indirect Kit (Perkin-Elmer; Boston, MA), iii) FITC-conjugated streptavidin (1:200; Molecular Probes). From this point onwards, tissue was isolated from ambient light during all incubations and rinses. Sections were then rinsed in PBS and incubated in i) 5% normal donkey serum (Jackson Laboratories, Bar Harbor, ME) in PBS with 0.3% Triton X-100, ii) a combination of mouse anti-GnRH (1:5000; HU4H) and rabbit anti-VIP (1:1000; Immunostar, St. Paul, MN) antisera for 48 hours at 4 degrees C, iii) a combination of Texas Red-conjugated donkey anti-mouse (1:200; Jackson) and Cy5-conjugated donkey anti-rabbit (1:200; Jackson) antisera. Sections were

mounted onto gelatin-coated slides and coverslipped with ProLong Gold antifade reagent (Sigma). Upon examination, VIP-ir fibers, while clearly visualized in and around the SCN as well as in the bed nuclei of the stria terminalis, were not reliably visualized in other areas previously shown to contain them (Mahoney and Smale, 2005b). For this reason, tissue was analyzed only for BDA-ir appositions.

GnRH neurons were examined for appositions with BDA-ir fibers under mercury vapor epifluorescence using a 40x objective. Those GnRH-ir neurons with apparent BDA-ir contacts were then examined on a Zeiss LSM 5 Pascal confocal microscope (Zeiss). Using a 63x oil immersion objective, GnRH neurons were optically sectioned through the cell body at 0.42 μm. Each z-stack was generated using 2 tracks. The first track visualized FITC (BDA) using a 488 nm argon-ion laser and a 123 μm pinhole diameter; the second track visualized Texas Red (GnRH) using a 543 nm helium-neon laser and a 108 μm pinhole diameter. All settings were kept constant for each z-stack. Contacts between BDA and GnRH neurons were verified using the LSM Image Browser (Zeiss) that allows reconstruction, rotation and viewing of z-stacks in 3 dimensions. 2-dimensional single frames and projections were converted to TIF format and adjusted in Photoshop as described above.

Results:

The distribution of GnRH-ir cells:

The appearance and distribution of GnRH neurons were similar to those described previously (McElhinny et al., 1999; Mahoney and Smale, 2005b). GnRH neurons had a fusiform appearance, with processes extending from both

ends of the cell, often for considerable distances. Rostrally, small numbers of GnRH neurons were observed in the MS and vertical DBB. These neurons were oriented dorsoventrally, and were most common on or close to the midline. Numbers of GnRH neurons increased dramatically around the OVLT and the adjacent DBB and rostral POA. In these regions GnRH neurons were oriented along a dorsomedial-ventrolateral axis close to the OVLT, and into the vertical DBB and septal region. Caudal to the OVLT, GnRH neurons became clustered in two areas. One group of cells was concentrated in the medial POA, whereas the other extended laterally and caudally parallel to the optic chiasm where they loosely surrounded the rostral and medial supraoptic nucleus. There were fewer GnRH neurons in the MS/DBB than in the OVLT or the POA/SCN.

BDA injection sites:

BDA injections were centered in the SCN in cases 74 and 81. Both injections filled the entire SCN, and in # 74 the injection did not extend beyond the borders of the SCN, whereas the injection in # 81 bled slightly into the RCh (Fig. 1). In both cases numerous BDA-ir fibers were apparent throughout the region in which GnRH neurons were distributed; the density of labeled fibers in this area was slightly higher in case 81 than 74. Overall, BDA-ir fibers were far more dense ipsilaterally than contralaterally, although certain targets exhibited highly bilateral innervation; these targets included the MS, the vertical limb of the DBB, the area surrounding the OVLT, and the POA.

BDA injections were centered around the SCN in 4 cases; of these, 2 were limited to the LSPV (34 and 61) and 2 extended beyond the LSPV laterally

and dorsally (40 and 75). In none of these 4 cases did the tracer bleed into the SCN. The distributions of BDA-ir fibers in 34 and 61 were very similar to those seen following SCN injections, with a slightly higher density of labeled fibers in case 61 than 34. Fiber densities through the region containing GnRH neurons were lower than those seen following SCN injections in all cases except for # 75. In cases 40 and 75, the distributions of BDA-ir fibers were generally similar to those of # 34 and # 61, although fibers extended further laterally past the DBB, and covered more of the mPOA, particularly in #75. Fiber densities through the areas containing GnRH neurons were also higher in both of these cases than in either # 34 or # 61. Overall, labeled fibers were more dense ipsilateral to the injection site, although contralateral fibers were evident, as was the case following injections into the SCN.

Appositions between GnRH-ir neurons and BDA-ir fibers:

Following injections into both the SCN and the LSPV, BDA-ir fibers were interspersed with GnRH-ir neurons at all rostrocaudal levels, but were most dense in and around the OVLT and the adjacent POA. Varicose BDA-ir fibers were often found in close association with GnRH-ir cell bodies and proximal processes (Fig. 2, 3), and in some cases these labeled fibers appeared to end in a large terminal bouton-like structure (Fig. 2a). In at least one case, a single BDA-ir fiber was observed to contact 2 GnRH-ir neurons in the same section (Fig. 3a, b). Varicose BDA-ir fibers were also frequently observed in apposition with GnRH-ir processes at some distance from the cell body (which was not

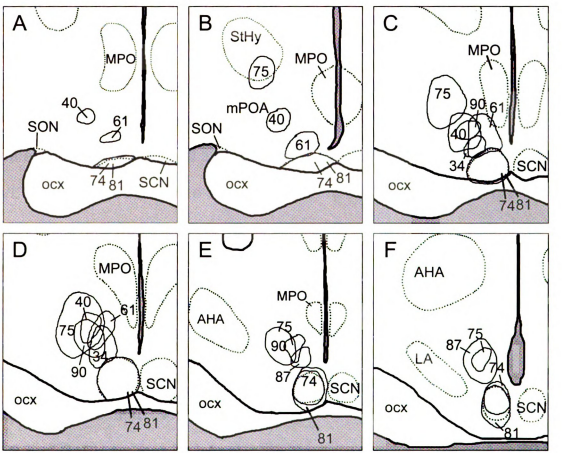

Figure 4.1: Schematic depiction of BDA injection sites in and around the SCN. See page *x-xii* for abbreviations.

always visible; Fig. 2e, 3d). These fiber-fiber appositions were observed throughout the region of the OVLT and adjacent POA.

Following BDA injections into the SCN, appositions were concentrated in the mid-to-caudal parts of the distribution of GnRH cells and were found on both sides of the brain. In the MS/DBB 17.2 % – 31.6 % of GnRH neurons were contacted by BDA-ir fibers (Table 4.1); these proportions were similar on the two sides of the brain. In the OVLT and POA/SCN, 53.1 % – 65.6 % and 44.2 % – 84.8 % of GnRH neurons, respectively, were contacted by BDA-ir fibers. The difference between ipsilateral and contralateral sides was low in the MS/DBB and OVLT. In the POA/SCN, there were more contacts on the side ipsilateral to the injection site; this was especially true in case 81, in which the tracer extended somewhat caudal to the SCN.

Following injections centered in the LSPV, appositions were concentrated in the mid-to-caudal parts of the distribution of GnRH neurons, where they were most numerous ipsilateral to the injection site. Rostrally, however, the projections were more evenly distributed. Specifically, in the MS/DBB 4.2 % – 26.8 % of GnRH neurons ipsilateral to the injection site were contacted by BDA fibers, while 16.7 % – 25.0 % of contralateral GnRH neurons apposed BDA fibers (Table 4.1). In the OVLT, 26.7 % – 73.5 % of GnRH neurons formed appositions with BDA-ir fibers from the LSPV, as did 17.3 % – 79.5 % of GnRH neurons in the POA/SCN area. In both regions, ipsilateral appositions increased with injection size. Numbers of appositions in the OVLT and POA/SCN were lower on the side contralateral to the injection site than ipsilateral to it in all 4 cases, and

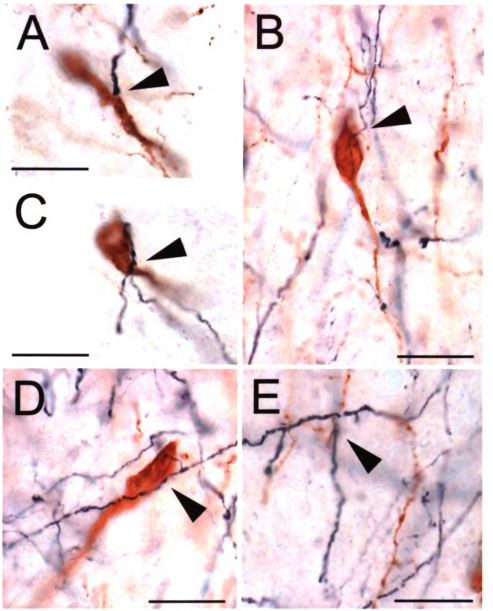

Figure 4.2: Photomicrographs of appositions between BDA-ir fibers (black) and GnRH neurons (brown; A – D) and processes (E) following injections centered in the SCN. BDA-ir fiber in (E) is not the same fiber pictured in (D). All images were taken using a 100x oil objective. Scale bar = 20 µm.

varied less from case to case (OVLT, 26.7 % - 37.5 %; POA/SCN, 17.3 % - 34.8 %). The distribution of GnRH neurons forming appositions with fibers from the LSPV was thus similar to that of neurons contacted by SCN fibers, in that appositions were more frequent in the OVLT and POA/SCN. However, LSPV efferents formed more appositions ipsilaterally than contralaterally in these areas, whereas SCN efferents projected more equally to the two sides.

Confocal imaging:

In two additional animals with BDA injections centered in the LSPV, confocal microscopy was used to examine the relationship between BDA-ir fibers and GnRH cell bodies in greater detail. In cases 87 and 90, injections were comparable in size to those of # 61 (Fig. 1). Case 87 was centered in the caudal LSPV, dorsolateral to the caudal SCN. In case 90, the injection was centered slightly more rostral than # 87, with significant coverage in the LSPV. In both cases, the distributions of BDA-ir fibers were consistent with those from the previously-described LSPV injections. BDA-ir fibers from the LSPV directly contacted GnRH-ir cell bodies and processes, forming appositions very similar in appearance to those observed using light-level microscopy (Fig. 4). This was confirmed by rotation of the image in 3 dimensions, as well as by examination of appositions in single optical sections (0.42 μm thickness; Fig. 4d). Varicose fibers coursed alongside GnRH neurons, forming multiple contacts along the entire length of the cell body (Fig. 4a). Often, BDA-ir fibers apposed GnRH neurons at the base of the processes (Fig. 4b). As was observed at the light

Subject		MS/DBB		OVLT		POA/SCN	
		ipsi	contra	ipsi	contra	ipsi	contra
SCN	74	18.9%	31.6%	65.6%	58.1%	51.3%	44.2%
	81	17.2%	17.9%	54.5%	53.1%	84.8%	57.9%
LSPV	34	26.8%	24.4%	27.3%	26.7%	36.4%	17.3%
	40	4.2%	16.7%	50.0%	32.0%	69.0%	21.4%
	61	26.7%	25.0%	43.8%	37.5%	48.4%	34.8%
	75	22.0%	20.7%	73.5%	27.9%	79.5%	24.5%

Table 4.1: Percentages of GnRH-ir neurons that formed appositions with BDA-labeled fibers. Values represent the percentage of the total number of GnRH neurons ipsilateral or contralateral to the BDA injection site with appositions in each of three rostrocaudal regions.

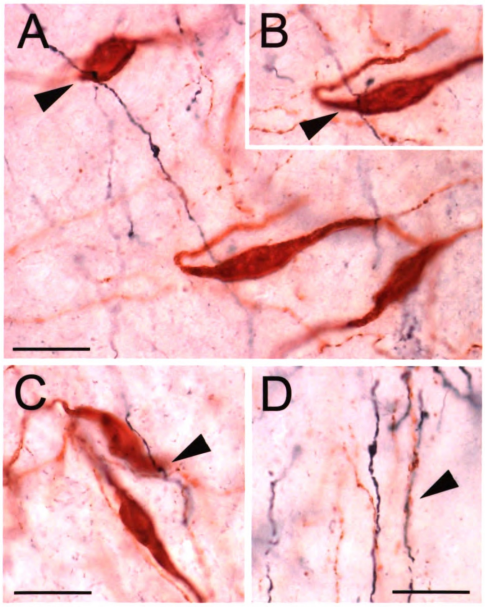

Figure 4.3: Photomicrographs of appositions between BDA-ir fibers (black) and GnRH-ir neurons (brown; A – C) and processes (D) following injections centered in the LSPV. GnRH neuron in (B) is the same neuron depicted in bottom center of (A). All images were taken using a 100x oil objective. Scale bar = 20 µm.

level, the density of appositions was low in the MS/DBB, highest in and around the OVLT, and decreased in frequency in the POA/SCN.

Discussion

Rhythms in activation of GnRH neurons associated with the LH surge require axonal outputs from the SCN (Meyer-Bernstein et al., 1999; de la Iglesia et al., 2003) and are reversed in diurnal and nocturnal species (McElhinny et al., 1999; Mahoney et al.; Mahoney and Smale, 2005a). However, the output pathways through which the SCN regulates these functions are not well-understood in diurnal species. In the present study, we asked whether the SCN and the LSPV might project to GnRH neurons. BDA-labeled fibers originating in the SCN appeared to contact GnRH neurons, as they do in nocturnal rodents. The appositions were most concentrated in and around the OVLT and the adjacent preoptic area; fewer appositions were present in the MS, rostral DBB and dorsal to the SON. BDA-labeled fibers coming from the LSPV also formed numerous appositions with GnRH neurons in the same areas, particularly in the OVLT and the rostral POA, where in several cases both SCN and LSPV fibers apposed more than 50% of the GnRH neurons. It is thus likely that some, and perhaps many, GnRH neurons receive input directly from both the SCN and the LSPV.

The appositions seen here with a light level microscope are highly suggestive of synaptic interaction between the SCN/LSPV efferents and GnRH neurons, but do not establish the presence of functional synapses. However, in nocturnal rodents, light-level techniques similar to those used here have revealed

contacts between SCN fibers and GnRH neurons and ER-positive neurons that were subsequently verified using electron microscopy (Watson et al., 1995; van der Beek et al., 1997b). Additionally, confocal analysis in the current study revealed appositions between varicose LSPV fibers and GnRH neurons in optical sections of less than 0.5 μm thickness, indicating that the labeled fibers were very likely to interact functionally with these cells. Taken together, these data provide strong evidence that the contacts observed here represent synapses between BDA-labeled fibers and GnRH neurons, as they do in lab rats.

The distribution of efferent fibers from the grass rat SCN is very similar to that seen in nocturnal lab rats and hamsters (Watts et al., 1987; Kriegsfeld et al., 2004) and includes prominent projections to the septum, diagonal band, OVLT and preoptic area. In the present study, labeled fibers from both the SCN and the LSPV formed appositions with GnRH neurons in all of these areas. However, the appositions with SCN fibers were bilaterally distributed in grass rats, whereas those with LSPV fibers were most heavily concentrated on the side ipsilateral to the BDA injection site. Although SCN input to contralateral GnRH neurons has been documented in lab rats, the degree of laterality has not yet been quantified in that species (Van der Beek et al., 1997a). At a more general level, SCN projections to the contralateral side of the brain have been reported in both lab rats and hamsters, though they are less pronounced than ipsilateral projections (Watts et al., 1987; Kriegsfeld et al., 2004). It is possible that differences in tracers used (*Phaseolus* vs. BDA in the present study), and/or the sizes and locations of injections, account for differences in the extent of

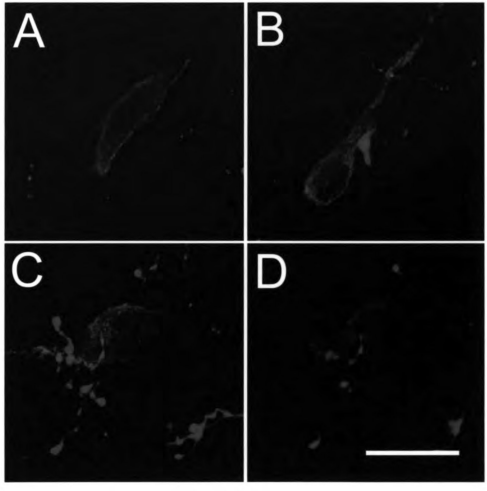

Figure 4.4: Confocal laser fluorescent images of appositions between BDA-ir fibers (green) and GnRH-ir cell bodies (red) following injections centered in the LSPV. A – C: projections of serial optical sections. D: single optical section from the cell depicted in (C). All images were taken using a 63x oil objective. Scale bar = 20 μm.

contralateral GnRH innervation between grass rats and lab rats. Alternatively, the relative degree to which the SCN projects to the contralateral population of GnRH neurons may differ in these species.

In nocturnal species, several lines of evidence suggest that at least some of the projection from the SCN to the GnRH neurons is composed of VIP fibers. Specifically, in lab rats VIP-ir fibers appose GnRH neurons (van der Beek et al., 1994; Kriegsfeld et al., 2002), GnRH neurons in the OVLT and POA express the VIP2 receptor (Smith et al., 2000) and VIP appositions decrease substantially following unilateral SCN lesions (van der Beek et al., 1993). In grass rats, VP- and VIP-ir fibers appear to contact GnRH neurons, and Mahoney and Smale (2005) suggested that at least some of these contacts represent direct input from the SCN. The present work provides further evidence that this may be the case, by showing that BDA-labeled fibers from the SCN form close appositions with GnRH neurons.

The SCN may also indirectly influence GnRH cell activity and the surge via its projections to the AVPV, a nucleus essential for the generation of an LH surge (Wiegand and Terasawa, 1982). In nocturnal species, SCN cells project to ER-positive neurons in the AVPV (de la Iglesia et al., 1995; Watson et al., 1995), and ER-ir cells in that nucleus project to regions containing GnRH neurons (Simonian et al., 1999). In female grass rats, appositions between VP- and VIP-ir fibers and ER-positive cells have also been seen (Mahoney and Smale, 2005b). The current data support the suggestion that these VIP- and VP-ir fibers could originate in the SCN. It thus appears likely that in diurnal rodents, as in

nocturnal ones, the SCN projects to GnRH neurons both directly and indirectly via the AVPV, and that these pathways are likely to include VIP- and VP-ir fibers.

The temporal patterns of VIP and VP signals to GnRH neurons from the SCN are likely to be the same in lab rats and grass rats, as rhythms in VP and VIP mRNA are similar (Krajnak et al., 1998; Mahoney et al., 2006). It is thus likely that GnRH neurons respond differently to these SCN signals in diurnal and nocturnal rodents. This may also be the case for rhythms in behavioral sensitivity to steroid hormones, which are also inverted in grass rats relative to lab rats (Mahoney et al., 2004). These time-dependent differences in sensitivity could reflect intrinsic properties of the GnRH neurons, or they could arise from rhythms in extra-SCN inputs to them. The present data suggest that the LSPV could represent one such input.

Appositions between GnRH cells and fibers emanating from the LSPV, as with those coming from the SCN, were most concentrated around the OVLT and adjacent POA. In lab rats, GnRH neurons in this area are preferentially activated during the LH surge (Lee et al., 1990; Lee et al., 1992; van der Beek et al., 1994), and the numbers of neurons expressing GnRH mRNA in this region, but not in more rostral or caudal areas, are increased during proestrus (Porkka-Heiskanen et al., 1994). The OVLT and rostral POA may therefore contain a high concentration of GnRH cells that are specialized for regulation of events occurring at estrus (Hiatt et al., 1992). The current observation of a relatively high concentration of appositions between LSPV efferent fibers and GnRH

neurons in this region suggest that the LSPV may also act on these cells to influence estrus-related events such as the LH surge and sex behavior.

In summary, the present data show that in grass rats, fibers emanating from the SCN and from the LSPV, a direct target of the SCN, form appositions with a group of GnRH cells concentrated in a region critical for the generation of the LH surge. The hypothesis that LSPV inputs influence the same GnRH neurons that receive input from the SCN is suggested by the extensive overlap in the distributions of GnRH neurons forming appositions with SCN and LSPV efferent fibers, and by the fact that in some areas over 50% of GnRH neurons receive input from the LSPV and SCN, respectively. Inputs from these areas differ with respect to their neurochemical signals, as LSPV neurons express neither VIP nor VP (Watts and Swanson, 1987; Smale and Boverhof, 1999). They are also unlikely to be the same in terms of their temporal pattern of signaling, as the grass rat SCN and LSPV exhibit different endogenous rhythms in cFos expression (Schwartz et al., 2004). The LSPV is thus in an ideal position to influence the circadian regulation of GnRH neurons, and to do so differently in diurnal and nocturnal species. The data also provide some support for the more general hypothesis that convergence of LSPV projections on SCN target neurons contributes to differences in circadian function of nocturnal and diurnal species.

CHAPTER 5

The effects of chemical lesions of the lower subparaventricular zone on general activity rhythms in the Nile grass rat

Introduction

Diurnal and nocturnal rodents exhibit dramatic differences in circadian rest-activity rhythms. However, the hypothalamic suprachiasmatic nucleus (SCN), which contains the primary circadian pacemaker in mammals (Moore and Eichler, 1972; Stephan and Zucker, 1972; Sato and Kawamura, 1984a; Ralph et al., 1990), is very similar in diurnal and nocturnal species. Rhythms in expression of the clock genes *per1* and *per2* peak during the subjective day in diurnal 13-lined ground squirrels (Mrosovsky et al., 2001), grass rats (Lambert et al., 2005); *Arvicanthis ansorgei*: (Caldelas et al., 2003) and in nocturnal laboratory rats (Rattus norvegicus, hereafter referred to as 'lab rats'; Yan et al., 1999), hamsters (Hamada et al., 2004) and mice (Hastings et al., 1999). Furthermore, rhythms in mRNA for the SCN output signals vasopressin (VP), vasoactive intestinal polypeptide (VIP) and prokineticin 2, do not differ in diurnal and nocturnal species (Krajnak et al., 1998; Lambert et al., 2005; Mahoney et al., 2006), suggesting that the phase of both the molecular clock in the SCN and several of its output signals are similar in diurnal and nocturnal rodents. Although it is still possible that SCN function differs in some important ways in diurnal and nocturnal species (Krajnak et al., 1997; Jiao et al., 1999), it is most likely that the fundamental difference in their activity rhythms is determined by mechanisms somewhere downstream of the SCN.

In nocturnal species, the SCN sends a major projection to the hypothalamic subparaventricular zone (sPVZ), which extends dorsally and caudally from the border of the SCN to the paraventricular nucleus of the hypothalamus (Watts and Swanson, 1987; Abrahamson and Moore, 2001). The sPVZ projects, in turn, to many of the same targets as the SCN (Watts et al., 1987; Morin et al., 1994), leading to speculation that it relays or amplifies signals emitted by the SCN (Watts, 1991; Saper et al., 2005). This hypothesis is supported by data showing that free-running circadian wheel-running rhythms in lab rats are attenuated by axon-sparing chemical lesions in the ventral sPVZ (Lu et al., 2001) and are abolished by electrolytic lesions of the sPVZ (Abrahamson and Moore, 2006). These data suggest that both cells in the sPVZ as well as fibers passing through it are important for maintaining locomotor rhythms. However, direct axonal projections from the SCN to the sPVZ are not necessary for maintenance of wheel running rhythms in lab rats, as these persist even after horizontal knife cuts have severed axonal connections between the SCN and the sPVZ (Brown and Nunez, 1986; Watts et al., 1989). Furthermore, in nocturnal hamsters wheel running rhythms may be maintained by a diffusible signal secreted by the SCN, as they persist following isolation of the SCN (Hakim et al., 1991). The sPVZ has been suggested as one possible target for such a signal (Abrahamson and Moore, 2006). Normal circadian regulation of locomotor activity in these species is thus likely to rely on multiple SCN outputs, axonal and/or diffusible (Silver et al., 1996a), at least one of which is likely to target the sPVZ.

In diurnal Nile grass rats, the lower part of the subparaventricular zone (LSPV) projects to nearly all of the same targets as the SCN (chapter 3), suggesting that circadian signals may be broadcast to other brain regions both directly from the SCN, and indirectly via the LSPV. The LSPV also displays a rhythm in cFos expression whose phase differs substantially from that of rhythms in the LSPV of lab rats, and which persists in constant darkness in grass rats but not in lab rats (Schwartz et al., 2004). These data suggest first, that in diurnal rodents, circadian signals emitted by the LSPV and SCN could differ substantially, and second, that LSPV signals could contribute to differences in the phases of behavioral and physiological rhythms of diurnal and nocturnal rodents. If this is the case, then a selective lesion of the LSPV, sparing both the SCN and the fibers that project from it, should significantly affect rhythms that are reversed in grass rats nocturnal lab rats.

The study described below examined the effects of bilateral destruction of the LSPV on general activity rhythms in grass rats. We used microinjections of the axon-sparing excitotoxin N-methyl-DL-aspartic acid (NMA; Stewart et al., 1986; NMA; Sisk et al., 1988) to destroy cell bodies in the LSPV. Because the SCN is resistant to this neurotoxin (Peterson and Moore, 1980; Hastings et al., 1985) its cell bodies and efferent fibers remained intact.

Experimental Procedures

Animals:

Animals were 29 adult male grass rats obtained from a breeding colony at Michigan State University (Katona and Smale, 1997). All animals were singly

housed in Plexiglas cages (34 x 28 x 17 cm) and were provided access to food (PMI Nutrition Prolab RMH 2000, Brentwood, MO) and water *ad libitum*. Animals were kept in a 12:12 light: dark cycle (LD; ~250 lux during the light phase; lights on at 06:00 h) with a red light (<5 lux) on constantly for animal care purposes. All experiments were performed in compliance with guidelines established by the Michigan State University All-University Committee on Animals Use and Care, and the NIH Guide for the Care and Use of Laboratory Animals. One preliminary group of animals (n = 5) was used to fully characterize the effects of lesions on the SCN and LSPV. A second, primary, group of animals (n = 21) was used to examine effects of the lesions on behavioral rhythms.

Surgical procedures:

All animals received a bilateral injection of 0.2 M NMA (Sigma, St. Louis MO) or control vehicle directed at the LSPV. Animals were deeply anesthetized with sodium pentobarbital (50mg/kg i.p.) prior to surgery, and then the head was shaved, wiped with betadine, and injected with lidocaine (0.03cc s.c.). The animal was then placed into a stereotaxic apparatus (Stoelting Co.; Wood Dale, IL) with the incisor bar set to -5.5 mm and the manipulator set vertically, and a 1-2 cm incision was made in the scalp to expose the skull. A small hole was drilled in the skull, and dura was gently broken to allow uninterrupted passage of the micropipette. All injections were made using a 10 μL Hamilton syringe (Hamilton; Reno, NV) in which the needle was cut to 2 cm in length. The syringe was filled with either NMA in 0.2 M saline or saline alone and lowered slowly to injection depth. Injection coordinates were: 1.4 mm anterior to bregma, ± 0.3 mm lateral

to bregma, and 6.3 mm ventral to dura. Animals were injected with 90 μL (n = 13) or 135 μL (n = 11) per side using a manual stereotaxic microinjector (Stoelting); this allowed the NMA to be delivered in small, precisely-measured volumes over the course of the injection. The incision was closed with autoclips, and animals were given 0.1 cc buprenorphine i.m. and 2.0 cc sterile saline s.c.

Assessment of lesions:

In order to characterize the full effects of the lesions we first examined three series of tissue taken from brains of five male grass rats that were lesioned, kept for at least three weeks in DD, and then perfused at CT 22, when cFos expression is high in the LSPV and low in the SCN (Schwartz et al., 2004). One series of tissue from these animals was thionin-stained, while the second and third were processed for cFos and VP-immunoreactivity, respectively. To characterize the location and spread of the lesion, thionin-stained tissue was examined for cell loss and gliosis. cFos expression was used to determine whether lesions destroyed the cells that are endogenously rhythmic in the grass rat LSPV. VP expression was used to verify that both VP-immunoreactive (-ir) dorsal SCN cells and their efferent fibers in the LSPV were spared by the lesions. Animals in the primary, behavioral, experiment were perfused at the end of the study between ZT 1 and ZT 2, when cFos expression is high in both the SCN and the LSPV of intact animals (Schwartz et al., 2004). This was used to assess both how completely the cFos-producing cells in the LSPV were destroyed and whether activity in the SCN was spared. One series of tissue from these

experimental animals was therefore processed for cFos expression while another was thionin-stained.

All animals were given an overdose of sodium pentobarbital and perfused transcardially with 0.01M phosphate-buffered saline (PBS), pH 7.2, followed by 4% paraformaldehyde (Sigma, St. Louis, MO) with lysine and sodium periodate in 0.1M phosphate buffer (PLP). Brains were post-fixed for 4 hours in PLP and then transferred to 20% sucrose solution overnight. Brains were sectioned coronally at 30 μm on a freezing microtome into 3 series of sections, which were then stored in cryoprotectant at -20°C until processing began. Unless noted otherwise, incubations were conducted at room temperature for 1 hour on a shaker, and tissue was rinsed 3 x 10 minutes in PBS between incubations. Free-floating sections were rinsed in PBS, and then incubated in (i) 5% normal serum in PBS with 0.3% Triton X-100, followed by (ii) primary antibody on a rotator for 48 hours at 4°C. Following primary incubation, tissue was incubated in (iii) biotinylated secondary antibody, followed by avidin-biotin peroxidase complex (ABC Vectastain Kit, Vector Laboratories, Burlingame, CA). Protein was visualized by reacting with diaminobenzidine (DAB; 0.5mg/mL; Sigma) in Trizma buffer (Sigma), catalyzed with hydrogen peroxide. For cFos immunostaining, nickel sulfate was added to the cFos reaction, yielding a blue-black rather than brown reaction product. Reagents for each reaction were as follows: cFos: (i) normal goat serum (Vector), (ii) rabbit anti-cFos (Santa Cruz Biochemistry, Santa Cruz, CA; 1:25,000), (iii) biotinylated goat anti-rabbit (Vector; 1:200). VP: (i) normal goat serum (Vector), (ii) guinea pig anti-VP (Peninsula Laboratories, San

Carlos, CA; 1:40,000); (iii) biotinylated goat anti-guinea pig (Vector; 1:200). Previous blocking experiments in which the primary antibodies were pre-incubated with their antigens eliminated all staining for both VP (Smale and Boverhof, 1999) and cFos (Schwartz et al., 2004). Tissue was mounted, dehydrated, and coverslipped with Permount.

To quantify the extent to which lesions impacted the LSPV region of special interest, two sections through the mid- to caudal SCN were selected from each animal for counts of cFos-ir cells. The boundaries of the SCN were first demarcated in thionin-stained sections, then superimposed onto adjacent cFos-stained sections. All cFos-positive neurons were counted within the SCN, and within a region of the LSPV defined by a 215 μm x 160 μm rectangle placed immediately dorsal to the SCN and lateral to the third ventricle. This method reliably samples a portion of the distribution of cFos-ir cells that is both clearly outside the SCN, and in which cFos expression is rhythmic in grass rats in both LD and DD (Schwartz et al., 2004). Bilateral counts were summed and expressed as the total number of cFos-positive cells in the SCN and LSPV.

Experimental Design:

All animals were housed in a 12:12 LD cycle (lights-on = 06:00 h) with infrared motion detectors placed directly over the cage to monitor general activity. Animals were stably entrained to the LD cycle for at least 10 days prior to the start of the experiment. General activity data were collected on a PC running the Vitalview program (Minimitter; Bend, OR). To ensure that activity data used for analysis represented stable, long-term patterns of rhythmicity,

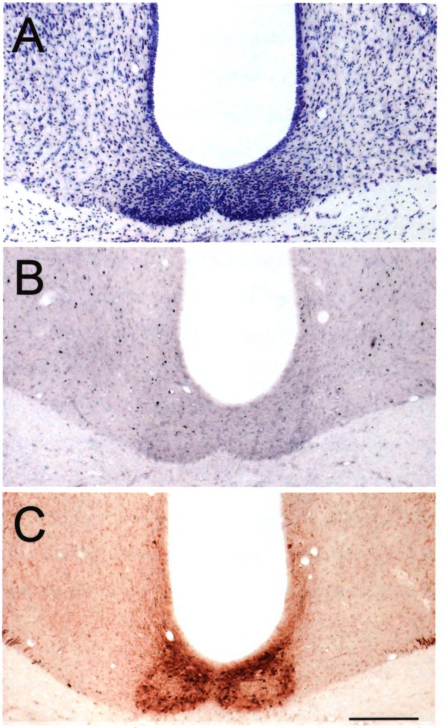

Figure 5.1: Photomicrographs of the SCN of a grass rat with a complete LSPV lesion that was perfused at CT 22. Alternate sections are stained for (A) Nissl, (B) cFos and (C) AVP. Scale bar = 200 µm.

animals were monitored for at least three weeks in each phase and a block representing approximately the final two weeks of each stage was selected for analysis (see below). In the preoperative phase (PREOP), baseline data were collected in LD for at least 21 days, of which the final 14 days prior to surgery were selected for analysis. Following PREOP, animals received intracranial injections of either NMA (n = 19) or vehicle (n = 5). Animals were kept in the same LD cycle following surgery for at least four weeks. General activity was recorded from them for at least the last three weeks of this period (LD1) and data from the final 12 days were selected for analysis. Animals were then released into constant darkness (DD) for four weeks, of which the final 14 days were selected for analysis. At the end of DD, 12:12 LD was resumed with the same phase as at the start of the study (lights-on at 06:00), and activity was recorded for another three weeks before animals were perfused (LD2). The sampling period analyzed for each individual in LD2 began on the day that rhythms in both the onset and the offset of activity were re-entrained, and ended on the day before sacrifice (mean number of days in sampling period for all animals = 14.67 $\pm$ 1.03 days).

Data analysis:

To assess rhythms in each stage, period (τ) and amplitude were calculated for each animal via chi-squared periodogram analysis in the Clocklab program (Actimetrics; Evanston, IL). Rhythmic patterns within the circadian range were considered significant at the $p = 0.05$ significance level. Total activity counts were summed for each stage and the percentage of activity in each day

occurring during the light phase was averaged for PREOP, LD1 and LD2. Additionally, daily onsets and offsets for the major daily activity bout were plotted in Clocklab. From these, the number of days to re-establish a stable phase angle with the light-dark cycle following the start of LD2 was determined. The day of entrainment was defined as the day on which the times of activity onset and offset no longer shifted more than 30 minutes for at least 3 consecutive days. Finally, we calculated the variance in the time of daily activity onset and offset for each animal at each stage of the experiment.

Six animals presented either unilateral lesions or no evidence of damage, and were not included in the ANOVA analyses. The remaining animals were classified as SHAM, LSPV-lesioned (LSPVx) or (MISS) based on 1) lesion placement determined from thionin-stained sections, and 2) the extent of LSPV damage in the lesion; these groups are described in detail in the results section. Separate 3 x 4 repeated-measures ANOVAs compared the influences of treatment group (LSPVx, MISS, SHAM) and stage (PREOP, LD1, DD, LD2) on the amplitude of activity rhythms, total activity counts, and variance in daily onset and offset. A 3 x 3 repeated-measures ANOVA compared the influences of treatment group (LSPVx, MISS, SHAM) and stage (PREOP, LD1, LD2) on the percentage of activity that occurred during the light phase of the 12:12 LD cycles. Lastly, one-way ANOVAs compared the effects of treatment on τ in DD, the number of days to re-entrainment of activity onset and offset following DD, and the number of cFos-ir cells in the SCN and the LSPV. All effects were considered significant at the $p = 0.05$ level. Where significant effects were

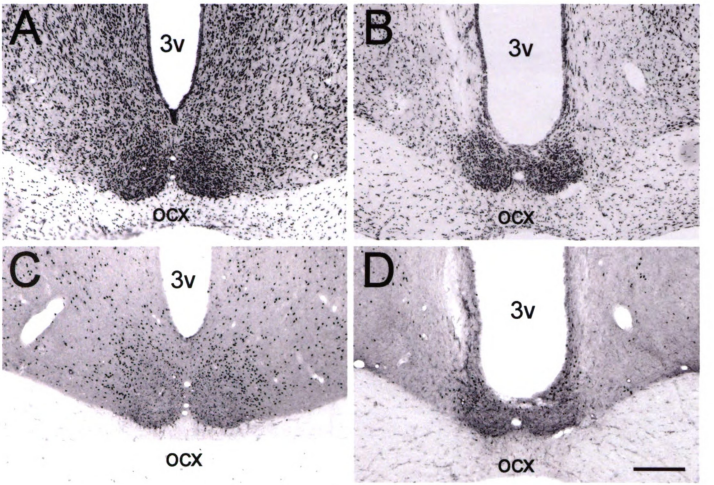

Figure 5.2: Photomicrographs of the SCN and LSPV of a representative SHAM (A, C) and LSPVx (B, D) grass rat perfused at ZT 1- ZT 2. Alternate sections are stained for (A, B) Nissl and (C, D) cFos. Scale bar = 200 µm.

detected, Fisher's posthoc tests were conducted to evaluate pairwise comparisons.

To assess relationships between the extent of cell loss in the LSPV and general activity rhythms, data from all animals (n = 21) were pooled. The number of cFos-ir cells in the SCN and LSPV were then correlated with the total activity counts and the amplitude of activity rhythms for each postoperative stage (LD1, DD, LD2). In addition, the number of cFos-ir cells in the SCN and LSPV was correlated with (1) the percent of activity that occurred during the light phase of the 12:12 LD cycles (LD1 and LD2), (2) τ in DD, and (3) the number of days to re-entrain activity onset and offset following DD. For analyses of these correlations, Pearson's *r* values were considered significant at the p = .05 level.

Results:

Histology:

In the five LSPV-lesioned animals perfused at CT 22 to characterize the NMA-induced damage, thionin-stained tissue revealed substantial gliosis and a near complete absence of neurons dorsal and, to a lesser extent, dorsolateral to the SCN (Fig. 5.5.1a). The area outside the Nissl-defined SCN border was almost completely devoid of cFos-positive cells (Fig. 5.5.1b). Very little cFos expression was observed within the SCN of these animals, as would be expected for grass rats perfused at CT 22. VP-ir cells formed a semicircular pattern with the most cells in the dorsal SCN, and some along the medial and lateral border of the SCN, as has been previously described in intact grass rats (Fig. 5.5.1c;

Smale and Boverhof, 1999; Fig. 5.5.1c; Schwartz et al., 2004). VP-ir fibers streamed dorsally from the SCN through the LSPV and sPVZ.

In SHAM animals in the primary behavioral study, the SCN and LSPV appeared as they have been described previously (Smale and Boverhof, 1999; Schwartz et al., 2004). In thionin-stained sections, cells in the SCN were small and tightly-packed, whereas cells in the area immediately dorsal to it were substantially larger and more dispersed (Fig. 5.5.2a). While a glial scar identifying the needle track was visible in several animals, there was no evidence of cellular trauma beyond the track mark, and neurons surrounding the glial scar were plentiful and healthy in appearance. The distributions of cFos expression in the SCN and LSPV of control animals perfused at ZT 1 and ZT 2 were also consistent with those observed previously in intact grass rats at ZT 1 (Fig. 5.5.2c; Nunez et al., 1999; Schwartz et al., 2004). cFos-ir cells filled the dorsal and ventral SCN and were relatively scarce in the central SCN. Dorsal and dorsolateral to the mid- to caudal portions of the SCN, cFos-ir cells extended from the periventricular nucleus to the anterior hypothalamic area. These cFos-ir cells were clearly outside the Nissl-defined border of the SCN, and were not observed directly lateral to the SCN.

The five lesioned animals with the fewest cFos-ir cells in the LSPV were classified as LSPVx. In these animals, lesions were centered in the LSPV and sPVZ (Fig. 5.3a) and left the SCN and the PVN intact (Fig. 5.2b). cFos immunoreactivity reflected the Nissl findings in LSPVx animals. That is, cFos-ir cells were plentiful within but not outside of the SCN (Fig. 5.2d). The numbers of

A

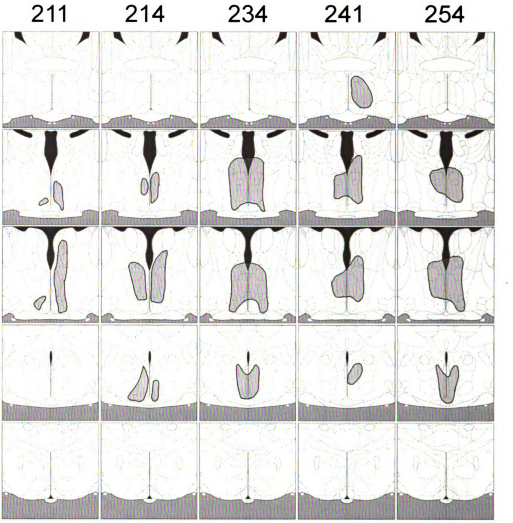

Figure 5.3: Schematic diagrams illustrating lesion placement in animals classified as LSPVx (A) and MISS (B). Atlas adapted from Paxinos & Watson (2005).

B

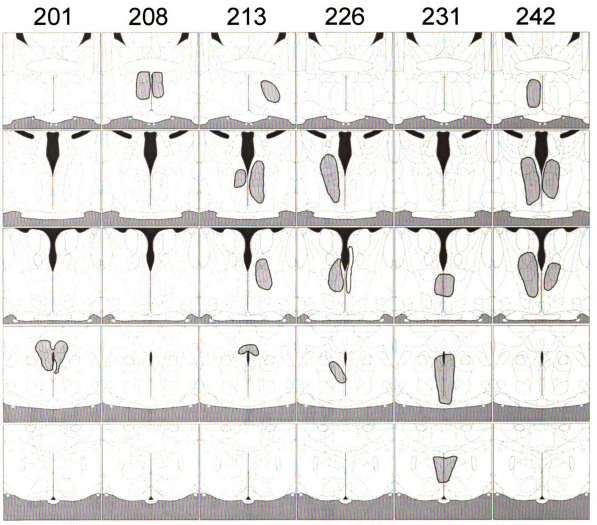

Figure 5.3 (continued).

	Total activity (counts)			Percent daytime activity			Onset variance (hrs)			Offset variance (hrs)		
	LSPV	**MISS**	**SHAM**	**LSPV**	**MISS**	**SHAM**	**LSPV**	**MISS**	**SHAM**	**LSPV**	**MISS**	**SHAM**
PRE	*24226.6**	*29431.5**	*26783.5**	60.2%	67.5%	61.2%	0.61	0.23	0.38	*0.23†*	0.25	0.21
± se	*2510.2*	*7670.8*	*9698.7*	3.5%	4.2%	1.4%	0.38	0.07	0.23	*0.09*	0.07	0.06
LD1	14915.6	18899.8	14635.5	55.1%	69.0%	61.0%	7.04	2.23	0.42	*18.55†*	2.54	0.54
± se	1881.2	6056.7	4276.2	4.9%	2.2%	6.2%	4.34	1.92	0.31	*7.27*	1.94	0.44
DD	12230.6	14688.7	22024.3	n/a	n/a	n/a	8.25	0.57	0.33	*17.08*†*	*6.21*†*	*0.09*†*
± se	2619.8	2178.2	6356.4	n/a	n/a	n/a	4.92	0.18	0.16	*8.43*	*4.08*	*0.03*
LD2	11618.8	13700.8	18094.3	59.3%	73.0%	68.9%	0.18	2.04	0.52	*3.53†*	0.33	0.08
± se	4031.4	2597.1	5894.5	5.5%	2.3%	5.0%	0.04	1.93	0.41	*3.00*	0.14	0.04

Table 5.1: Total levels of activity, percentage of activity in the daytime, variance in daily onset and variance in daily offset in each stage for LSPVx, MISS and SHAM animals. * = significant main effect of stage; † = significant main effect of group.

cFos-ir cells in the LSPV of these animals ranged from 15.9 % to 56.8 % of those obtained from controls.

Among the 6 animals classified as MISS, most lesions were centered in the mid- to dorsal sPVZ, and either missed or only slightly damaged the LSPV (Fig. 5.3b). In one of these animals, the lesion destroyed a large portion of the mPOA, and in another case the lesion was centered in the rostral and mid-PVN. The smallest bilateral lesion in this group covered approximately half of the sPVZ, whereas the largest encompassed most of the sPVZ, as well as the anterior and mid-PVN. In some MISS individuals, as with some LSPVx animals, the shape of the SCN was slightly distorted and the 3v was distended. cFos-ir cells in the LSPV of MISS animals were between 70.2 % and 121.8 % of average control values. The number of cFos-positive cells in the LSPV was significantly lower in LSPVx animals than either MISS or SHAM animals, which were similar to each other ($F_{2,12} = 16.501$, $p < 0.001$). The surgeries did not affect the number of cFos-positive cells in the SCN ($F_{2,12} = 1.560$, $p = 0.250$).

Activity rhythms

All animals had robust daily activity rhythms prior to surgery (Fig. 5.4). Several individuals exhibited crepuscular tendencies, and one of these was slightly more active in the dark phase than in the light because of a single large activity peak centered around lights-off; (in this individual 46.9 % of total daily activity occurred in the light phase; Fig. 5.5c). In all other animals activity was concentrated in the light phase (Table 1).

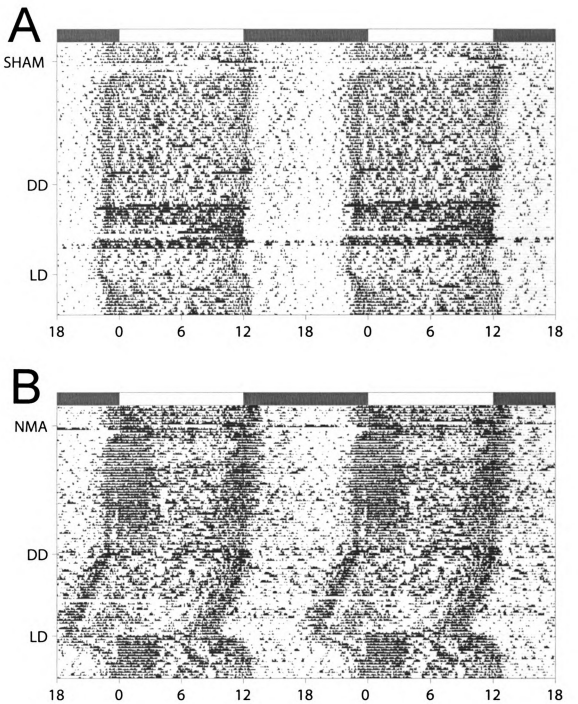

Figure 5.4: Representative double-plotted actograms of a SHAM (A) and MISS (B) grass rats. LD cycles are indicated at top, time of day (ZT) at bottom. In each actogram, date of lesion surgery (NMA or SHAM) and changes in lighting conditions (LD, DD) are indicated along the left side of each actogram.

Figure 5.5: Representative double-plotted actograms of three LSPVx animals, # 234 (A), # 241 (B) and # 254 (C). LD cycles are indicated at top, time of day (ZT) at bottom. In each actogram, date of lesion surgery (NMA or SHAM) and changes in lighting conditions (LD, DD) are indicated along the left side of each actogram.

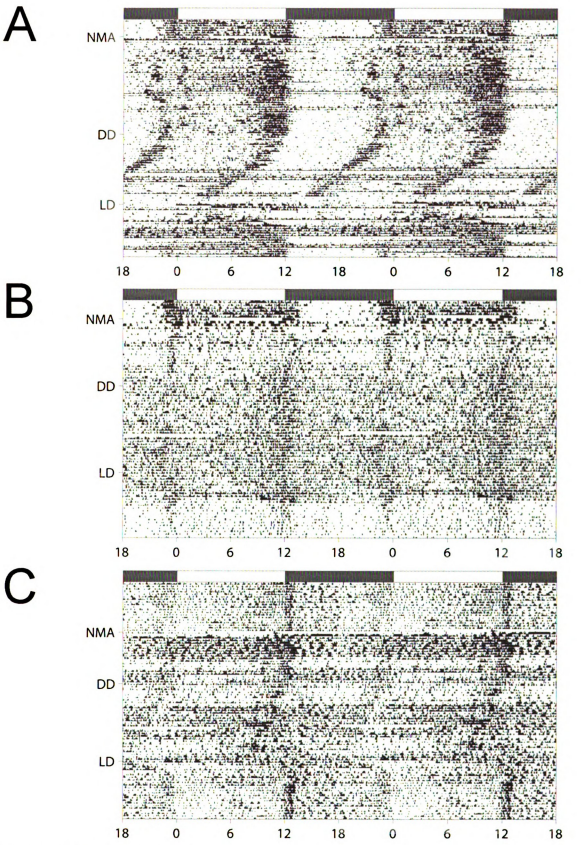
A
NMA
DD
LD
18
0
6
12
18
0
6
12
18
B
NMA
DD
LD
18
0
6
12
18
0
6
12
18
C
NMA
DD
LD
18
0
6
12
18
0
6
12
18

Figure 5.5.

Injections of both NMA and of vehicle were associated with short-term and long-term nonspecific behavioral effects. The short-term effect was a brief period of arrhythmicity in the first several days after surgery. Animals were hyperactive and in some cases displayed an ultradian component to their activity pattern that persisted for several days during this phase (Fig. 5.5). In all cases, these effects subsided within seven days; we did not include behavior from this first post-surgical week in our analyses.

There was also a long-term nonspecific effect of surgery on total activity. Specifically, total activity counts were reduced in all three postoperative stages compared to the PREOP period ($F_{3,36} = 6.938$, $p < 0.001$; Table 1), but were not affected by treatment ($F_{2,12} = 0.353$, $p = 0.709$), and there was no interaction between stage and group ($F_{3,36} = 0.593$, $p = 0.734$). There was also no correlation between the total amount of activity and cFos expression in the LSPV or the SCN (Table 2). Thus, total activity counts decreased similarly following surgery in the three treatment groups at all stages of the experiment, and were unrelated to cell loss in the LSPV or SCN. Effects of treatment on activity rhythms are therefore not likely to have been caused by a decrease in overall activity levels.

Rhythms of all animals were entrained in LD and free-ran in DD. Free-running periods (τ) were less than 24 hours in all but one animal ($\tau = 24.16$ h), and did not differ among groups ($F_{2,12} = 1.000$, $p = 0.454$; Table 1). However, activity rhythms became noticeably less precise in several individuals after they had been lesioned (Fig. 5.5). Amplitude was not affected by group ($F_{2,12} = 1.778$,

$p = 0.211$), but there was an interaction between group and stage ($F_{6,36} = 2.900$, $p = 0.021$). Specifically, activity rhythms in LSPVx animals in LD1, DD and LD2 were of lower amplitude than they were during the PREOP stage, whereas in MISS animals, only the amplitude in DD was lower than in the PREOP period (Fig. 5.6). In SHAM animals, by contrast, amplitude was higher in LD2 than in any other condition. Amplitude was positively correlated with cFos expression in the LSPV in DD, but not at any other stage, and amplitude was not related to cFos expression in the SCN (Table 2). Thus, although all animals were rhythmic following surgery, LSPVx animals had lower-amplitude activity rhythms at all postoperative stages, and cFos-ir cell loss in the LSPV was more closely related to the amplitude of free-running activity rhythms than entrained ones.

Several lesioned animals exhibited disorganized activity following surgery, particularly during and following the period in DD. Some of these were nearly arrhythmic (Fig. 5.5b), whereas others had rhythms that were disrupted by arrhythmic episodes that lasted up to five days (Fig. 5.5a, c). The variability of daily activity offsets was affected by group ($F_{2,12} = 7.43$, $p = 0.008$) and stage ($F_{3,36} = 2.894$, $p = 0.048$), with no interaction between these variables ($F_{6,36} = 1.579$, $p = 0.182$). Specifically, offset variance was higher in LSPVx animals than in MISS and SHAM animals, and was higher in DD compared to PREOP conditions (Table 1). Although the variance in daily activity onset appeared slightly elevated in LSPVx animals (Table 1), it was not significantly affected by treatment group ($F_{2,12} = 3.121$, $p = 0.081$), stage ($F_{3,36} = 1.311$, $p = 0.286$) nor the interaction between these variables ($F_{6,36} = 1.17$, $p = 0.340$). Offset variance was

	total activity counts		amplitude		Percent daytime activity	
	SCN	**LSPV**	**SCN**	**LSPV**	**SCN**	**LSPV**
PRE	0.0131	-0.034	-0.1502	-0.0306	-0.0652	0.0546
LD1	0.2091	0.0153	-0.046	0.1218	0.1192	0.3179
DD	-0.1196	0.076	0.1657	*0.5185**	n/a	n/a
LD2	-0.3116	-0.017	-0.0737	0.3683	0.1217	*0.4676**

Table 5.2: Correlations between the number of cFos-immunoreactive cells in the SCN and LSPV and total levels of activity, amplitude of activity rhythms, and percentage of activity in the daytime in each stage. * = significant correlation.

thus higher in LSPVx animals compared to MISS and SHAM animals, and onset variance exhibited a nonsignificant trend in the same direction.

Following the transition from DD to LD all control animals re-entrained within 5-9 days. Activity rhythms also re-entrained in all NMA-injected animals, but the rates at which this occurred were highly variable, ranging from 5 days to 21 days, and the animal that took the longest to re-entrain was the one sustaining the most complete lesion (Fig. 5.5a). Animals that took the longest time to re-entrain often displayed sudden phase jumps, or prolonged arrhythmic bouts as seen in DD (Fig. 5.5a, c). LSPVx animals exhibited somewhat slower re-entrainment rates than either MISS or SHAM animals, but these differences did not reach statistical significance (onset, $F_{2,12} = 3.427$, $p = 0.066$; offset, $F_{2,12} = 2.846$, $p = 0.097$; Fig. 5.7). However, the number of days to re-entrain onsets as well as offsets was negatively correlated with the number of cFos-positive cells in the LSPV (onset, $r = -0.457$, $p = 0.037$; offset, $r = -0.557$, $p = 0.009$), but not in the SCN (onset, $r = -0.215$, $p = 0.350$; offset, $r = -0.227$, $p = 0.321$). The distribution of activity following surgery was also highly variable between, and in some cases within, animals. Postoperative changes in activity distributions included increased crepuscular and nocturnal tendencies; this can be seen most strikingly in # 254, in which daytime activity represented only 30.1 % of total daily activity in LD2 (Fig. 5.5c). However, there were no effects of treatment group ($F_{2,12} = 2.649$, $p = 0.111$) or stage ($F_{2,24} = 1.112$, $p = 0.345$) on the percentage of activity that occurred during the daytime, and there was no interaction between these variables ($F_{4,2} = 1.271$, $p = 0.309$; Table 1). The percentage of activity

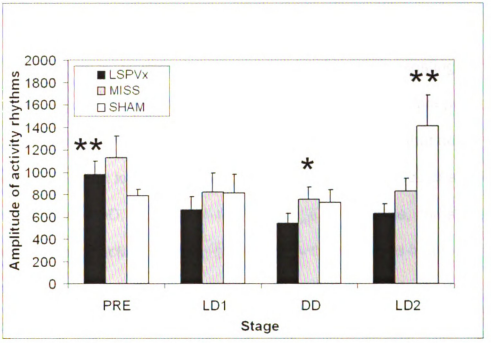

Fig.ure 5.6: Amplitude of activity rhythms of LSPVx (black), MISS (gray) and SHAM (white) grass rats in each stage. * = significantly different from PREOP within group. ** = significantly different from all other stages within group.

occurring in the daytime was, however, positively correlated with cFos expression in the LSPV in LD2, but not LD1, and was not related to cFos expression in the SCN (Table 2). In other words, animals with fewer Fos-ir cells in the LSPV were proportionally more active at night after they had been in DD for several weeks, but not prior to that.

Discussion:

The LSPV is a major target of the SCN, and in turn projects to many of the same areas as the SCN, raising the possibility that signals emanating from these two regions interact to regulate circadian rhythms. The current data provide support for that hypothesis by showing that excitotoxic lesions that destroyed cells in the LSPV but left the SCN intact decreased the amplitude of activity rhythms in LD and DD, impaired re-entrainment to an LD cycle, and shifted the distribution of daily activity towards the nighttime after rhythms had re-entrained. These changes were unrelated to cFos expression in the SCN, and were absent in animals with lesions that spared the LSPV. Cells in the grass rat LSPV thus appear to be an important part of the output pathways used by the pacemaker within the SCN to communicate circadian information to other brain regions.

Histology:

The SCN of NMA-injected animals appeared normal in thionin-stained sections, suggesting that it is resistant to chemical lesion in grass rats as is the case in lab rats (Peterson and Moore, 1980; Hastings et al., 1985). VP-ir neurons in the dorsal SCN and fibers passing through the LSPV were spared, further indicating that the SCN was intact in animals receiving NMA injections.

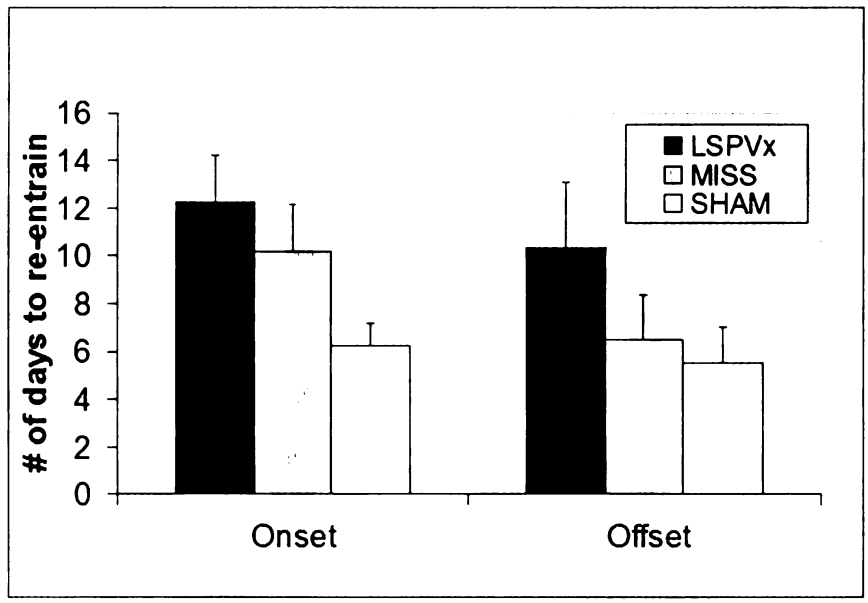

Figure 5.7: Number of days to re-entrain daily activity onset (left) and offset (right) for LSPVx (black), MISS (gray) and SHAM (white) grass rats following free-run.

Furthermore, cFos-ir staining in the SCN of lesioned animals perfused at ZT 1-2 was similar to that of SHAM animals and to that seen previously in intact grass rats (Nunez et al., 1999; Schwartz et al., 2004), suggesting that SCN neurons were functioning normally. cFos expression in the SCN was also not correlated with any of the observed changes in activity seen in LSPV-lesioned animals. Thus, the SCN was both intact and functional following NMA lesions, as indicated by basic morphology and assays of cellular activity.

All lesions that damaged the LSPV also damaged parts of the upper sPVZ. However, it is unlikely that changes in behavior in LSPV-lesioned animals were due to collateral damage sustained by the upper sPVZ. Many MISSes had large lesions centered in the upper sPVZ, so if the patterns seen in LSPVx animals were caused by damage to the upper sPVZ, they should have been seen in both groups. While MISSes did exhibit reduced-amplitude rhythms in DD compared the PREOP phase of the study, amplitudes in LD1 and LD2 did not differ from those seen during the PREOP period, and MISSes were similar to SHAMs on all other behavioral measures. Thus, the behavioral effects of lesions that included the LSPV were different and far more severe than those that did not, suggesting that these effects were due specifically to damage within the lower part of the sPVZ (i.e. the LSPV) rather than to other portions of it.

Free-running rhythms in LSPV-lesioned animals:

Activity rhythms were profoundly disrupted in LSPV-damaged animals. LSPVx animals had lower-amplitude activity rhythms in all postoperative conditions compared to the PREOP condition, and were more variable than

MISS or SHAM animals with respect to daily offset times. These deficits were most apparent in DD, when amplitude was lowest in animals with the most damage in the LSPV. However, activity in lesioned animals was not completely arrhythmic in constant conditions. In some animals, activity was disorganized, but still weakly rhythmic in DD, and in others free-running activity rhythms were disrupted by arrhythmic episodes lasting several days. However, these animals eventually resumed activity rhythms that free-ran with a phase that could be predicted from that of the preceding rhythm. Thus, although LSPV-damaged grass rats were unable to maintain a consistently stable endogenous activity rhythm, the clock normally governing that activity appears to have been undisturbed. In lab rats, free-running locomotor rhythms were also attenuated following excitotoxic lesions that included the LSPV (Lu et al., 2001), and were abolished following electrolytic lesions that destroyed both cells and fibers in the sPVZ (Abrahamson and Moore, 2006). This raises the possibility that cells in the LSPV act to reinforce the normal patterns of coupling between the clock and general activity, and is consistent with the hypothesis that differences in this coupling seen in diurnal and nocturnal rodents could be mediated in part by the LSPV.

It is unclear what triggered arrhythmic episodes in LSPV-damaged animals. They appeared to increase in frequency and last longer over time, suggesting that prolonged exposure to constant conditions may be necessary for them to emerge. We are not aware of similar phenomena in other species.

Further research should investigate whether these arrhythmias are evident in functions other than activity, and whether they are unique to grass rats.

Entrainment in LSPV-lesioned animals:

LSPV lesions did not initially disrupt rhythms of animals maintained in an LD cycle, but did slow re-entrainment to an LD cycle when grass rats were returned to LD from DD. Although all animals re-entrained following re-instatement of the LD cycle, animals with reduced cFos expression in the LSPV took longer to do so than those whose LSPV was intact. The effect of the lesions on re-entrainment was not secondary to an effect on the phase of the clock rhythm in DD, as lesions did not systematically affect τ. Rather, lesions could have affected the recovery of entrainment via one or both of two mechanisms. First, signals from the LSPV to the SCN may influence basic entrainment mechanisms that couple the clock to the LD cycle. Alternatively, coupling of the pacemaker in the SCN to activity could have been significantly weakened in LSPV-damaged animals such that re-entrainment of activity rhythms lagged behind that of the clock. Bouts of arrhythmia in lesioned animals, in LD2 (as in DD), suggest that the LSPV may ordinarily facilitate this coupling by aiding in the suppression of activity during the night (or subjective night), enhancing the ability of the pacemaker to drive or entrain rhythms in downstream targets. We view this as the most parsimonious explanation.

When animals did re-establish entrainment, the resulting activity rhythms were less diurnal in animals with the most damage to the LSPV. Reduced diurnality in LD2 did not simply reflect a decrease in the amplitude of the rhythm

in lesioned animals. cFos expression in the LSPV was not correlated with either amplitude or total activity levels at this stage, and neither the amplitude nor total activity levels of LSPVx animals differed in LD1 and LD2. However, there was no relationship between cFos in the LSPV and diurnality in LD1, suggesting that exposure to DD and/or difficulties related to re-entrainment may have induced a shift in activity distribution. Lesions may have led to a more general vulnerability of the circadian system to perturbation that became apparent when it was challenged by transitions from LD to DD and back, consistent with the hypothesis that the LSPV reinforces the coupling between the cock and activity. We do not know if such vulnerability is unique to diurnal species as there are presently no data on re-entrainment in LSPV- or sPVZ-lesioned nocturnal ones.

LSPV destruction does, however, appear to have a greater effect on entrained activity rhythms in grass rats than lab rats in which chemical lesions that included the LSPV did not affect locomotor activity rhythms in LD immediately following surgery in lab rats (Lu et al., 2001). However, in that study animals were only monitored for five days in LD following surgery, leaving open the possibility that rhythms could have degraded over a longer period of time (as they did in the present study). In another study, electrolytic sPVZ lesions abolished locomotor rhythms in lab rats kept in LD as well as DD (Abrahamson and Moore, 2006), and partial sPVZ ablation via wire knife lesions (Moore and Danchenko, 2002) attenuated rhythms in DD and LD in proportion to the extent of sPVZ damage. However, the methods used in these studies are likely to have destroyed both cell bodies in the sPVZ and SCN efferents passing though it. The

extent to which the effects of sPVZ lesions in those studies might have been due to damage to its lower (ventral) region, versus destruction of SCN projections beyond the LSPV, is thus not clear. In the present study, LSPV-damaged grass rats took longer to entrain to an LD cycle than did animals whose LSPV was intact, and once re-entrained were also less diurnal. Because SCN efferents were intact in these animals, the behavioral effects must be a result of damage to cells in the LSPV.

Conclusions:

In grass rats, the LSPV is likely to transmit circadian signals to other brain regions via projections that parallel those of the SCN, extending to the same set of hypothalamic and limbic forebrain targets (Watts et al., 1987; Morin et al., 1994). They may even project to the same cells, as neurons in the grass rat LSPV and SCN both form appositions with gonadotropin-releasing hormone neurons (chapter 4) and orexin neurons (Schwartz and Smale, 2006), two cell populations whose rhythmic activity is reversed in diurnal and nocturnal species (McElhinny et al., 1999; Martinez et al., 2002; Mahoney et al., 2004). The LSPV thus exhibits the anatomical connectivity necessary to communicate circadian signals to targets that regulate functions that are rhythmically inverted in nocturnal and diurnal species.

The LSPV of grass rats is similar in some ways and very different in others from that of lab rats. In both species the LSPV is devoid of signaling molecules that are present in the SCN, such as VP, vasoactive intestinal polypeptide, or prokineticin 2, (Smale and Boverhof, 1999; Schwartz et al., 2004; Lambert et al.,

2005). Thus, although these two regions project to the same areas, the signals they communicate are different, in both species. However, grass rats differ from lab rats with respect to the phase of the rhythm in the LSPV relative to that of the SCN (and to the LD cycle), and with respect to the dependence of that rhythm on an LD cycle (Schwartz et al., 2004). The present study provides experimental evidence for the first time that the grass rat LSPV is involved with the organization of stable activity rhythms in both LD and DD conditions, that it affects re-entrainment rates and that its role may be different from that of the LSPV of nocturnal species. Taken together, these data suggest that the LSPV, like the SCN, communicates circadian signals necessary for the expression of normal activity rhythms, and that species differences in signals coming from the LSPV may contribute to the differences between diurnal and nocturnal rodents.

CHAPTER 6

Conclusions

Circadian rhythms in physiology and behavior are dramatically different in diurnal and nocturnal rodents. However, the SCN, that houses the circadian pacemaker, exhibits similar rhythms in clock gene expression (Hastings et al., 1999; Bae et al., 2001; Mrosovsky et al., 2001; Yan and Okamura, 2002; Caldelas et al., 2003; Lambert and Weaver, 2006; Novak et al., 2006), metabolic activity (Schwartz, 1991), and firing rate (Kubota et al., 1981; Sato and Kawamura, 1984b; Kurumiya and Kawamura, 1988). Furthermore, rhythms in synthesis of three SCN output signals that have been examined are similar in diurnal and nocturnal rodents (Krajnak et al., 1998; Lambert and Weaver, 2006; Mahoney et al., 2006). Together, these data suggest that the primary neural mechanisms determining whether an animal is diurnal or nocturnal are unlikely to reside within the SCN. Rather, circadian signals from the SCN are probably modulated by downstream mechanisms in ways that contribute to determination of whether an animal has a diurnal or nocturnal pattern of rhythmicity. The experiments in this thesis evaluated this hypothesis by exploring the function and anatomy of the LSPV, a major target of the SCN (Watts et al., 1987) that functions differently in diurnal and nocturnal rodents (Nunez et al., 1999).

In Chapter 2, cFos rhythms in the LSPV were assessed in lab rats and grass rats housed in LD and in DD. The rising phase of the rhythm in cFos expression in the LSPV was advanced by roughly 8 hours in grass rats compared to lab rats, and this rhythm was endogenous in the former but not the

latter species. cFos expression in the LSPV was clearly outside the SCN's borders as defined by Nissl staining and AVP-ir. The grass rat LSPV thus represents a region receiving major inputs from the SCN (Watts et al., 1987; Smale and Boverhof, 1999) that exhibits dramatically different patterns of rhythmicity in grass rats and lab rats.

In Chapter 3, the efferent projections of the SCN and LSPV were mapped using injections of the anterograde tracer BDA. This study revealed that the SCN and the LSPV project in parallel to a nearly identical set of targets within the hypothalamus, midline thalamus, septal region and basal forebrain. Furthermore, the distributions of efferent fibers from the grass rat SCN and LSPV appear to be very similar to those of nocturnal lab rats and hamsters (Watts and Swanson, 1987; Watts et al., 1987; Morin et al., 1994; Kriegsfeld et al., 2004). These parallelisms suggest that in diurnal and nocturnal species the SCN communicates with targets both directly via its own axonal projections, and indirectly via the LSPV. Signals carried along these direct and indirect pathways likely affect their targets differently, as their temporal patterns of function and their neuropeptide content are not the same. These signals are also likely to differ in lab rats and grass rats, as rhythms in the LSPV are quite different in these two species.

Chapter 4 followed up on this idea by examining SCN and LSPV projections to GnRH neurons, a specific population of cells whose rhythmic activity is reversed in grass rats relative to lab rats (McElhinny et al., 1999; Mahoney et al., 2004). Fibers from both the SCN and the LSPV formed

numerous appositions with GnRH neurons, including more than half of those counted in the OVLT and rostral POA. Thus, the pattern of parallel innervation by the SCN and LSPV is maintained in specific cell populations known to exhibit reversed patterns of rhythmic activity in diurnal and nocturnal rodents. The pattern also raises the possibility that individual GnRH neurons receive input from both the SCN and the LSPV.

In Chapter 5, LSPV function was assessed via chemical lesions that spared both the SCN and its efferents. Free-running general activity rhythms and re-entrainment of these rhythms to an LD cycle were profoundly disturbed in grass rats with LSPV lesions. Thus, the coordination of circadian behavioral rhythms is influenced by the LSPV. However, lesioned animals were still capable of maintaining and entraining low-amplitude activity rhythms, indicating that the core oscillatory mechanisms underlying circadian activity rhythms were preserved. The LSPV is therefore not essential for maintaining circadian activity rhythms, or for a diurnal phase preference, but it is clearly essential for the normal expression of both.

Together, these experiments suggest that the grass rat LSPV is involved in transmitting circadian signals to the same suite of targets as does the SCN. The LSPV expressed endogenous cFos rhythms that were nearly 8 hours advanced relative to cFos rhythms in the SCN. The LSPV of grass rats also expresses daily rhythms in Per1 and Per2 whose phase differs from that of Per rhythms in the SCN (Ramanathan et al., 2006). These data are consistent with a role for the LSPV in communication of circadian signals to other brain regions

and that these signals differ from those transmitted by the SCN. When signaling from the LSPV was eliminated via neuron-specific lesions, general activity frequently appeared to become decoupled from the circadian clock, but circadian control was always re-established within several days. This decoupling was especially common in situations where external time cues were absent (as in DD) or in conflict with internal signals (as in re-entrainment to a new LD cycle). However, LSPV lesions, while causing disruptions in activity rhythms, neither abolished them nor caused stable long-term alterations in their phase. The LSPV is thus not essential for the basic diurnal pattern of activity rhythms in these animals. Rather, it may strengthen or reinforce the coupling between the SCN and its targets such that a stable, diurnal pattern is maintained.

Diurnality in grass rats may ordinarily be determined primarily by the nature of the direct coupling between the SCN and targets regulating locomotor activity. For example, the SCN could emit patterns of signals that determine whether an animal has a diurnal or nocturnal pattern of activity, although the available evidence suggests that this is unlikely to be the case. Alternatively, phase preference could be determined by the coupling between the SCN and a network of key intermediates, of which the LSPV is only one. The highly interconnected nature of major SCN and LSPV targets (POA, PVT, PVN, DMH, VMH) is consistent with the hypothesis that phase preference emerges from a networked organization. What the data in this thesis have established is that the LSPV contributes to the regulation of diurnality, and that it is not likely to do this on its own. More broadly speaking, phase preference, be it diurnal or nocturnal,

is likely to arise from the interactions of multiple direct and indirect output pathways from the SCN as well as from other sources of temporal information. For example, the presence or absence of light may also influence the behavior of targets downstream of the SCN via masking. Pathways from the SCN to the LSPV, and from the LSPV to targets that also receive direct input from the SCN, appear to represent an important part of this system.

The mechanisms by which the LSPV regulates rhythmic activity in conjunction with the SCN must be related to both its inputs and its outputs. Inputs to neurons in the grass rat LSPV lead to expression of cFos in response to phase-shifting light pulses (Mahoney et al., 2001), and, as described in Chapter 5, circadian rhythms were most strongly perturbed after prolonged exposure to DD and during re-entrainment to an LD cycle, suggesting that LSPV cells are involved in the entrainment processes. Further research should thus assess the extent to which activity in the LSPV is sensitive to entraining stimuli, such as light. Rhythmic activity in LSPV neurons, as measured by cFos expression and Per expression, should be examined under free-running, phase-shifted and entrained conditions in both diurnal and nocturnal rodents, to compare the time course of entrainment of rhythms in the LSPV to that of SCN rhythms. In this way, it may be possible to determine whether cells in the LSPV respond directly to entraining signals, are synchronized by signals from the SCN, or both. It will also be important to evaluate the extent to which the LSPV of nocturnal species is involved in entrainment, as this is presently unknown.

Further research should also evaluate whether cells in the LSPV integrate circadian signals with information pertaining to internal variables such as arousal state, as has been suggested in nocturnal species (Saper et al., 2005). Initial studies suggest that cFos rhythms in the grass rat LSPV are unaffected by variation in sleep-wake schedule (Schwartz and Smale, 2005), but it is not known whether the same is true in nocturnal species. To this end, description of the major inputs to the grass rat LSPV via injection of retrograde tracers may identify areas that contribute to the rhythmic activity of LSPV cells, and possibly to species differences in LSPV activity. For example, cholinergic innervation of the SCN and LSPV is more dense in lab rats than grass rats (Castillo-Ruiz, unpublished data), which is consistent with the idea that LSPV activity is less sensitive to variations in sleep-wake state in grass rats than in lab rats.

The LSPV's influence on rhythms of multiple behavioral and physiological parameters should also be examined more carefully. In nocturnal rodents, different types of lesions around the SCN have different effects on activity, core body temperature, drinking and neuroendocrine rhythms (Nunez and Stephan, 1977; Stephan and Nunez, 1977; Nunez and Casati, 1979; Dark, 1980; Brown and Nunez, 1986; Watts et al., 1989; Lu et al., 2001; Moore and Danchenko, 2002; Abrahamson and Moore, 2006). Furthermore, certain rhythms, such as that of pineal melatonin secretion, are not reversed in diurnal and nocturnal species (Reiter et al., 1982; Maywood et al., 1993; Klante et al., 1999; Garidou et al., 2002; Perreau-Lenz et al., 2003). These data raise the possibility that LSPV neurons could regulate some but not all circadian rhythms. For example, the

area above the SCN may be unrelated to pineal function but very much involved in rhythms associated with the hypothalamic-pituitary-gonadal (HPG) axis. Lesions (Docke et al., 1982), knife cuts (Nunez and Stephan, 1977) and electrical stimulation (Arendash and Gallo, 1979) centered in the area above the SCN affect the ability of rats to generate an LH surge, and daily rhythms in glial activity above the SCN are related to the ability of lab rats to generate an LH surge (Fernandez-Galaz et al., 1999). In chapter four, both SCN and LSPV neurons were found to project directly onto GnRH neurons in grass rats, suggesting that circadian signals from both areas may be important for maintaining a diurnal phase preference in the HPG axis. Future research should evaluate this hypothesis by determining whether axon-sparing LSPV lesions affect the GnRH neurons and their ability to coordinate the LH surge in grass rats.

In summary, the LSPV, a principal target of the SCN in diurnal and nocturnal rodents, exhibits the basic functional and anatomical characteristics necessary to communicate circadian signals originating in the SCN to other brain regions. Differences in the timing and the persistence of rhythmic activity in the grass rat LSPV suggest that this region could modulate those signals differently in diurnal and nocturnal rodents. Finally, signals from the LSPV contribute to rhythmic precision and stability in grass rats, as destruction of the LSPV causes profound disturbances in free-running activity rhythms and in entrainment of those rhythms to a light: dark cycle. Together, these results suggest that a normally functioning circadian system is likely to depend on contributions from

multiple oscillators that are ultimately coordinated by the master pacemaker in the SCN, and that the LSPV is one of those oscillators.

References

Abrahamson EE, Moore RY (2001) Suprachiasmatic nucleus in the mouse: retinal innervation, intrinsic organization and efferent projections. Brain Res 916:172-191.

Abrahamson EE, Moore RY (2006) Lesions of suprachiasmatic nucleus efferents selectively affect rest-activity rhythm. Mol Cell Endocrinol 252:46-56.

Allen G, Rappe J, Earnest DJ, Cassone VM (2001) Oscillating on borrowed time: diffusible signals from immortalized suprachiasmatic nucleus cells regulate circadian rhythmicity in cultured fibroblasts. J Neurosci 21:7937-7943.

Amir S, Lamont EW, Robinson B, Stewart J (2004) A circadian rhythm in the expression of PERIOD2 protein reveals a novel SCN-controlled oscillator in the oval nucleus of the bed nucleus of the stria terminalis. J Neurosci 24:781-790.

Antle MC, Silver R (2005) Orchestrating time: arrangements of the brain circadian clock. Trends Neurosci 28:145-151.

Arendash GW, Gallo RV (1979) Regional differences in response to electrical stimulation within the medial preoptic-suprachiasmatic region on blood luteinizing hormone levels in ovariectomized and ovariectomized, estrogen-primed rats. Endocrinology 104:333-343.

Bae K, Jin X, Maywood ES, Hastings MH, Reppert SM, Weaver DR (2001) Differential functions of mPer1, mPer2, and mPer3 in the SCN circadian clock. Neuron 30:525-536.

Beaule C, Arvanitogiannis A, Amir S (2001) Light suppresses Fos expression in the shell region of the suprachiasmatic nucleus at dusk and dawn: implications for photic entrainment of circadian rhythms. Neuroscience 106:249-254.

Bell-Pedersen D, Cassone VM, Earnest DJ, Golden SS, Hardin PE, Thomas TL, Zoran MJ (2005) Circadian rhythms from multiple oscillators: lessons from diverse organisms. Nat Rev Genet 6:544-556.

Brown MH, Nunez AA (1986) Hypothalamic circuits and circadian rhythms: effects of knife cuts vary with their placement within the suprachiasmatic area. Brain Res Bull 16:705-711.

Caldelas I, Poirel VJ, Sicard B, Pevet P, Challet E (2003) Circadian profile and photic regulation of clock genes in the suprachiasmatic nucleus of a diurnal mammal arvicanthis ansorgei. Neuroscience 116:583-591.

Card JP, Moore RY (1989) Organization of lateral geniculate-hypothalamic connections in the rat. J Comp Neurol 284:135-147.

Cheng MY, Bullock CM, Li C, Lee AG, Bermak JC, Belluzzi J, Weaver DR, Leslie FM, Zhou QY (2002) Prokineticin 2 transmits the behavioural circadian rhythm of the suprachiasmatic nucleus. Nature 417:405-410.

Cheung PW, McCormack CE (1983) Splitting of the locomotor activity rhythm in rats by exposure to continuous light. Am J Physiol 244:R573-576.

Dardente H, Menet JS, Challet E, Tournier BB, Pevet P, Masson-Pevet M (2004) Daily and circadian expression of neuropeptides in the suprachiasmatic nuclei of nocturnal and diurnal rodents. Brain Res Mol Brain Res 124:143-151.

Dark J (1980) Partial isolation of the suprachiasmatic nuclei: effects on circadian rhythms of rat drinking behavior. Physiol Behav 25:863-873.

de la Iglesia HO, Schwartz WJ (2006) Minireview: timely ovulation: circadian regulation of the female hypothalamo-pituitary-gonadal axis. Endocrinology 147:1148-1153.

de la Iglesia HO, Blaustein JD, Bittman EL (1995) The suprachiasmatic area in the female hamster projects to neurons containing estrogen receptors and GnRH. Neuroreport 6:1715-1722.

de la Iglesia HO, Meyer J, Schwartz WJ (2003) Lateralization of circadian pacemaker output: Activation of left- and right-sided luteinizing hormone-releasing hormone neurons involves a neural rather than a humoral pathway. J Neurosci 23:7412-7414.

Deurveilher S, Semba K (2003) Indirect projections from the suprachiasmatic nucleus to the median preoptic nucleus in rat. Brain Res 987:100-106.

Deurveilher S, Semba K (2004) Indirect projections from the suprachiasmatic nucleus to major arousal-promoting cell groups in rat: Implications for the circadian control of behavioural state. Neuroscience 130:165-183.

Deurveilher S, Burns J, Semba K (2002) Indirect projections from the suprachiasmatic nucleus to the ventrolateral preoptic nucleus: a dual tract-tracing study in rat. Eur J Neurosci 16:1195-1213.

Docke F, Lung DN, Rohde W, Dorner G (1982) Perisuprachiasmatic lesions enhance the increase of gonadotropin secretion in acutely ovariectomized rats. Endokrinologie 79:311-314.

Dunlap JC (1999) Molecular bases for circadian clocks. Cell 96:271-290.

Dunlap JC, Loros JJ, DeCoursey PJ (2004) Chronobiology: biological timekeeping. Sunderland, Mass.: Sinauer Associates.

Everett JW, Sawyer CH (1950) A 24-Hour Periodicity in the Lh-Release Apparatus of Female Rats, Disclosed by Barbiturate Sedation. Endocrinology 47:198-218.

Fernandez-Galaz MC, Martinez Munoz R, Villanua MA, Garcia-Segura LM (1999) Diurnal oscillation in glial fibrillary acidic protein in a perisuprachiasmatic area and its relationship to the luteinizing hormone surge in the female rat. Neuroendocrinology 70:368-376.

Field MD, Maywood ES, O'Brien JA, Weaver DR, Reppert SM, Hastings MH (2000) Analysis of clock proteins in mouse SCN demonstrates phylogenetic divergence of the circadian clockwork and resetting mechanisms. Neuron 25:437-447.

Garidou ML, Gauer F, Vivien-Roels B, Sicard B, Pevet P, Simonneaux V (2002) Pineal arylalkylamine N-acetyltransferase gene expression is highly stimulated at night in the diurnal rodent, Arvicanthis ansorgei. Eur J Neurosci 15:1632-1640.

Green DJ, Gillette R (1982) Circadian rhythm of firing rate recorded from single cells in the rat suprachiasmatic brain slice. Brain Res 245:198-200.

Gu GB, Simerly RB (1997) Projections of the sexually dimorphic anteroventral periventricular nucleus in the female rat. J Comp Neurol 384:142-164.

Guido ME, de Guido LB, Goguen D, Robertson HA, Rusak B (1999a) Daily rhythm of spontaneous immediate-early gene expression in the rat suprachiasmatic nucleus. J Biol Rhythms 14:275-280.

Guido ME, Goguen D, De Guido L, Robertson HA, Rusak B (1999b) Circadian and photic regulation of immediate-early gene expression in the hamster suprachiasmatic nucleus. Neuroscience 90:555-571.

Guo H, Brewer JM, Lehman MN, Bittman EL (2006) Suprachiasmatic regulation of circadian rhythms of gene expression in hamster peripheral organs: effects of transplanting the pacemaker. J Neurosci 26:6406-6412.

Hakim H, DeBernardo AP, Silver R (1991) Circadian locomotor rhythms, but not photoperiodic responses, survive surgical isolation of the SCN in hamsters. J Biol Rhythms 6:97-113.

Hamada T, Antle MC, Silver R (2004) Temporal and spatial expression patterns of canonical clock genes and clock-controlled genes in the suprachiasmatic nucleus. Eur J Neurosci 19:1741-1748.

Hamada T, LeSauter J, Lokshin M, Romero MT, Yan L, Venuti JM, Silver R (2003) Calbindin influences response to photic input in suprachiasmatic nucleus. J Neurosci 23:8820-8826.

Hastings MH, Roberts AC, Herbert J (1985) Neurotoxic lesions of the anterior hypothalamus disrupt the photoperiodic but not the circadian system of the Syrian hamster. Neuroendocrinology 40:316-324.

Hastings MH, Field MD, Maywood ES, Weaver DR, Reppert SM (1999) Differential regulation of mPER1 and mTIM proteins in the mouse suprachiasmatic nuclei: new insights into a core clock mechanism. J Neurosci 19:RC11.

Hiatt ES, Brunetta PG, Seiler GR, Barney SA, Selles WD, Wooledge KH, King JC (1992) Subgroups of luteinizing hormone-releasing hormone perikarya defined by computer analyses in the basal forebrain of intact female rats. Endocrinology 130:1030-1043.

Inouye ST, Kawamura H (1979) Persistence of circadian rhythmicity in a mammalian hypothalamic "island" containing the suprachiasmatic nucleus. Proc Natl Acad Sci U S A 76:5962-5966.

Jiao YY, Lee TM, Rusak B (1999) Photic responses of suprachiasmatic area neurons in diurnal degus (Octodon degus) and nocturnal rats (Rattus norvegicus). Brain Res 817:93-103.

Jobst EE, Allen CN (2002) Calbindin neurons in the hamster suprachiasmatic nucleus do not exhibit a circadian variation in spontaneous firing rate. Eur J Neurosci 16:2469-2474.

Jobst EE, Robinson DW, Allen CN (2004) Potential pathways for intercellular communication within the calbindin subnucleus of the hamster suprachiasmatic nucleus. Neuroscience 123:87-99.

Kalamatianos T, Kallo I, Goubillon ML, Coen CW (2004) Cellular expression of V1a vasopressin receptor mRNA in the female rat preoptic area: effects of oestrogen. J Neuroendocrinol 16:525-533.

Katona C, Smale L (1997) Wheel-running rhythms in Arvicanthis niloticus. Physiol Behav 61:365-372.

Katona C, Rose S, Smale L (1998) The expression of Fos within the suprachiasmatic nucleus of the diurnal rodent Arvicanthis niloticus. Brain Res 791:27-34.

Klante G, Secci K, Masson-Pevet M, Pevet P, Vivien-Roels B, Steinlechner S, Wollnik F (1999) Interstrain differences in activity pattern, pineal function, and SCN melatonin receptor density of rats. Am J Physiol 276:R1078-1086.

Konopka RJ, Benzer S (1971) Clock mutants of Drosophila melanogaster. Proc Natl Acad Sci U S A 68:2112-2116.

Krajnak K, Dickenson L, Lee TM (1997) The induction of Fos-like proteins in the suprachiasmatic nuclei and intergeniculate leaflet by light pulses in degus (Octodon degus) and rats. J Biol Rhythms 12:401-412.

Krajnak K, Kashon ML, Rosewell KL, Wise PM (1998) Sex differences in the daily rhythm of vasoactive intestinal polypeptide but not arginine vasopressin messenger ribonucleic acid in the suprachiasmatic nuclei. Endocrinology 139:4189-4196.

Kramer A, Yang FC, Snodgrass P, Li X, Scammell TE, Davis FC, Weitz CJ (2001) Regulation of daily locomotor activity and sleep by hypothalamic EGF receptor signaling. Science 294:2511-2515.

Kraves S, Weitz CJ (2006) A role for cardiotrophin-like cytokine in the circadian control of mammalian locomotor activity. Nat Neurosci 9:212-219.

Kriegsfeld LJ, Silver R (2006) The regulation of neuroendocrine function: Timing is everything. Horm Behav 49:557-574.

Kriegsfeld LJ, Silver R, Gore AC, Crews D (2002) Vasoactive intestinal polypeptide contacts on gonadotropin-releasing hormone neurones increase following puberty in female rats. J Neuroendocrinol 14:685-690.

Kriegsfeld LJ, Leak RK, Yackulic CB, LeSauter J, Silver R (2004) Organization of suprachiasmatic nucleus projections in Syrian hamsters (Mesocricetus auratus): an anterograde and retrograde analysis. J Comp Neurol 468:361-379.

Kubota A, Inouye ST, Kawamura H (1981) Reversal of multiunit activity within and outside the suprachiasmatic nucleus in the rat. Neurosci Lett 27:303-308.

Kurumiya S, Kawamura H (1988) Circadian oscillation of the multiple unit activity in the guinea pig suprachiasmatic nucleus. J Comp Physiol [A] 162:301-308.

Lambert CM, Weaver DR (2006) Peripheral gene expression rhythms in a diurnal rodent. J Biol Rhythms 21:77-79.

Lambert CM, Machida KK, Smale L, Nunez AA, Weaver DR (2005) Analysis of the prokineticin 2 system in a diurnal rodent, the unstriped Nile grass rat (Arvicanthis niloticus). J Biol Rhythms 20:206-218.

Leak RK, Moore RY (2001) Topographic organization of suprachiasmatic nucleus projection neurons. J Comp Neurol 433:312-334.

Lee WS, Smith MS, Hoffman GE (1990) Luteinizing hormone-releasing hormone neurons express Fos protein during the proestrous surge of luteinizing hormone. Proc Natl Acad Sci U S A 87:5163-5167.

Lee WS, Abbud R, Smith MS, Hoffman GE (1992) LHRH neurons express cJun protein during the proestrous surge of luteinizing hormone. Endocrinology 130:3101-3103.

Legan SJ, Karsch FJ (1975) Daily Signal for Lh Surge in Rat. Endocrinology 96:57-62.

LeSauter J, Silver R (1999) Localization of a suprachiasmatic nucleus subregion regulating locomotor rhythmicity. J Neurosci 19:5574-5585.

LeSauter J, Kriegsfeld LJ, Hon J, Silver R (2002) Calbindin-D(28K) cells selectively contact intra-SCN neurons. Neuroscience 111:575-585.

Lu J, Zhang YH, Chou TC, Gaus SE, Elmquist JK, Shiromani P, Saper CB (2001) Contrasting effects of ibotenate lesions of the paraventricular nucleus and subparaventricular zone on sleep-wake cycle and temperature regulation. J Neurosci 21:4864-4874.

Mahoney M, Bult A, Smale L (2001) Phase response curve and light-induced fos expression in the suprachiasmatic nucleus and adjacent hypothalamus of Arvicanthis niloticus. J Biol Rhythms 16:149-162.

Mahoney MM, Smale L (2005a) A daily rhythm in mating behavior in a diurnal murid rodent Arvicanthis niloticus. Horm Behav 47:8-13.

Mahoney MM, Smale L (2005b) Arginine vasopressin and vasoactive intestinal polypeptide fibers make appositions with gonadotropin-releasing hormone and estrogen receptor cells in the diurnal rodent Arvicanthis niloticus. Brain Res 1049:156-164.

Mahoney MM, Nunez AA, Smale L (2000) Calbindin and Fos within the suprachiasmatic nucleus and the adjacent hypothalamus of Arvicanthis niloticus and Rattus norvegicus. Neuroscience 99:565-575.

Mahoney MM, Sisk C, Ross HE, Smale L (2004) Circadian regulation of gonadotropin-releasing hormone neurons and the preovulatory surge in luteinizing hormone in the diurnal rodent, Arvicanthis niloticus, and in a nocturnal rodent, Rattus norvegicus. Biol Reprod 70:1049-1054.

Mahoney MM, Ramanathan C, Hagenauer MH, Smale L, Lee TM. A comparison of mRNA rhythms in vasoactive intestinal polypeptide and vasopressin in the suprachiasmatic nucleus of male and female grass rats. Program no.

P95. Society for Research on Biological Rhythms. Destin: Tenth Meeting, Society for Research on Biological Rhythms, 2006.

Martinez GS, Smale L, Nunez AA (2002) Diurnal and nocturnal rodents show rhythms in orexinergic neurons. Brain Res 955:1-7.

Maywood ES, Hastings MH, Max M, Ampleford E, Menaker M, Loudon AS (1993) Circadian and daily rhythms of melatonin in the blood and pineal gland of free-running and entrained Syrian hamsters. J Endocrinol 136:65-73.

McElhinny TL, Sisk CL, Holekamp KE, Smale L (1999) A morning surge in plasma luteinizing hormone coincides with elevated Fos expression in gonadotropin-releasing hormone-immunoreactive neurons in the diurnal rodent, Arvicanthis niloticus. Biol Reprod 61:1115-1122.

Meyer-Bernstein EL, Jetton AE, Matsumoto SI, Markuns JF, Lehman MN, Bittman EL (1999) Effects of suprachiasmatic transplants on circadian rhythms of neuroendocrine function in golden hamsters. Endocrinology 140:207-218.

Moga MM, Weis RP, Moore RY (1995) Efferent projections of the paraventricular thalamic nucleus in the rat. J Comp Neurol 359:221-238.

Moore-Ede MC, Sulzman FM, Fuller CA (1982) The clocks that time us: physiology of the circadian timing system. Cambridge, Mass.: Harvard University Press.

Moore RY, Eichler VB (1972) Loss of a circadian adrenal corticosterone rhythm following suprachiasmatic lesions in the rat. Brain Res 42:201-206.

Moore RY, Card JP (1994) Intergeniculate leaflet: an anatomically and functionally distinct subdivision of the lateral geniculate complex. J Comp Neurol 344:403-430.

Moore RY, Silver R (1998) Suprachiasmatic nucleus organization. Chronobiol Int 15:475-487.

Moore RY, Leak RK (2001) Suprachiasmatic Nucleus. In: Handbook of Behavioral Neurobiology, Vol. 12: Circadian Clocks, 1 Edition (Takahashi JS, Turek, F.W., Moore, R. Y., ed), pp 141-179. New York: Kluwer Academic/Plenum Publishers.

Moore RY, Danchenko RL (2002) Paraventricular-subparaventricular hypothalamic lesions selectively affect circadian function. Chronobiol Int 19:345-360.

Morin LP, Blanchard J, Moore RY (1992) Intergeniculate leaflet and suprachiasmatic nucleus organization and connections in the golden hamster. Vis Neurosci 8:219-230.

Morin LP, Goodless-Sanchez N, Smale L, Moore RY (1994) Projections of the suprachiasmatic nuclei, subparaventricular zone and retrochiasmatic area in the golden hamster. Neuroscience 61:391-410.

Morin LP, Shivers KY, Blanchard JH, Muscat L (2006) Complex organization of mouse and rat suprachiasmatic nucleus. Neuroscience 137:1285-1297.

Mrosovsky N, Edelstein K, Hastings MH, Maywood ES (2001) Cycle of period gene expression in a diurnal mammal (Spermophilus tridecemlineatus): implications for nonphotic phase shifting. J Biol Rhythms 16:471-478.

Novak CM, Nunez AA (1998) Daily rhythms in Fos activity in the rat ventrolateral preoptic area and midline thalamic nuclei. Am J Physiol 275:R1620-1626.

Novak CM, Albers HE (2004) Novel phase-shifting effects of GABAA receptor activation in the suprachiasmatic nucleus of a diurnal rodent. Am J Physiol Regul Integr Comp Physiol 286:R820-825.

Novak CM, Smale L, Nunez AA (2000) Rhythms in Fos expression in brain areas related to the sleep-wake cycle in the diurnal Arvicanthis niloticus. Am J Physiol Regul Integr Comp Physiol 278:R1267-1274.

Novak CM, Ehlen JC, Paul KN, Fukuhara C, Albers HE (2006) Light and GABA-A receptor activation alter Period mRNA levels in the SCN of diurnal Nile grass rats. In.

Nuesslein-Hildesheim B, O'Brien JA, Ebling FJ, Maywood ES, Hastings MH (2000) The circadian cycle of mPER clock gene products in the suprachiasmatic nucleus of the siberian hamster encodes both daily and seasonal time. Eur J Neurosci 12:2856-2864.

Nunez AA, Stephan FK (1977) The effects of hypothalamic knife cuts on drinking rhythms and the estrus cycle of the rat. Behav Biol 20:224-234.

Nunez AA, Casati MJ (1979) The role of efferent connections of the suprachiasmatic nucleus in the control of circadian rhythms. Behav Neural Biol 25:263-267.

Nunez AA, Bult A, McElhinny TL, Smale L (1999) Daily rhythms of Fos expression in hypothalamic targets of the suprachiasmatic nucleus in diurnal and nocturnal rodents. J Biol Rhythms 14:300-306.

Orpen BG, Steiner M (1994) Neural connections of the suprachiasmatic nucleus and medial hypothalamus of the Syrian hamster (Mesocricetus auratus). J Anat 184 (Pt 1):23-33.

Paxinos G, Watson C (2005) The rat brain in stereotaxic coordinates, 5th Edition. Amsterdam; Boston: Elsevier Academic Press.

Perreau-Lenz S, Kalsbeek A, Garidou ML, Wortel J, van der Vliet J, van Heijningen C, Simonneaux V, Pevet P, Buijs RM (2003) Suprachiasmatic control of melatonin synthesis in rats: inhibitory and stimulatory mechanisms. Eur J Neurosci 17:221-228.

Peterson GM, Moore RY (1980) Selective effects of kainic acid on diencephalic neurons. Brain Res 202:165-182.

Porkka-Heiskanen T, Urban JH, Turek FW, Levine JE (1994) Gene expression in a subpopulation of luteinizing hormone-releasing hormone (LHRH) neurons prior to the preovulatory gonadotropin surge. J Neurosci 14:5548-5558.

Ralph MR, Menaker M (1988) A mutation of the circadian system in golden hamsters. Science 241:1225-1227.

Ralph MR, Foster RG, Davis FC, Menaker M (1990) Transplanted suprachiasmatic nucleus determines circadian period. Science 247:975-978.

Ramanathan C, Nunez AA, Martinez GS, Schwartz MD, Smale L (2006) Temporal and spatial distribution of immunoreactive PER1 and PER2 proteins in the suprachiasmatic nucleus and peri-suprachiasmatic region of the diurnal grass rat (Arvicanthis niloticus). Brain Res 1073-1074:348-358.

Reiner A, Veenman CL, Medina L, Jiao Y, Del Mar N, Honig MG (2000) Pathway tracing using biotinylated dextran amines. J Neurosci Methods 103:23-37.

Reiter RJ, King TS, Richardson BA, Hurlbut EC (1982) Studies on pineal melatonin levels in a diurnal species, the eastern chipmunk (Tamias striatus): effects of light at night, propranolol administration or superior cervical ganglionectomy. J Neural Transm 54:275-284.

Reppert SM, Weaver DR (2002) Coordination of circadian timing in mammals. Nature 418:935-941.

Reppert SM, Schwartz WJ, Artman HG, Fisher DA (1983) Comparison of the temporal profiles of vasopressin and oxytocin in the cerebrospinal fluid of the cat, monkey and rat. Brain Res 261:341-345.

Salazar-Juarez A, Escobar C, Aguilar-Roblero R (2002) Anterior paraventricular thalamus modulates light-induced phase shifts in circadian rhythmicity in rats. Am J Physiol Regul Integr Comp Physiol 283:R897-904.

Saper CB, Lu J, Chou TC, Gooley J (2005) The hypothalamic integrator for circadian rhythms. Trends Neurosci 28:152-157.

Sato T, Kawamura H (1984a) Effects of bilateral suprachiasmatic nucleus lesions on the circadian rhythms in a diurnal rodent, the Siberian chipmunk (*Eutamias sibericus*). J Comp Physiol 155:745-752.

Sato T, Kawamura H (1984b) Circadian rhythms in multiple unit activity inside and outside the suprachiasmatic nucleus in the diurnal chipmunk (Eutamias sibiricus). Neurosci Res 1:45-52.

Schwartz MD, Smale L (2005) Individual differences in rhythms of behavioral sleep and its neural substrates in nile grass rats. J Biol Rhythms 20:526-537.

Schwartz MD, Smale L The suprachiasmatic nucleus and the lower subparaventricular zone project onto orexin-A neurons in a diurnal rodent Atlanta 2006 Society for Neuroscience. 'Online.'

Schwartz MD, Nunez AA, Smale L (2004) Differences in the suprachiasmatic nucleus and lower subparaventricular zone of diurnal and nocturnal rodents. Neuroscience 127:13-23.

Schwartz WJ (1991) SCN metabolic activity in vivo. In: Suprachiasmatic Nucleus: The Mind's Clock (Klein DC, Moore, R.Y., and Reppert, S.M., ed), pp 144-156. New York: Oxford University Press.

Schwartz WJ, Carpino A, Jr., de la Iglesia HO, Baler R, Klein DC, Nakabeppu Y, Aronin N (2000) Differential regulation of fos family genes in the ventrolateral and dorsomedial subdivisions of the rat suprachiasmatic nucleus. Neuroscience 98:535-547.

Silver R, LeSauter J, Tresco PA, Lehman MN (1996a) A diffusible coupling signal from the transplanted suprachiasmatic nucleus controlling circadian locomotor rhythms. Nature 382:810-813.

Silver R, Romero MT, Besmer HR, Leak R, Nunez JM, LeSauter J (1996b) Calbindin-D28K cells in the hamster SCN express light-induced Fos. Neuroreport 7:1224-1228.

Simerly RB, Swanson LW (1986) The organization of neural inputs to the medial preoptic nucleus of the rat. J Comp Neurol 246:312-342.

Simerly RB, Swanson LW (1988) Projections of the medial preoptic nucleus: a Phaseolus vulgaris leucoagglutinin anterograde tract-tracing study in the rat. J Comp Neurol 270:209-242.

Simonian SX, Spratt DP, Herbison AE (1999) Identification and characterization of estrogen receptor alpha-containing neurons projecting to the vicinity of the gonadotropin-releasing hormone perikarya in the rostral preoptic area of the rat. J Comp Neurol 411:346-358.

Sisk CL, Nunez AA, Thebert MM (1988) Differential effects of electrolytic and chemical hypothalamic lesions on LH pulses in rats. Am J Physiol 255:E583-590.

Smale L, Boverhof J (1999) The suprachiasmatic nucleus and intergeniculate leaflet of Arvicanthis niloticus, a diurnal murid rodent from East Africa. J Comp Neurol 403:190-208.

Smale L, Castleberry C, Nunez AA (2001) Fos rhythms in the hypothalamus of Rattus and Arvicanthis that exhibit nocturnal and diurnal patterns of rhythmicity. Brain Res 899:101-105.

Smale L, Lee TM, Nunez AA (2003) Mammalian Diurnality: Some Facts and Gaps. J Biol Rhythms 18:356-366.

Smith MJ, Jiennes L, Wise PM (2000) Localization of the VIP2 receptor protein on GnRH neurons in the female rat. Endocrinology 141:4317-4320.

Stephan FK, Zucker I (1972) Circadian rhythms in drinking behavior and locomotor activity of rats are eliminated by hypothalamic lesions. Proc Natl Acad Sci U S A 69:1583-1586.

Stephan FK, Nunez AA (1977) Elimination of circadian rhythms in drinking, activity, sleep, and temperature by isolation of the suprachiasmatic nuclei. Behav Biol 20:1-61.

Stewart GR, Price M, Olney JW, Hartman BK, Cozzari C (1986) N-methylaspartate: an effective tool for lesioning basal forebrain cholinergic neurons of the rat. Brain Res 369:377-382.

Sumova A, Travnickova Z, Mikkelsen JD, Illnerova H (1998) Spontaneous rhythm in c-Fos immunoreactivity in the dorsomedial part of the rat suprachiasmatic nucleus. Brain Res 801:254-258.

Swanson LW (2000) Cerebral hemisphere regulation of motivated behavior. Brain Res 886:113-164.

Sylvester CM, Krout KE, Loewy AD (2002) Suprachiasmatic nucleus projection to the medial prefrontal cortex: a viral transneuronal tracing study. Neuroscience 114:1071-1080.

Takeo Y (1984) Influence of continuous illumination on estrous cycle of rats: time course of changes in levels of gonadotropins and ovarian steroids until occurrence of persistent estrus. Neuroendocrinology 39:97-104.

ter Horst GJ, Luiten PG (1986) The projections of the dorsomedial hypothalamic nucleus in the rat. Brain Res Bull 16:231-248.

Thompson RH, Swanson LW (1998) Organization of inputs to the dorsomedial nucleus of the hypothalamus: a reexamination with Fluorogold and PHAL in the rat. Brain Res Brain Res Rev 27:89-118.

Thompson RH, Canteras NS, Swanson LW (1996) Organization of projections from the dorsomedial nucleus of the hypothalamus: a PHA-L study in the rat. J Comp Neurol 376:143-173.

Urbanski HF (1991) Monoclonal antibodies to luteinizing hormone-releasing hormone: production, characterization, and immunocytochemical application. Biol Reprod 44:681-686.

van der Beek EM, Wiegant VM, van der Donk HA, van den Hurk R, Buijs RM (1993) Lesions of the suprachiasmatic nucleus indicate the presence of a direct vasoactive intestinal polypeptide-containing projection to gonadotrophin-releasing hormone neurons in the female rat. J Neuroendocrinol 5:137-144.

Van der Beek EM, Horvath TL, Wiegant VM, Van den Hurk R, Buijs RM (1997a) Evidence for a direct neuronal pathway from the suprachiasmatic nucleus to the gonadotropin-releasing hormone system: combined tracing and light and electron microscopic immunocytochemical studies. J Comp Neurol 384:569-579.

van der Beek EM, van Oudheusden HJ, Buijs RM, van der Donk HA, van den Hurk R, Wiegant VM (1994) Preferential induction of c-fos immunoreactivity in vasoactive intestinal polypeptide-innervated gonadotropin-releasing hormone neurons during a steroid-induced luteinizing hormone surge in the female rat. Endocrinology 134:2636-2644.

van der Beek EM, Wiegant VM, van Oudheusden HJ, van der Donk HA, van den Hurk R, Buijs RM (1997b) Synaptic contacts between gonadotropin-releasing hormone-containing fibers and neurons in the suprachiasmatic nucleus and perichiasmatic area: an anatomical substrate for feedback regulation? Brain Res 755:101-111.

Vidal L, Blanchard J, Morin LP (2005) Hypothalamic and zona incerta neurons expressing hypocretin, but not melanin concentrating hormone, project to the hamster intergeniculate leaflet. Neuroscience 134:1081-1090.

Vitaterna MH, King DP, Chang AM, Kornhauser JM, Lowrey PL, McDonald JD, Dove WF, Pinto LH, Turek FW, Takahashi JS (1994) Mutagenesis and mapping of a mouse gene, Clock, essential for circadian behavior. Science 264:719-725.

Vrang N, Mrosovsky N, Mikkelsen JD (2003) Afferent projections to the hamster intergeniculate leaflet demonstrated by retrograde and anterograde tracing. Brain Res Bull 59:267-288.

Watson RE, Jr., Langub MC, Jr., Engle MG, Maley BE (1995) Estrogen-receptive neurons in the anteroventral periventricular nucleus are synaptic targets of the suprachiasmatic nucleus and peri- suprachiasmatic region. Brain Res 689:254-264.

Watts AG (1991) The efferent projections of the suprachiasmatic nucleus: anatomical insights into the control of circadian rhythms. In: Suprachiasmatic Nucleus: The Mind's Clock (Klein DC, Moore, R.Y., and Reppert, S.M., ed), pp 77-106. New York: Oxford University Press.

Watts AG, Swanson LW (1987) Efferent projections of the suprachiasmatic nucleus: II. Studies using retrograde transport of fluorescent dyes and simultaneous peptide immunohistochemistry in the rat. J Comp Neurol 258:230-252.

Watts AG, Swanson LW, Sanchez-Watts G (1987) Efferent projections of the suprachiasmatic nucleus: I. Studies using anterograde transport of Phaseolus vulgaris leucoagglutinin in the rat. J Comp Neurol 258:204-229.

Watts AG, Sheward WJ, Whale D, Fink G (1989) The effects of knife cuts in the sub-paraventricular zone of the female rat hypothalamus on oestrogen-induced diurnal surges of plasma prolactin and LH, and circadian wheel-running activity. J Endocrinol 122:593-604.

Weaver DR (1998) The suprachiasmatic nucleus: a 25-year retrospective. J Biol Rhythms 13:100-112.

Wiegand SJ, Terasawa E (1982) Discrete lesions reveal functional heterogeneity of suprachiasmatic structures in regulation of gonadotropin secretion in the female rat. Neuroendocrinology 34:395-404.

Yamazaki S, Numano R, Abe M, Hida A, Takahashi R, Ueda M, Block GD, Sakaki Y, Menaker M, Tei H (2000) Resetting central and peripheral circadian oscillators in transgenic rats. Science 288:682-685.

Yan L, Okamura H (2002) Gradients in the circadian expression of Per1 and Per2 genes in the rat suprachiasmatic nucleus. Eur J Neurosci 15:1153-1162.

Yan L, Takekida S, Shigeyoshi Y, Okamura H (1999) Per1 and Per2 gene expression in the rat suprachiasmatic nucleus: circadian profile and the compartment-specific response to light. Neuroscience 94:141-150.


MICHIGAN STATE UNIVERSITY LIBRARIES
3 1293 02845 6444